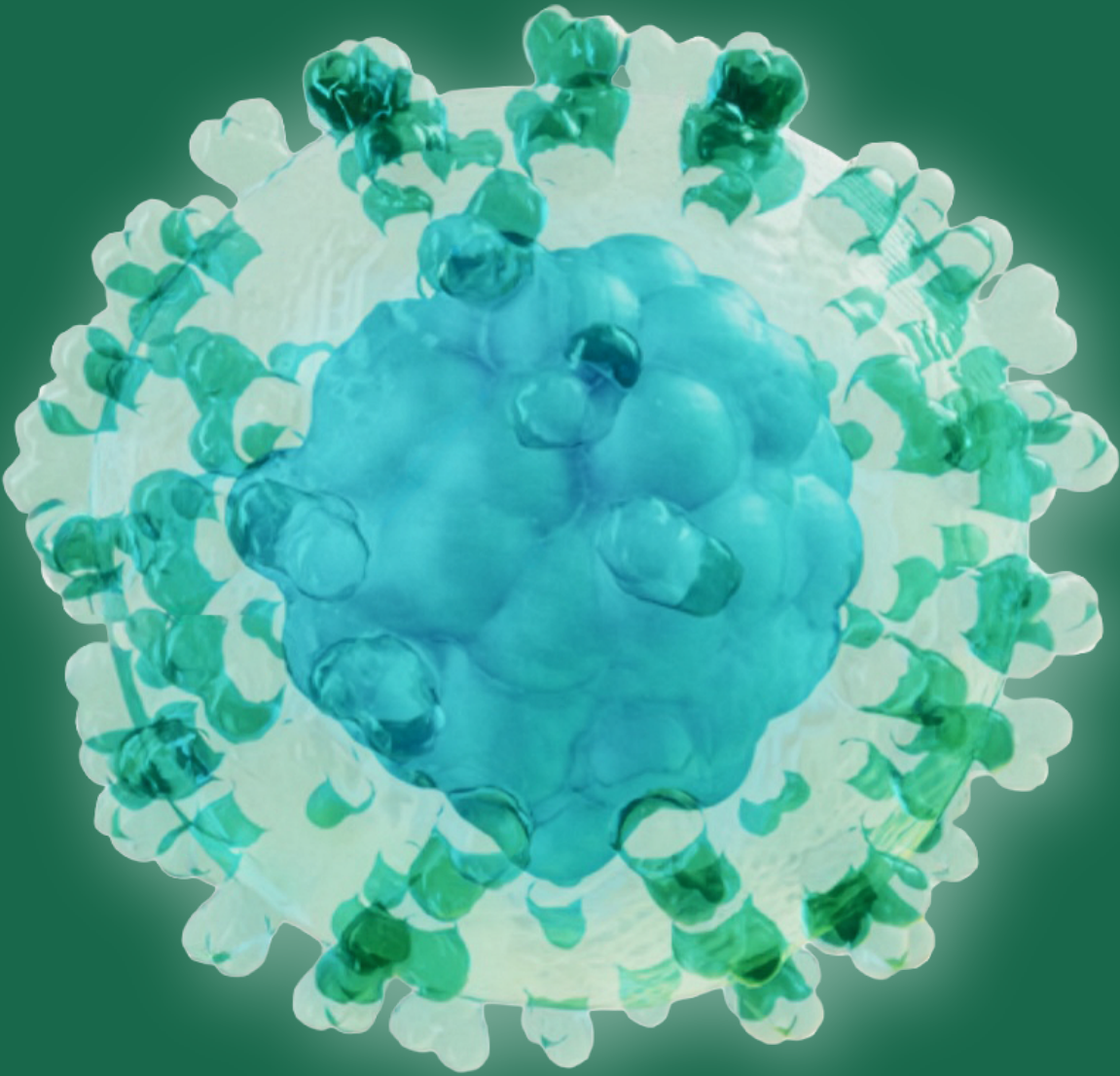


# TURKISH JOURNAL OF IMMUNOLOGY

**13**  
Volume  
**3**  
Issue



## Editor-in-Chief

### Prof. Günnur Deniz, PhD

İstanbul University, Aziz Sancar Institute of  
Experimental Medicine, Department of  
Immunology, İstanbul, Türkiye  
gdeniz@istanbul.edu.tr  
ORCID: 0000-0002-0721-6213

## Managing Editor

### Prof. Akif Turna, MD, PhD

İstanbul University-Cerrahpasa, Cerrahpasa  
Faculty of Medicine, Department of Thoracic  
Surgery, İstanbul, Türkiye  
akif.turna@gmail.com  
ORCID: 0000-0003-3229-830X

## Executive Office

### Türk İmmünoloji Derneği

Doğpa Ticaret AŞ Blok Yıldız Cad No 55  
34353 Beşiktaş - İstanbul, Türkiye  
turkimmunolojidernegi@gmail.com  
+90 212 - 414 20 97

## Publication Secretary

### Esra Dizdar

Turkish Society of Immunology  
(Türk İmmünoloji Derneği)  
turkimmunolojidernegi@gmail.com

## Assistant Editors

### Prof. Arzu Aral, MD, PhD

Yeditepe University Faculty of Medicine,  
Department of Immunology, İstanbul, Türkiye  
arzuaral@gmail.com  
ORCID: 0000-0002-7300-1624

### Prof. Ceren Çıracı, PhD

İstanbul Technical University Faculty of Science  
and Literature, Department of Molecular  
Biology and Genetics, İstanbul, Türkiye  
cerenciraci@gmail.com  
ORCID: 0000-0003-2162-0930

### Asst. Prof. Tolga Sütü, PhD

Acibadem University Faculty of Engineering  
and Natural Sciences, Department of Molecular  
Biology and Genetics, İstanbul, Türkiye  
Tolga.Sutlu@acibadem.edu.tr  
ORCID: 0000-0002-7813-8734

### Prof. Ali Önder Yıldırım, MD, PhD

Helmholtz Zentrum München, Germany  
oender.yildirim@helmholtz-muenchen.de  
ORCID: 0000-0003-1969-480X

## English Language Editor

### Rabia Ünal

DOC Tasarım ve Bilişim Ltd. Şti., İstanbul, Türkiye



**TÜRK  
İMMÜNOLOJİ  
DERNEĞİ**

## Owner

Owned by on behalf of the Turkish Society of Immunology:  
Prof. İhsan Gürsel

**.doc**

## Publication and Design

DOC Design and Informatics Co. Ltd.

E-mail: info@dotdoc.com.tr

Web page: www.dotdoc.com.tr

## Publishing Coordinator

Gizem Pakdil

## Design Lead

Ali Pekşen

## Software

Asım Demirağ

## Informatics

Nuh Naci Kışnişçi

## Typesetting

A Manikandaprabhu

## EDITORIAL BOARD

**Prof. Ali Önder Yıldırım, MD, PhD**

Helmholtz Zentrum München, Germany  
oender.yildirim@helmholtz-muenchen.de  
ORCID: 0000-0003-1969-480X

**Prof. Barbaros Oral, MD, PhD**

Bursa Uludag University Faculty of Medicine,  
Department of Immunology, Bursa, Türkiye  
oralb@uludag.edu.tr  
ORCID: 0000-0003-0463-6818

**Prof. Cevayir Çoban, MD, PhD**

The Institute of Medical Science (IMSUT), The University  
of Tokyo Division of Malaria Immunology, Japan  
ccoban@ims.u-tokyo.ac.jp  
ORCID: 0000-0002-4467-7799

**Prof. Cezmi Akdiş, MD**

Swiss Institute of Allergy and Asthma, Davos,  
Switzerland  
akdisac@siaf.uzh.ch  
ORCID: 0000-0001-8020-019X

**Prof. Derya Unutmaz, MD**

The Jackson Laboratory, Bar Harbor, USA  
derya@mac.com  
ORCID: 0000-0001-8898-6633

**Prof. Dicle Güç, MD, PhD**

Hacettepe University, Basic Oncology Institute, Retired  
Lecturer, Ankara, Türkiye  
dicleguc17@gmail.com  
ORCID: 0000-0003-1203-2109

**Prof. Güher Saruhan Direskeneli, MD, PhD**

İstanbul University, İstanbul Faculty of Medicine,  
Department of Physiology, İstanbul, Türkiye  
gsaruhan@istanbul.edu.tr  
ORCID: 0000-0002-6903-7173

**Prof. Haner Direskeneli, MD**

Marmara University Faculty of Medicine, Department  
of Internal Medicine, Department of Rheumatology,  
İstanbul, Türkiye  
hanerdireskeneli@gmail.com  
ORCID: 0000-0003-2598-5806

**Prof. İhsan Gürsel, PhD**

Bilkent University, Department of Molecular Biology and  
Genetics, Ankara, Türkiye  
ihsangursel@bilkent.edu.tr  
ORCID: 0000-0003-3761-1166

**Prof. Ken J. Ishii, MD, PhD**

Tokyo University, Institute of Medical Science, Division  
of Vaccine Science, Department of Microbiology and  
Immunology, Japan  
kenishii@ims.u-tokyo.ac.jp  
ORCID: 0000-0002-6728-3872

**Prof. Mayda Gürsel, PhD**

Middle East Technical University, Department of  
Biological Sciences, Ankara, Türkiye  
mgursel@metu.edu.tr  
ORCID: 0000-0003-0044-9054

**Prof. Moshe Ariditi, MD**

Cedars-Sinai Medical Center, Department of Pediatrics,  
USA  
Moshe.Arditi@cshs.org  
ORCID: 0000-0001-9042-2909

**Oral Alpan, MD**

Amerimmune Clinic, Fairfax, USA  
Oalpan@me.com  
ORCID: 0000-0001-7467-8541

**Prof. Sühendan Ekmekcioğlu, PhD**

MD Anderson Cancer Center, Department of Melanoma  
Medical Oncology, Division of Cancer Medicine, Huston,  
USA  
sekmekcioglu@mdanderson.org  
ORCID: 0000-0003-4079-6632

**Prof. Şefik Şanal Alkan, PhD**

Alkan Consulting LLC, Switzerland  
sefik.alkan@gmail.com  
ORCID: 0000-0001-8922-6337

**Prof. Yıldız Camcıoğlu, MD**

İstanbul University-Cerrahpasa, Cerrahpasa Faculty of  
Medicine, Department of Pediatrics, Retired Lecturer,  
İstanbul, Türkiye  
camciy@yahoo.com  
ORCID: 0000-0002-4796-6828

## ADVISORY BOARD

**Adil Doğanay Duru, MD**

Glycostem Therapeutics, Oss, The Netherlands

**Prof. Ahmet Özen, MD**

Marmara University Faculty of Medicine, Department of Pediatric Allergy-Immunology, İstanbul, Türkiye

**Assoc. Prof. Ahmet Eken, PhD**

Erciyes University Faculty of Medicine, Department of Medical Biology, Kayseri, Türkiye

**Assoc. Prof. Ayça Aslan Kıyıkım, MD**

İstanbul University-Cerrahpasa, Cerrahpasa Faculty of Medicine, Department of Pediatric Allergy-Immunology, İstanbul, Türkiye

**Assoc. Prof. Ayça Sayı Yazgan, PhD**

İstanbul Teknik University, Department of Molecular Biology and Genetics, İstanbul, Türkiye

**Assoc. Prof. Ayten Nalbant, PhD**

Izmir Institute of Technology, Department of Molecular Biology and Genetics, Izmir, Türkiye

**Prof. Batu Erman, PhD**

Bogazici University Faculty of Medicine, Department of Molecular Biology and Genetics, İstanbul, Türkiye

**Asst. Prof. Baran Erman, PhD**

Hacettepe University, Child Health Institute, Department of Pediatric Basic Sciences, HÜGEN, Can Sucak Translational Immunology Research Laboratory, Ankara, Türkiye

**Prof. Cem Ar, MD, PhD**

İstanbul University-Cerrahpasa, Cerrahpasa Faculty of Medicine, Department of Hematology, İstanbul, Türkiye

**Assoc. Prof. Çağman Tan, PhD**

Hacettepe University Faculty of Medicine, Child Health Institute, Department of Child Health and Diseases, Division of Pediatric Immunology, Ankara, Türkiye

**Prof. Deniz Nazire Çağdaş Ayvaz, MD**

Hacettepe University Faculty of Medicine, Child Health Institute, Department of Child Health and Diseases, Division of Pediatric Immunology, Ankara, Türkiye

**Asst. Prof. Diğdem Yöyen Ermiş, PhD**

Bursa Uludag University Faculty of Medicine, Department of Immunology, Bursa, Türkiye

**Assoc. Prof. Duygu Sağ, PhD**

Dokuz Eylul University, Izmir Biomedicine and Genome Center, Izmir, Türkiye

**Prof. Elif Aydın, MD**

Marmara University Faculty of Medicine, Department of Pediatric Allergy-Immunology, İstanbul, Türkiye

**Prof. Emel Ekşioğlu Demiralp, MD, PhD**

İstanbul Memorial Hospital, Tissue Type and Immunology Laboratory, İstanbul, Türkiye

**Prof. Erdem Tüzün, MD**

İstanbul University, Aziz Sancar Institute of Experimental Medicine, Department of Neuroscience, İstanbul, Türkiye

**Dr. Esen Şefik, PhD**

Yale University, Dr. Diane Mathis ve Dr. Christophe Benoist Laboratory, USA

**Prof. Esin Aktaş, PhD**

İstanbul University, Aziz Sancar Institute of Experimental Medicine, Department of Immunology, İstanbul, Türkiye

**Assoc. Prof. Fatih Kocabaş, MD**

Yeditepe University Faculty of Medicine, Department of Molecular Biology and Genetics, İstanbul, Türkiye

**Prof. Ferah Budak, PhD**

Bursa Uludag University Faculty of Medicine, Department of Immunology, Bursa, Türkiye

**Prof. Gaye Erten Yurdağül, MD, PhD**

İstanbul University, Aziz Sancar Institute of Experimental Medicine, Department of Immunology, İstanbul, Türkiye

**Prof. Gülderen Yanıkkaya Demirel, MD, PhD**

Yeditepe University Faculty of Medicine, Department of Immunology, İstanbul, Türkiye

**Prof. Güneş Esendağlı, PhD**

Hacettepe University, Basic Oncology Institute, Ankara, Türkiye

**Assoc. Prof. Gürcan Günaydın, MD, PhD**

Hacettepe University, Cancer Institute, Department of Basic Oncology, Ankara, Türkiye



**Prof. Hasibe Artaç, MD**

Selcuk University Faculty of Medicine, Department of Immunology, Konya, Türkiye

**Assoc. Prof. Hande Canpınar, PhD**

Hacettepe University, Cancer Institute, Department of Basic Oncology, Ankara, Türkiye

**Prof. İlgin Özden, MD**

İstanbul University-İstanbul Faculty of Medicine, Department of General Surgery, İstanbul, Türkiye

**Assoc. Prof. Jülide Duymaz, PhD**

Trakya University, Vocational School of Health Services, Edirne, Türkiye

**Assoc. Prof. Leyla Pur, MD, PhD**

University of Hospitals of Leicester NHS Trust, England

**Prof. Murat İnanç, MD**

İstanbul University-İstanbul Faculty of Medicine, Department of Internal Medicine, Division of Rheumatology, İstanbul, Türkiye

**Dr. Mustafa Diken, MD**

TRON - Translational Oncology at University Medical Center of Johannes Gutenberg University, Germany

**Assoc. Prof. Neşe Akış, PhD**

Trakya University Faculty of Medicine, Department of Medical Microbiology, Edirne, Türkiye

**Prof. Neslihan Cabioğlu, MD, PhD**

İstanbul University-İstanbul Faculty of Medicine, Department of Surgery, İstanbul, Türkiye

**Prof. Nesrin Özören, PhD**

Bogazici University, Department of Molecular Biology and Genetics, İstanbul, Türkiye

**Prof. Safa Barış, MD**

Marmara University Faculty of Medicine Hospital, Department of Pediatric Allergy-Immunology, İstanbul, Türkiye

**Dr. Semir Beyaz, PhD**

Cold Spring Harbor Laboratory, Immunology, USA

**Prof. Suzan Adın Çınar, PhD**

İstanbul University, Aziz Sancar Institute of Experimental Medicine, Department of Immunology, İstanbul, Türkiye

**Asst. Prof. Timuçin Avcı, PhD**

Bahcesehir University Faculty of Medicine, Department of Medical Biology, İstanbul, Türkiye

**Prof. Tunç Akkoç, PhD**

Marmara University Faculty of Medicine, Department of Pediatric Allergy-Immunology, İstanbul, Türkiye

**Assoc. Prof. Umut Can Küçüksezer, PhD**

İstanbul University, Aziz Sancar Institute of Experimental Medicine, Department of Immunology, İstanbul, Türkiye

**Assoc. Prof. Vuslat Yılmaz, PhD**

İstanbul University, Aziz Sancar Institute of Experimental Medicine, Department of Neuroscience, İstanbul, Türkiye

## CONTENT

### EDITORIAL

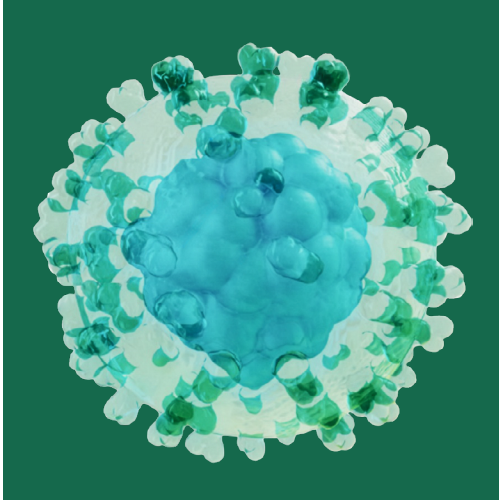
- 121** Highlights from This Issue and Perspectives for the New Year  
Günnur Deniz

### REVIEW ARTICLE

- 122** Role of Circular RNAs in Cancer Immune Checkpoint Therapy: Focus on Anti-PD-1 Treatment  
Duygu Kırkık, Furkan Aydın, Sevgi Kalkanlı Taş

### ORIGINAL RESEARCH

- 132** Understanding Allosteric Stabilization of pMHC by Peptide Ligands Through Molecular Dynamics Simulations  
Onur Serçinoğlu
- 146** Integrated Clinical and *In Silico* Analysis of Hypomorphic *DCLRE1C* Variants: Predicting Malignancy and Autoimmunity Risk  
Serkan Küçüktürk, Ali Şahin, Mehmet Ali Karaselek, Tuğçe Duran, Şükrü Nail Güner, Sevgi Keleş, İsmail Reislı
- 158** Dose-Dependent Effects of Maternal Vitamin D<sub>3</sub> on Offspring IL-6 and IL-1 $\beta$  in a Rat Model  
Kurnia Maidarmi Handayani, Widia Sari, Ghaniyyatul Khudri, Alief Dhuha, Rifkind Malik, Melya Susanti, Laura Zeffira, Annisa Lidra Maribeth
- 169** Effects of Typeable and Non-typeable *Haemophilus influenzae* on Human CD4<sup>+</sup> T Cell Proliferation and Production of Th1 and Th2 Cytokines  
Abdel Rahman Youssef
- 177** Effects of HLA Typing Resolution on Hardy-Weinberg Equilibrium, Linkage Disequilibrium, and Hidden Heterozygosity  
Emel Yantır



## COVER IMAGE

Human CD4+ T cells

### Image Credit:

Charles River Laboratories.

Available from: <https://www.criver.com/products-services/cell-sourcing/human-immune-cells/t-cells/cd4-t-cells-helper?region=3701>

# Highlights from This Issue and Perspectives for the New Year

## Dear Colleagues,

It is my pleasure to introduce the current issue of the *Turkish Journal of Immunology*, which brings together a series of original studies reflecting continued scientific progress in our field. This issue features contributions from Türkiye (4 articles), Indonesia (1 article), and Saudi Arabia (1 article), demonstrating both the journal's expanding international engagement and the strong research activity within our region.


This issue also includes a review article that examines the role of circular RNAs in cancer immune checkpoint therapy, with a particular focus on anti-PD-1 treatment. This comprehensive analysis highlights the emerging regulatory functions of circRNAs and their potential to influence therapeutic responses, offering new perspectives for the future of cancer immunotherapy.

The original articles presented here address important and diverse areas of immunology. One study employs molecular dynamics simulations to explore the allosteric stabilization of pMHC complexes, contributing to our understanding of peptide design and T-cell epitope prediction. Another study integrates clinical data with *in silico* modelling to evaluate the pathogenic potential of hypomorphic *DNA cross-link repair 1C* (DCL-RE1C) variants, offering refined perspectives on malignancy and autoimmunity risk.

Research on the dose-dependent effects of maternal vitamin D<sub>3</sub> supplementation provides valuable insights into the regulation of IL-6 and IL-1 $\beta$  in offspring, expanding our understanding of prenatal immunomodulation. The analysis of typeable and non-typeable *Haemophilus influenzae* strains offers important observations regarding their influence on CD4<sup>+</sup> T-cell proliferation and Th1/Th2 cytokine responses. Finally, an investigation into the impact of different human leukocyte antigen (HLA) typing resolutions on population genetic parameters highlights considerations of significance for immunogenetics and transplantation studies.

As we bring this year to a close, I warmly thank all our authors, reviewers, and readers for their invaluable contributions and unwavering support. May the new year bring you health, peace, and renewed enthusiasm for scientific discovery. We look forward to another year of collaboration and advancement together.

Wishing you all a happy, healthy, and successful New Year!  
With warm regards,

Prof. Günnur Deniz   
On behalf of the Editorial Board  
*Turkish Journal of Immunology*

## Correspondence

Günnur Deniz

## E-mail

gdeniz@istanbul.edu.tr

## Published

December 4, 2025

## Suggested Citation

Deniz G. Highlights from this issue and perspectives for the new year. *Turk J Immunol.* 2025;13(3):121.




## DOI

10.36519/tji.2025.951



This work is licensed under the Creative Commons Attribution-NonCommercial-Non-Derivatives 4.0 International License (CC BY-NC-ND 4.0).

# Role of Circular RNAs in Cancer Immune Checkpoint Therapy: Focus on Anti-PD-1 Treatment

Duygu Kırkık<sup>1,3</sup> , Furkan Aydın<sup>2,3</sup> , Sevgi Kalkanlı Taş<sup>3</sup> 

<sup>1</sup>University of Health Sciences Hamidiye Medicine Faculty, Department of Medical Biology, İstanbul, Türkiye; <sup>2</sup>Yeditepe University Faculty of Medicine, Department of Immunology, İstanbul, Türkiye; <sup>3</sup>University of Health Sciences Hamidiye Medicine Faculty, Department of Immunology, İstanbul, Türkiye

## Abstract

Circular RNAs (circRNAs) have gained attention in cancer immunotherapy, particularly in the context of immune checkpoint blockade therapies targeting programmed cell death 1 (PD-1). In this review, we aimed to elucidate the complex interactions between circRNAs and the PD-1 axis across various malignancies, highlighting their pivotal roles in modulating tumor immunity and influencing therapeutic responses in *in vitro*, *in vivo*, and in clinical studies. Beginning with an overview of circRNA biogenesis and functionalities, we examine circRNA-mediated mechanisms that impact the PD-1 pathway in cancers such as colorectal, gastric, pancreatic, hepatocellular, bladder, breast, lung, and metastatic melanoma. CircRNAs exhibit diverse functions, including acting as microRNA (miRNA) and protein sponges, translational modulators, and gene expression regulators, thereby intricately modulating the efficacy of PD-1 blockade therapy. Despite remarkable advancements, the field necessitates further investigation to unravel the full spectrum of circRNA-PD-1 interactions and translate these findings into clinical practice effectively. Our review underscores the significant translational potential of circRNAs in cancer immunotherapy, highlighting their multifaceted role in shaping innovative therapeutic strategies. These circRNAs offer insights into the molecular mechanisms of malignancies and hold promise as reliable biomarkers for early detection, prognosis, and monitoring of treatment responses. By integrating circRNA profiling into clinical practice, we envision the development of more personalized treatment approaches that cater to the unique molecular and immune landscapes of individual patients, ultimately revolutionizing cancer management and improving patient outcomes.

**Keywords:** Circular RNA, programmed cell death 1, immune checkpoints

## Introduction

### Immune Checkpoints and Anti-PD-1 Therapy

Immunotherapies refer to the usage of stimulative or suppressive substances in order to change the outcomes of immune system interactions and antagonize the

### Correspondence

Duygu Kırkık

### E-mail

dygkirkik@gmail.com

### Received

May 20, 2025

### Accepted

October 6, 2025

### Published

December 4, 2025

### Suggested Citation

Kırkık D, Aydın F, Kalkanlı Taş S. Role of circular RNAs in cancer immune checkpoint therapy: Focus on anti-PD-1 treatment. Turk J Immunol. 2025;13(3):122-31.

### DOI

10.36519/TJI.2025.711



This work is licensed under the Creative Commons Attribution-NonCommercial-Non-Derivatives 4.0 International License (CC BY-NC-ND 4.0).



disease progression (1). In cancer immunotherapies, it is provided by cancer vaccines, adoptive cell therapies with tumor-infiltrating lymphocytes, chimeric antigen receptor (CAR) T-cell therapies, and immune checkpoint blockade.

Immune checkpoints (ICPs) typically function to suppress overactivated cell-mediated immune responses, thereby maintaining homeostasis, particularly normal anti-tumor immunity; concurrently, they prevent peripheral tissue damage (2). Examples of immune checkpoint proteins are programmed cell death 1 (PD-1), programmed cell death ligand 1 (PD-L1), cytotoxic T-lymphocyte-associated antigen 4 (CTLA-4), lymphocyte activation gene 3 (LAG3), T-cell immunoglobulin (Ig) and mucin domain (TIM3), and V-domain Ig suppressor of T-cell activation (VISTA) (3). However, cancer cells acquired the ability to activate these ICPs to evade immune surveillance. For this reason, potential chemopreventive strategies should be developed to counteract the diminished or decreased immune cell activity in cancer treatment by ICP inhibitors (4). Immune checkpoint inhibitors (ICIs) represent a transformative therapeutic strategy designed to reverse this tumor-induced immune suppression (5). The core concept behind ICIs is to release the “brakes” placed on the immune system by the malignant cells, thereby restoring the effector T-cell capacity to recognize and eliminate the tumor (6). This novel mechanism of action has led to remarkable clinical success and significant improvements in patient outcomes across numerous solid tumors (7).

Nevertheless, the therapeutic utility of ICIs remains challenged by considerable patient response variability, the development of acquired resistance, and the potential for immune-related adverse events, necessitating ongoing research into predictive biomarkers and rational combination strategies (8,9).

Programmed cell death 1, which is also depicted as CD279, is an example of the immune checkpoint and can be found on the surfaces of activated T cells, B cells, dendritic cells (DCs), regulatory T cells (Tregs), and tumor-associated macrophages (TAMs) (2). Structurally, PD-1 protein contains a monomeric extracellular domain (ECD), transmembrane domain (TMD), and intracellular domain (ICD). In the tumor microenvironment (TME), T cell and PD-1 interacts with PD-L1 expressed in tumor cells (10). After the PD-1/PD-L1 interaction, immunoreceptor tyrosine-based inhibitory (ITIM) or switch

motifs (ITSM) are activated, and later this interaction suppresses downstream T-cell receptor (TCR) signaling pathways and therefore inhibits T cell proliferation and the production of cytokines like interferon-gamma (IFN- $\gamma$ ) and interleukin-2 (IL-2) (11). In this way, tumor cells make the immune cells vulnerable while performing their functions (12). Recent research has uncovered that non-coding RNAs, especially circular RNAs (circRNAs), may play a significant role in influencing immune checkpoint pathways like PD-1, providing new opportunities for therapeutic interventions.

### Biogenesis and Functions of circular RNAs

After the discovery of its role in viral replication in RNA viruses by Sanger et al. (13) in 1976, circRNAs were found to have distinct features, particularly in their unique structure among non-coding RNAs (ncRNAs), and are responsible for a vast number of both physiological and pathophysiological events, as discussed in detail elsewhere (14). Biogenesis of these special ncRNAs is dependent on the circularization of linear sequences of both exons and/or introns throughout the interaction with 5'-cap and 3'-poly-A tail, which are

### Highlights

- Circular RNAs (circRNAs) have emerged as critical regulators of immune evasion in cancer by modulating programmed cell death 1 (PD-1) and programmed cell death ligand 1 (PD-L1) signaling pathways.
- Recent studies demonstrate that specific circRNAs can directly or indirectly influence PD-1 expression, affecting T cell exhaustion and immune checkpoint blockade efficacy.
- Circular RNA-mediated competitive endogenous RNA (ceRNA) networks represent promising therapeutic targets to enhance the response to PD-1 inhibitors.
- Major unanswered questions include the precise mechanisms by which circRNAs modulate immune cell phenotypes within the tumor microenvironment and their clinical utility as predictive biomarkers.
- Future perspectives suggest integrating circRNA profiles into immunotherapy decision algorithms and exploring circRNA-based therapeutics in combination with immune checkpoint blockade.

covalently bound and do not have the site for binding the RNA exonucleases, which drives downregulation of RNA components in the environment (15). After their biogenesis, circRNAs act like sponges to certain microRNAs (miRNAs), which are other ncRNAs that have diverse functions either inhibiting or activating the downstream effect of miRNA-associated pathways. It has been identified as a key regulator of gene expression pathways, functioning through interactions with enhancer and silencer proteins, mediating RNA splicing to generate diverse transcript variants, and contributing to protein translation processes (16). Although they are synthesized in the nucleus, they transfer to the cytoplasm and then eventually can be found in different body sites and cellular components such as exosomes, plasma, and interstitial fluids (17).

### Circular RNAs in Tumorigenesis and Cancer Progression

Circular RNAs are emerging as critical regulators of immune cell function, influencing processes such as activation, differentiation, and immune evasion, particularly within the TME (18,19). By acting as sponges for specific miRNAs, circRNAs modulate gene expression in immune cells, shaping their activity and interactions. In T cells, circRNAs like circNCOA3 and circFGFR1 suppress cytotoxic responses by indirectly promoting the recruitment of immunosuppressive cells or reducing CD8<sup>+</sup> T cells infiltration into tumors. Similarly, circRNAs regulate DCs by affecting their antigen-presenting capacity and cytokine production, as seen with circDLG1, which recruits myeloid-derived suppressor cells (MDSCs) and impairs T cell activation (20-22). These effects collectively hinder effective anti-tumor immunity, making circRNAs key players in immune regulation. In addition to their roles in T cells and DCs, circRNAs significantly influence macrophages, particularly TAMs, by driving their polarization toward an immunosuppressive M2 phenotype (23-25). For instance, circPRDM4 enhances this polarization via the hypoxia-inducible factor-1 $\alpha$  (HIF-1 $\alpha$ ) pathway, supporting tumor immune evasion (26)

Circular RNAs also regulate other immune cells, such as Tregs, where they contribute to maintaining immune suppression in pathological conditions (27). In acute respiratory distress syndrome, circFLNA increases PD-1 expression on Tregs, promoting their anti-inflammatory functions (27,28). These findings underscore the diverse and interconnected roles of circRNAs across immune cell populations, highlighting their potential as targets

for therapeutic intervention in diseases like cancer and inflammatory disorders (29-31).

In this review, we aimed to reveal the influence of circRNAs on anti-programmed cell death 1 (anti-PD-1) therapy and their underlying pathways, which give us insights into considering circRNAs either as interrupting or promoting the therapeutic efficacy. After a literature search on databases such as Scopus, Web of Science, and PubMed, all the relevant information was summarized for each different malignancy, separated by the subheadings. Critically, the mechanisms discussed, and data compiled integrate findings from both *in vitro* (cell lines) and *in vivo* (animal and clinical) studies, providing a holistic view of the circRNA-PD-1 axis. The identifier of the circRNAs and their downstream pathways were indicated in Figure 1. The affected protein expression levels and the relationship with anti-PD-1 therapeutic efficacy were summarized in Table 1.

### Circular RNAs and Programmed Cell Death 1 (PD-1) Axis in Multiple Malignancies

#### Colorectal Cancer

In a study that investigated colorectal cancer (CRC) patients who underwent PD-1 immune checkpoint blockade therapy, it was determined that hsa\_circ\_0060627, also known as circNCOA3, was associated with an increase in metastatic ability and tumor mass. Furthermore, levels of circNCOA3 were found to be correlated with low overall survival and progression-free survival. Also in this study, results were confirmed to be from the activity of circNCOA3 as miR-203a-3p.1 sponge, which eventually inhibits the C-X-C motif chemokine ligand 1 (CXCL1) mRNA transcription. The downstream effect of these mechanisms can be summarized as the accumulation of MDSCs, which usually prevent the effector functions of immune cells in the tumor microenvironment. Also, it was proposed to be a means suitable for possible therapeutic intervention as augmenting PD-1 responsiveness (20).

#### Gastric Cancer

There is just one study that explores the axis in which gastric cancer (GC) and circRNA are investigated together. As reported by Chen et al. (21), circDLG1 (hsa\_circ\_0008583) causes the attraction of MDSCs to the tumor site through the C-X-C motif chemokine ligand 12 (CXCL12), which facilitates this migration when circDLG1 performs miR-141-3p sponge activity. The overall ef-

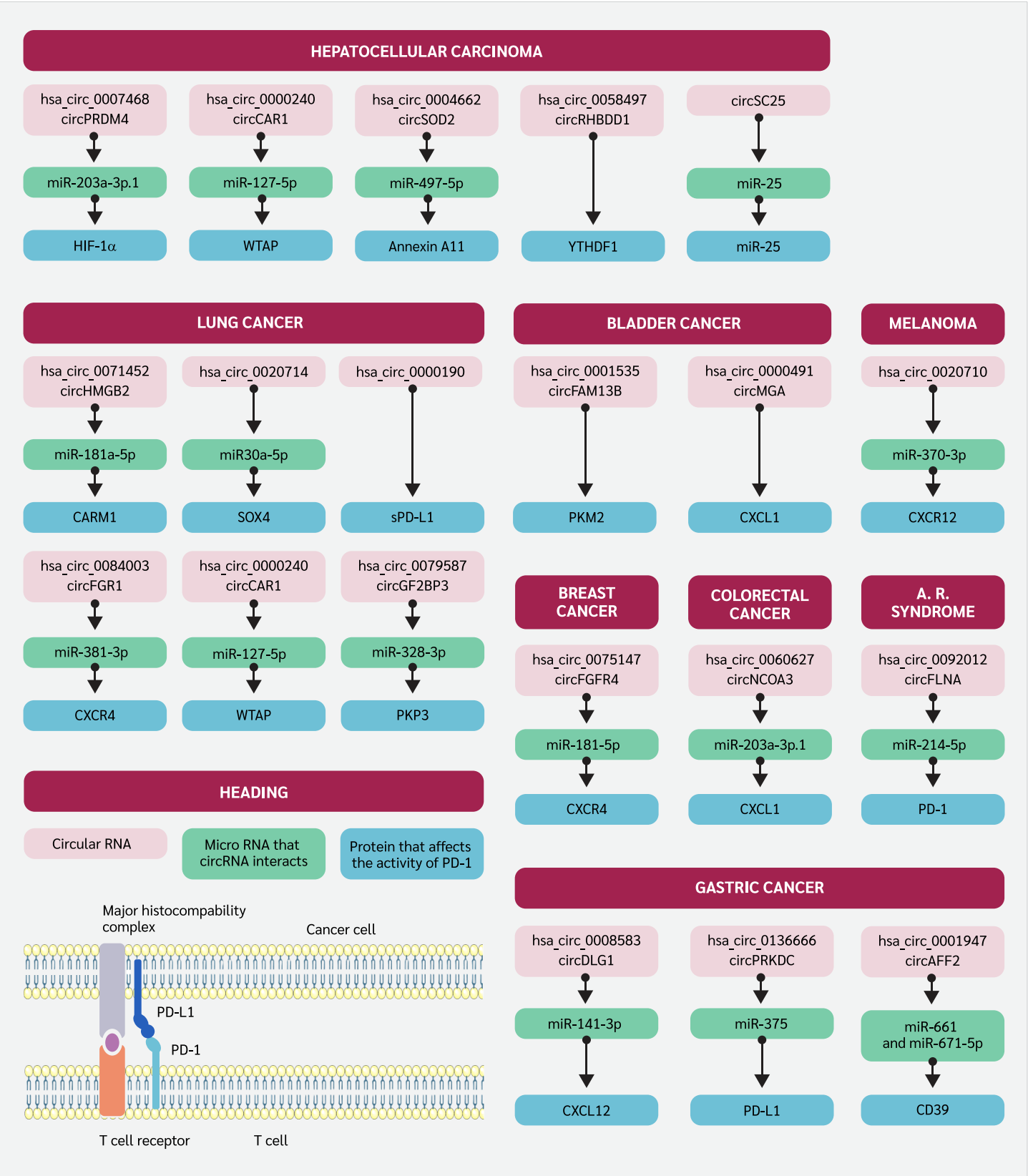


**Figure 1.** Summary of the circRNAs in the axis of PD-1 therapy and its efficacy. The names of the circRNAs were indicated in pink, while miRNAs that interfere with the circRNA function were indicated in green. Blue boxes were designed to indicate the affected protein that eventually interferes with the anti-PD-1 therapeutic efficacy.

**Table 1.** Expression levels of circular RNA molecules for each cancer group and their effects on the therapeutic effectiveness of anti-PD-1 therapy.

Disease type	circRNA	CircBase ID	MicroRNA that circRNA interacts	Targets	Expression level	Effect on PD-1 therapy effectiveness
Colorectal cancer	circNCOA3	hsa_circ_0060627	miR-203a-3p.1	CXCL1	Increased	Decreased
Gastric cancer	circDLG1	hsa_circ_0008583	miR-141-3p	CXCL12	Increased	Decreased
Gastric cancer	circPRKDC	hsa_circ_0136666	miR-375	PD-L1	Increased	Decreased
Gastric cancer	circAFF2	hsa_circ_0001947	miR-661 and miR-671-5p	CD39	Increased	Decreased
Pancreatic cancer	circUBAP2	hsa_circ_0007367	miR-494	CXCR4 and ZEB1	Increased	Decreased
Hepatocellular carcinoma	circPRDM4	hsa_circ_0007468	miR-203a-3p.1	HIF-1 $\alpha$	Increased	Decreased
Hepatocellular carcinoma	circCAR1	hsa_circ_0000240	miR-127-5p	WTAP	Increased	Decreased
Hepatocellular carcinoma	circSOD2	hsa_circ_0004662	miR-497-5p	Annexin A11	Increased	Decreased
Hepatocellular carcinoma	circRHBD1	hsa_circ_0058497	-	YTHDF1	Increased	Decreased
Hepatocellular carcinoma	circSC25	-	miR-25	miR-25	Decreased	Increased
Bladder cancer	circMGA	hsa_circ_0000491	-	CXCL1	Increased	Decreased
Bladder cancer	circFAM13B	hsa_circ_0001535	-	PKM2	Increased	Decreased
Breast cancer	circFGFR4	hsa_circ_0075147	miR-185-5p	CXCR4	Increased	Decreased
Lung cancer	circHSP90A	hsa_circ_0033393	miR-424-5p	HSP90A	Increased	Decreased
Lung cancer	circSOD2	hsa_circ_001678	miR-326	ZEB1	Increased	Decreased
Lung cancer	circHMGB2	hsa_circ_0071452	miR-181a-5p	CARM1	Increased	Decreased
Lung cancer	-	hsa_circ_0020714	miR30a-5p	SOX4	Increased	Decreased
Lung cancer	-	hsa_circ_0000190	-	sPD-L1	Increased	Decreased
Lung cancer	circFGFR1	hsa_circ_0084003	miR-381-3p	CXCR4	Increased	Decreased
Melanoma	-	hsa_circ_0020710	miR-370-3p	CXCL12	Increased	Decreased
Acute respiratory syndrome	circFLNA	hsa_circ_0092012	miR-214-5p	PD-1	Increased	Decreased

fects of this migration can be summarized as diminished cancer cell detection and killing, and insensitivity to anti-PD-1 treatment. Further research revealed that circ\_0001947, encapsulated within small extracellular vesicles (sEVs) derived from GC cells, is markedly upregulated in GC and is associated with unfavorable clinical outcomes. Functionally, elevated circ\_0001947 levels enhance GC cell proliferation, migration, and invasion. Mechanistically, circ\_0001947 functions as a molecular sponge for miR-661 and miR-671-5p, resulting in increased CD39 expression, which in turn promotes CD8<sup>+</sup> T cell exhaustion and contributes to immune evasion. In contrast, inhibition of circ\_0001947 mitigates CD8<sup>+</sup> T cell exhaustion and improves the efficacy of anti-PD-1 therapy (31). Additionally, hsa\_circ\_0136666 has been shown to act by sponging miR-375-3p to competitive-

ly upregulate protein kinase, DNA-activated, catalytic subunit (PRKDC) expression, which regulates immune checkpoint proteins and promotes PD-L1 phosphorylation to prevent its degradation, thereby driving PD-L1 aggregation and suppressing immune function (33).

### **Pancreatic Cancer**

According to a study by Zhao et al. (34) covering pancreatic adenocarcinoma, the researchers specifically examined the involvement of circ-UBAP2 within the circRNA network. Through their analysis, circ-UBAP2 was identified as a key regulator influencing the expression of pivotal genes, including C-X-C motif chemokine receptor 4 (CXCR4) and zinc finger E-box binding homeobox 1 (ZEB1), in tumor tissues. Furthermore, it was observed that circ-UBAP2 interacts with hsa-miR-494 to modulate

the expression levels of these genes. This interaction underlines the potential role of circ-UBAP2 in orchestrating immune modulation within the tumor site, potentially impacting immune cell infiltration and function through increased PD-1 levels.

### Hepatocellular Carcinoma

In hepatocellular carcinoma (HCC), according to a study done by Chen et al. (26), hsa\_circ\_0007468, also known as circPRDM4, was evaluated in hypoxic conditions. It was found that circPRDM4 was associated with increased PD-L1 levels through the HIF-1 $\alpha$  pathway, which is correlated with the positive response to anti-PD-1 therapy with good prognostic markers; however, downstream activation of PD-L1 was reported as diminishing anti-tumor response to the cancerous cells, resulting in immune evasion. In addition, a microarray study comprising HCC patients and their circRNA levels was assessed by Hu et al. (35), and circCCAR1 (hsa\_circ\_0000240) was discovered to be abundant in patients' plasma samples, especially located in exosomal content. CircCCAR1 was associated with the regulation of PD-1 through post-transcriptional events, as high circCCAR1 levels were correlated with the diminished proteolysis of PD-1 and ubiquitination, which all affect the resistance to inhibition of PD-1. By using BALB/c nude mice, Ye et al. (36) established a mice xenograft tumor assay for understanding the role of hsa\_circ\_0004662 or circSOD2 in HCC, as a result of the study it was confirmed that circSOD2 through sponging the miR-497-5p upregulate the oncogene expression such as Annexin A11 (ANXA11) which is also thought to be involved in cancer hallmarks as favoring tumor survival. This pathway and its axis were also found to be correlated with poor response to anti-PD1 therapy. CircRHBDD1 (hsa\_circ\_0058497) in HCC throughout the mechanism that upregulates glycolysis, as its elevated levels were identified to be associated with prolonged HCC progression. The underlying mechanism in the context of glycolysis and circRHBDD1 was considered as YTH domain-containing family protein 1 (YTHDF1), as they recognize post-transcriptional RNA modification m<sup>6</sup>A and upregulate the translational activity of phosphoinositide-3-kinase regulatory subunit 1 (PIK3R1). Also, when considering circRHBDD1 as an indicator of the potency of PD-1 blockade, elevated levels were detected in patients with low response rates to the anti-PD-1 therapy (37). In another study, Lai et al. (38). developed an innovative, multifunctional engineered circRNA for HCC therapy, designed to execute a dual therapeutic function: it acts as a sponge for the oncogenic miR-25 while simultaneously

expressing an anti-PD-1 single-chain variable fragment (scFv). This circRNA-based construct successfully inhibited HCC cell proliferation and suppressed angiogenesis *in vitro* by effectively sequestering miR-25. Furthermore, the expression of the anti-PD-1 scFv significantly bolstered the cytotoxic T-cell response against the cancer cells, indicating enhanced immunotherapeutic action. The combined mechanism proved highly effective *in vivo*, resulting in a significant reduction in tumor volume and prolonged survival in treated mouse models compared to controls, thereby demonstrating a promising strategy for combined gene- and immuno-therapy in HCC

### Bladder Cancer

Via utilizing NOG (NOD/Shi-scid/IL-2R $\gamma^{\text{null}}$ ) mice, which are immunodeficient as they do not have some of the immune cells or even their immune regulatory functions are diminished, the researchers created a humanized (HuNOG) bladder cancer model by injecting human peripheral blood mononuclear cells (PBMCs) and bladder cancer cell line T24. NOG mice are immunodeficient as they do not have some immune cells or their immune regulatory functions are diminished. Researchers created a humanized (HuNOG) bladder cancer model by injecting PBMC and the bladder cancer cell line T24. This model is used to study the interactions between the human immune system and cancer cells. By working with HuNOG, Lv et al. (39) stated that, after two weeks of PD-1 immunotherapy, circFAM13B was found to be as effective in improving therapeutic efficacy in the case of bladder cancer as compared to mice with suppressed circFAM13B expression through reversing the enzymes promoting lactic acid formation (pyruvate kinase muscle isozyme M2 [PKM2]) and eventually increased pH levels can restore effector functions of immune cells in the TME.

Furthermore, hsa\_circ\_0000591 (circMGA) was found to be correlated with an increased level of chemokine ligand 5 (CCL5), which is responsible for the enrollment of CD8<sup>+</sup> cytotoxic T cells to the TME through the mechanism of CCL5 mRNA stabilization with the help of heterogeneous nuclear ribonucleoprotein L (HNRNPL) and these results reflected the capability of this mechanism to induce efficient anti-PD-1 therapy (40).

### Breast Cancer

With the research done by Wang et al. (41) in triple-negative breast cancer (TNBC) lesions, it was found that the severity of the disease course was correlated with the



elevated levels of circFGFR4 (hsa\_circ\_0075147). The research findings demonstrated that circFGFR4 promotes immune escape in TNBC and is a predictive biomarker for anti-PD-1 immunotherapy responsiveness.

Mechanistically, circFGFR4, when overexpressed, competitively sequesters miR-185-5p (acts like a sponge), preventing the suppression of CXCR4 expression and thereby hindering CD8<sup>+</sup> cytotoxic T cell infiltration into TNBC lesions in both human and mice. Moreover, circFGFR4 emerges as a potential therapeutic target in TNBC patients, particularly those undergoing anti-PD-1 immunotherapy.

### Lung Cancer

The dual effect of circHSP90A (hsa\_circ\_0033393) was shown as an activator of the signal transducer and activator of transcription 3 (STAT3) pathway and elevated levels of PD-L1 in non-small cell lung cancer (NSCLC). Circ\_HSP90A recruits and increases the levels of ubiquitin-specific peptidase 30 (USP30), which is responsible for the downstream activation of heat shock protein 90 A (HSP90A) via ubiquitination and eventually STAT3 activation that is thought to be related to the upregulation in cancer stem cell formation, invasion, and migratory ability. On the other hand, throughout the miR-424-5p sponge effect, circ\_HSP90A increases the level of PD-L1 expression, which ultimately causes programmed cell death of CD8<sup>+</sup> cytotoxic T cells, characterized by diminished anti-tumor response (42). Another study, revealing the circRNA and NSCLC axis, was done by Tian et al. (43), who stated that circ\_001678, which captures miR-326, leads to diminished miR-326 levels. This study has governed the rise in the levels of PD-L1 throughout the ZEB1 protein, causing lung cancer cell proliferation and depletion in apoptosis or cytotoxicity maintained by CD8<sup>+</sup> T cells via PD-L1 overexpression. In NSCLC, circHMGB2 (hsa\_circ\_0071452) showed increased expression in lung tumor tissues, correlating with poor prognosis in both adenocarcinoma and squamous cell carcinoma patients, which are the common subtypes of NSCLC. While its impact on cell proliferation was moderate, circHMGB2 notably influenced the TME by inducing antitumor immune cell exhaustion, which ultimately downregulates the effectiveness of monoclonal antibody therapy targeting PD-1. circHMGB2 facilitated the downregulation of the type 1 interferon response by sponging miR-181a-5p, thereby enhancing coactivator-arginine methyltransferase 1 (CARM1) activity (44). As remarked by a study done by Wu et al. (45), a high level of hsa\_circ\_0020714

expression was defined in NSCLC tumors as compared to surrounding healthy tissue. By sponging miR-30a-5p, this context results in an increased expression of transcription factor ex-determining region Y-box 4 (SOX4), which is classified as an oncogene and eventually causes impairment in response to anti-PD-1 therapy. Hsa\_circ\_0000190, another type of circular RNA, has been identified as a potential biomarker for monitoring the progression of NSCLC and assessing the effectiveness of immunotherapy. Research conducted by Luo et al. (46) suggested that elevated levels of hsa\_circ\_0000190 may contribute to poor prognosis in NSCLC patients by regulating the expression of soluble PD-L1 (sPD-L1), which has a negative influence on anti-PD-L1 antibody therapeutic efficiency and cytotoxic T-cell activation. This study implies a role for hsa\_circ\_0000190 in promoting tumorigenesis and immune evasion in NSCLC, which suggests an antagonistic approach to defined circRNAs' levels could potentially enhance the effectiveness of immunotherapy in treating NSCLC. In addition, Zhang et al. (47) delved into the upregulated expression of circFGFR1 within NSCLC tissues, correlating with an adverse clinical profile and poor prognosis in NSCLC patients. Insights from this research underline circFGFR1's role as directly sponging miR-381-3p and downregulating its downstream target, CXCR4. This intricate regulatory network orchestrated by circFGFR1 confers NSCLC progression and resistance to anti-PD-1 immunotherapy. Lastly, in NSCLC, increased expression of circIGF2BP3 was found to be associated with reduced CD8<sup>+</sup> T cell infiltration and compromised anti-tumor immunity in mice, mediated by plakophilin 3 (PKP3) and PD-L1. Via revealing the pathways correlated with the circIGF2BP3, N6-adenosine-methyltransferase 70 kDa subunit (METTL3) facilitates the modification of circIGF2BP3, which competitively upregulates PKP3 by sponging miR-328-3p and miR-3173-5p. Another finding that researchers postulated implies that inhibition of circIGF2BP3/PKP3 enhances the effectiveness of anti-PD-1 therapy in NSCLC mouse models, which is thought to be a possible therapeutic strategy (48).

### Metastatic Melanoma

By using the bioinformatics analysis of RNA sequence data taken from different databases, metastatic melanoma (MM) patients who are on the course of anti-PD-1 treatment alone were analyzed to elucidate circRNAs that hold the potential to emphasize prognostic markers related to the monotherapy of PD-1 blockade. Among more than 74,000 distinct circRNAs, five of them were

statistically shown to be related to response or survival rates in MM patients throughout the treatment regime, either pembrolizumab or nivolumab, as PD-1 blockers (49). RNA sequencing of cutaneous melanoma patients' formalin-fixed and paraffin-embedded samples with a history of metastasis was done to define possible circRNA candidates that are potential markers of therapeutic efficacy among the patient cohort taking nivolumab as chemotherapy, which is an anti-PD-1 monoclonal antibody. Together with the other circRNA candidates, it was shown that the hsa\_CDR1\_0001 significantly increased, and it is thought to be associated with response to nivolumab chemotherapy according to statistical analysis, which needs further validation with *in vitro* or *in vivo* studies (50). Researchers discovered that circ\_0020710, found in higher levels in melanoma samples, correlates with more aggressive cancer behavior and poorer patient prognosis. Formation of this circRNA causes upregulation in CXCL12 expression through miR-370-3p sponging, which ultimately leads to activation of biochemical pathways that are essential for tumor progression and even calls out MDSCs, which promotes an unfavorable environment for efficient response to cancer cells by cytotoxic T cells. Researchers also postulated that combining AMD3100 and anti-PD-1 therapies effectively slows tumor growth, offering a potential treatment approach for melanoma (51).

### Other Pathologies

As stated by Zhong et al. (26), elevated levels of circFLNA (or hsa\_circ\_0092012) were found to be associated with the severity of acute respiratory distress syndrome (ARDS) induced by sepsis as examined via bronchoalveolar lavage of the patients and mice, and also with the lung tissue of mice. Inhibition of circFLNA led to a notable increase in CD4<sup>+</sup>CD25<sup>+</sup>FoxP3<sup>+</sup> Tregs and suppressed the release of inflammatory cytokines in ARDS mice. miR-214-5p, which circFLNA behaves like a sponge to it, played a crucial role in modulating these effects by targeting PD-1, suggesting its potential as a therapeutic target for ARDS. These findings highlight the intricate regulatory network involving circFLNA, miR-214-5p, and PD-1 in the pathogenesis and treatment of ARDS. In a study comparing PD-1 antagonist-treated A/PR8(H1N1) influenza A-infected mice lungs to control groups, differential expression analysis revealed significant changes in various types of non-coding RNA molecules. Specifically, 22 differentially expressed circRNAs were identified in the lungs, while in the spleens of mice, 24 circRNAs showed differential expression. However, it was not

shown which circRNA is responsible for impairment in antiviral immunity or the essential pathways regulating viral infection-associated comorbidities; overall results can express their possible role in PD-1 checkpoint blockade treatment (52).

## Conclusion

In summary, circRNAs have emerged as a research interest within cancer immunotherapy research, exhibiting considerable potential and clinical relevance, particularly in the context of PD-1 blockade therapy across diverse cancer types. Our literature review of circRNA biogenesis and functionalities has given novel insights into their molecular mechanisms in the context of PD-1 blockade in cancer. CircRNAs exhibit a widened array of functions, serving as miRNA and protein sponges, translational modulators, and gene expression regulators, collectively modulating the efficacy of PD-1 blockade therapy. Nevertheless, despite notable advancements, the exploration of the circRNA-PD-1 blockade axis remains limited and needs further research to apply circRNA-based interventions to clinical practice effectively. Here are some points that need to be addressed: firstly, while studies have postulated individual pathways, a better understanding of multiple pathways' modulating circRNA's downstream effects and their synergistic effects is needed to ease our understanding of the circRNA network's molecular interactions. Secondly, particular attention should be given to exosomal circRNAs, as they have distinct biological functions, which hold promise in increasing the efficacy of PD-1 blockade therapy. Thirdly, while most of the techniques primarily rely on *in vitro* cellular assays, blood-based assays, and animal models, extensive clinical investigations and multicenter trials are necessary to advance our understanding of circRNAs in clinical settings. Utilizing new technologies is also important in elucidating the physiological importance of circRNAs, so that it will be possible to integrate them into diagnostic and therapeutic approaches related to PD-1 blockade therapy across different cancer types. Efforts given by researchers will give rise to new therapeutic approaches in cancer immunotherapy, such as involving circRNA in their experimental setup, which may even lead to a new era in cancer treatment. Further studies are needed to determine the therapeutic potential of circRNAs in specific cancer types.

**Ethical Approval:** N.A.

**Informed Consent:** N.A.

**Peer-review:** Externally peer-reviewed

**Author Contributions:** Concept – D.K., F.A., S.K.T.; Design – D.K., F.A.; Supervision – D.K., F.A., S.K.T.; Data Collection and/or Process-

ing – D.K., F.A.; Analysis and/or Interpretation – D.K., F.A.; Literature Review – D.K., F.A.; Writer – D.K.; Critical Reviews – D.K., F.A., S.K.T.

**Conflict of Interest:** The authors declare no conflict of interest.


**Financial Disclosure:** The authors declared that this study has received no financial support.

## References

- 1 Esfahani K, Roudaia L, Buhlaiga N, Del Rincon SV, Papneja N, Miller WH Jr. A review of cancer immunotherapy: from the past, to the present, to the future. *Curr Oncol.* 2020;27(Suppl 2):S87-S97. [\[CrossRef\]](#)
- 2 Wu X, Meng Y, Liu L, Gong G, Zhang H, Hou Y, et al. Insights into non-peptide small-molecule inhibitors of the PD-1/PD-L1 interaction: Development and perspective. *Bioorg Med Chem.* 2021;33:116038. [\[CrossRef\]](#)
- 3 Lee JB, Ha SJ, Kim HR. Clinical insights into novel immune checkpoint inhibitors. *Front Pharmacol.* 2021;12:681320. [\[CrossRef\]](#)
- 4 Lin X, Lu X, Luo G, Xiang H. Progress in PD-1/PD-L1 pathway inhibitors: From biomacromolecules to small molecules. *Eur J Med Chem.* 2020;186:111876. [\[CrossRef\]](#)
- 5 Alturki NA. Review of the immune checkpoint inhibitors in the context of cancer treatment. *J Clin Med.* 2023;12(13):4301. [\[CrossRef\]](#)
- 6 Li Y, Yang L, Liu Z. Combination of immune checkpoint inhibitors and anti-angiogenic agents: An emerging strategy for cancer therapy. *Crit Rev Oncol Hematol.* 2025;215:104883. [\[CrossRef\]](#)
- 7 Nielsen DL, Juhl CB, Chen IM, Wang Y, Nielsen OH, Santomaso BD. Immune checkpoint inhibitor-related neurotoxicity: Incidence and management. A systematic review and meta-analysis. *Cancer Treat Rev.* 2025;140:103011. [\[CrossRef\]](#)
- 8 Kong X, Ou S, Wei Z, Ye X, Chen S, Shi X, et al. Transforming the "cold" tumors to "hot" tumors: strategies for immune activation. *Biochem Pharmacol.* 2025;241:117194. [\[CrossRef\]](#)
- 9 Darvin P, Toor SM, Sasidharan Nair V, Elkord E. Immune checkpoint inhibitors: recent progress and potential biomarkers. *Exp Mol Med.* 2018;50(12):1-11. [\[CrossRef\]](#)
- 10 Zak KM, Grudnik P, Magiera K, Dömling A, Dubin G, Holak TA. Structural biology of the immune checkpoint receptor PD-1 and its ligands PD-L1/PD-L2. *Structure.* 2017;25(8):1163-74. [\[CrossRef\]](#)
- 11 Ai L, Xu A, Xu J. Roles of PD-1/PD-L1 pathway: signaling, cancer, and beyond. *Adv Exp Med Biol.* 2020;1248:33-59. [\[CrossRef\]](#)
- 12 Han Y, Liu D, Li L. PD-1/PD-L1 pathway: current researches in cancer. *Am J Cancer Res.* 2020;10(3):727-42.
- 13 Sanger F, Nicklen S, Coulson AR. DNA sequencing with chain-terminating inhibitors. *Proc Natl Acad Sci U S A.* 1977;74(12):5463-7. [\[CrossRef\]](#)
- 14 Liu J, Zhao F, Chen LL, Su S. Dysregulation of circular RNAs in inflammation and cancers. *Fundam Res.* 2023;3(5):683-91. [\[CrossRef\]](#)
- 15 Liu Q, Li S. Exosomal circRNAs: Novel biomarkers and therapeutic targets for urinary tumors. *Cancer Lett.* 2024;588:216759. [\[CrossRef\]](#)
- 16 Saleem A, Khan MU, Zahid T, Khurram I, Ghani MU, Ullah I, et al. Biological role and regulation of circular RNA as an emerging biomarker and potential therapeutic target for cancer. *Mol Biol Rep.* 2024;51(1):296. [\[CrossRef\]](#)
- 17 Sun X, Zhao X, Xu Y, Yan Y, Han L, Wei M, et al. Potential therapeutic strategy for cancer: Multi-dimensional cross-talk between circRNAs and parental genes. *Cancer Lett.* 2024;588:216794. [\[CrossRef\]](#)
- 18 Ashrafizadeh M, Dai J, Torabian P, Nabavi N, Aref AR, Aljabali AAA, et al. Circular RNAs in EMT-driven metastasis regulation: modulation of cancer cell plasticity, tumorigenesis and therapy resistance. *Cell Mol Life Sci.* 2024;81(1):214. [\[CrossRef\]](#)
- 19 Guan L, Hao Q, Shi F, Gao B, Wang M, Zhou X, et al. Regulation of the tumor immune microenvironment by cancer-derived circular RNAs. *Cell Death Dis.* 2023;14(2):132. [\[CrossRef\]](#)
- 20 Chen DL, Chen N, Sheng H, Zhang DS. Circular RNA circNCOA3 promotes tumor progression and anti-PD-1 resistance in colorectal cancer. *Cancer Drug Resist.* 2024;7:9. [\[CrossRef\]](#)
- 21 Chen DL, Sheng H, Zhang DS, Jin Y, Zhao BT, Chen N, et al. The circular RNA circDLG1 promotes gastric cancer progression and anti-PD-1 resistance through the regulation of CXCL12 by sponging miR-141-3p. *Mol Cancer.* 2021;20(1):166. [\[CrossRef\]](#)
- 22 Panda AC. Circular RNAs act as miRNA sponges. *Adv Exp Med Biol.* 2018;1087:67-79. [\[CrossRef\]](#)
- 23 Duan S, Wang S, Huang T, Wang J, Yuan X. circRNAs: Insight into their role in tumor-associated macrophages. *Front Oncol.* 2021;11:780744. [\[CrossRef\]](#)
- 24 Lv C, Chen J, Wang Y, Lin Y. Immunoregulatory role of exosomal circRNAs in the tumor microenvironment. *Front Oncol.* 2025;15:1453786. [\[CrossRef\]](#)
- 25 Yu S, Su S, Wang P, Li J, Chen C, Xin H, et al. Tumor-associated macrophage-induced circMRCK $\alpha$  encodes a peptide to promote glycolysis and progression in hepatocellular carcinoma. *Cancer Lett.* 2024;591:216872. [\[CrossRef\]](#)
- 26 Chen ZQ, Zuo XL, Cai J, Zhang Y, Han GY, Zhang L, et al. Hypoxia-associated circPRDM4 promotes immune escape via HIF-1 $\alpha$

- regulation of PD-L1 in hepatocellular carcinoma. *Exp Hematol Oncol.* 2023;12(1):17. [\[CrossRef\]](#)
- 27 Wang L, Liang Y, Zhao C, Ma P, Zeng S, Ju D, et al. Regulatory T cells in homeostasis and disease: molecular mechanisms and therapeutic potential. *Signal Transduct Target Ther.* 2025;10(1):345. [\[CrossRef\]](#)
  - 28 Zhong J, Zhang W, Zhang L, Li J, Kang L, Li X. CircFLNA/miR-214 modulates regulatory T cells by regulating PD-1 in acute lung injury induced by sepsis. *Autoimmunity.* 2023;56(1):2259131. [\[CrossRef\]](#)
  - 29 Liu X, Zhang Y, Zhou S, Dain L, Mei L, Zhu G. Circular RNA: An emerging frontier in RNA therapeutic targets, RNA therapeutics, and mRNA vaccines. *J Control Release.* 2022;348:84-94. [\[Cross-Ref\]](#)
  - 30 Xu T, Wang M, Jiang L, Ma L, Wan L, Chen Q, et al. CircRNAs in anticancer drug resistance: recent advances and future potential. *Mol Cancer.* 2020;19(1):127. [\[CrossRef\]](#)
  - 31 He AT, Liu J, Li F, Yang BB. Targeting circular RNAs as a therapeutic approach: current strategies and challenges. *Signal Transduct Target Ther.* 2021;6(1):185. [\[CrossRef\]](#)
  - 32 Wang B, Liu W, Zhang M, Li Y, Tang H, Wang Y, et al. Circ\_0001947 encapsulated by small extracellular vesicles promotes gastric cancer progression and anti-PD-1 resistance by modulating CD8<sup>+</sup> T cell exhaustion. *J Nanobiotechnology.* 2024;22(1):563. [\[CrossRef\]](#)
  - 33 Miao Z, Li J, Wang Y, Shi M, Gu X, Zhang X, et al. Hsa\_circ\_0136666 stimulates gastric cancer progression and tumor immune escape by regulating the miR-375/PRKDC Axis and PD-L1 phosphorylation. *Mol Cancer.* 2023;22(1):205. [\[CrossRef\]](#)
  - 34 Zhao R, Ni J, Lu S, Jiang S, You L, Liu H, et al. CircUBAP2-mediated competing endogenous RNA network modulates tumorigenesis in pancreatic adenocarcinoma. *Aging (Albany NY).* 2019;11(19):8484-501. [\[CrossRef\]](#)
  - 35 Hu Z, Chen G, Zhao Y, Gao H, Li L, Yin Y, et al. Exosome-derived circCCAR1 promotes CD8<sup>+</sup> T-cell dysfunction and anti-PD1 resistance in hepatocellular carcinoma. *Mol Cancer.* 2023;22(1):55. [\[CrossRef\]](#)
  - 36 Ye R, Lu X, Liu J, Duan Q, Xiao J, Duan X, et al. CircSOD2 contributes to tumor progression, immune evasion and anti-PD-1 resistance in hepatocellular carcinoma by targeting miR-497-5p/ANXA11 axis. *Biochem Genet.* 2023;61(2):597-614. [\[CrossRef\]](#)
  - 37 Cai J, Chen Z, Zhang Y, Wang J, Zhang Z, Wu J, et al. CircRHBDD1 augments metabolic rewiring and restricts immunotherapy efficacy via m<sup>6</sup>A modification in hepatocellular carcinoma. *Mol Ther Oncolytics.* 2022;24:755-71. [\[CrossRef\]](#)
  - 38 Lai Y, Wang F, Cai G, Li Y, Weng J, Cai F, et al. Utilization of artificial circular RNAs as miRNA sponges and anti-PD-1 scFv expression platforms to suppress hepatocellular carcinoma progression. *Front Immunol.* 2025;16:1609165. [\[CrossRef\]](#)
  - 39 Lv J, Li K, Yu H, Han J, Zhuang J, Yu R, et al. HNRNPL induced circFAM13B increased bladder cancer immunotherapy sensitivity via inhibiting glycolysis through IGF2BP1/PKM2 pathway. *J Exp Clin Cancer Res.* 2023;42(1):41. [\[CrossRef\]](#)
  - 40 Sun J, Zhang H, Wei W, Xiao X, Huang C, Wang L, et al. Regulation of CD8<sup>+</sup> T cells infiltration and immunotherapy by circMGA/HN-RNPL complex in bladder cancer. *Oncogene.* 2023;42(15):1247-62. [\[CrossRef\]](#)
  - 41 Wang F, Lu Q, Yu H, Zhang XM. The Circular RNA circFGFR4 facilitates resistance to anti-PD-1 of triple-negative breast cancer by targeting the miR-185-5p/CXCR4 axis. *Cancer Manag Res.* 2023;15:825-35. [\[CrossRef\]](#)
  - 42 Lei J, Zhu J, Hui B, Jia C, Yan X, Jiang T, et al. Circ-HSP90A expedites cell growth, stemness, and immune evasion in non-small cell lung cancer by regulating STAT3 signaling and PD-1/PD-L1 checkpoint. *Cancer Immunol Immunother.* 2023;72(1):101-24. [\[CrossRef\]](#)
  - 43 Tian Q, Wu T, Zhang X, Xu K, Yin X, Wang X, et al. Immunomodulatory functions of the circ\_001678/miRNA-326/ZEB1 axis in non-small cell lung cancer via the regulation of PD-1/PD-L1 pathway. *Hum Mol Genet.* 2022;31(23):4094-106. [\[CrossRef\]](#)
  - 44 Zhang LX, Gao J, Long X, Zhang PF, Yang X, Zhu SQ, et al. The circular RNA circHMGB2 drives immunosuppression and anti-PD-1 resistance in lung adenocarcinomas and squamous cell carcinomas via the miR-181a-5p/CARM1 axis. *Mol Cancer.* 2022;21(1):110. [\[CrossRef\]](#)
  - 45 Wu J, Zhu MX, Li KS, Peng L, Zhang PF. Circular RNA drives resistance to anti-PD-1 immunotherapy by regulating the miR-30a-5p/SOX4 axis in non-small cell lung cancer. *Cancer Drug Resist.* 2022;5(2):261-70. [\[CrossRef\]](#)
  - 46 Luo YH, Yang YP, Chien CS, Yarmishyn AA, Adekunle Ishola A, Chien Y, et al. Circular RNA hsa\_circ\_0000190 facilitates the tumorigenesis and immune evasion by upregulating the expression of soluble PD-L1 in non-small-cell lung cancer. *Int J Mol Sci.* 2021;23(1):64. [\[CrossRef\]](#)
  - 47 Zhang PF, Pei X, Li KS, Jin LN, Wang F, Wu J, et al. Circular RNA circFGFR1 promotes progression and anti-PD-1 resistance by sponging miR-381-3p in non-small cell lung cancer cells. *Mol Cancer.* 2019;18(1):179. Erratum in: *Mol Cancer.* 2020;19(1):21. [\[CrossRef\]](#)
  - 48 Liu Z, Wang T, She Y, Wu K, Gu S, Li L, et al. N<sup>6</sup>-methyladenosine-modified circIGF2BP3 inhibits CD8<sup>+</sup> T-cell responses to facilitate tumor immune evasion by promoting the deubiquitination of PD-L1 in non-small cell lung cancer. *Mol Cancer.* 2021;20(1):105. [\[CrossRef\]](#)
  - 49 Oliver J, Onieva JL, Garrido-Barros M, Berciano-Guerrero MÁ, Sánchez-Muñoz A, José Lozano M, et al. Association of circular RNA and long non-coding RNA dysregulation with the clinical response to immune checkpoint blockade in cutaneous metastatic melanoma. *Biomedicines.* 2022;10(10):2419. [\[CrossRef\]](#)
  - 50 Zhou JG, Liang R, Wang HT, Jin SH, Hu W, Frey B, et al. Identification and characterization of circular RNAs as novel putative biomarkers to predict anti-PD-1 monotherapy response in metastatic melanoma patients - Knowledge from two independent international studies. *Neoplasia.* 2023;37:100877. [\[CrossRef\]](#)
  - 51 Wei CY, Zhu MX, Lu NH, Liu JQ, Yang YW, Zhang Y, et al. Circular RNA circ\_0020710 drives tumor progression and immune evasion by regulating the miR-370-3p/CXCL12 axis in melanoma. *Mol Cancer.* 2020;19(1):84. [\[CrossRef\]](#)
  - 52 Ou H, Chen K, Chen L, Wu H. Bioinformatic analysis of PD-1 checkpoint blockade response in influenza infection. *BMC Genom Data.* 2022;23(1):65. [\[CrossRef\]](#)

# Understanding Allosteric Stabilization of pMHC by Peptide Ligands Through Molecular Dynamics Simulations

Onur Serçinoğlu<sup>1</sup> 

<sup>1</sup> Gebze Technical University School of Engineering, Department of Bioengineering, Kocaeli, Türkiye

## Abstract

**Objective:** The dynamic interaction between peptide ligands and major histocompatibility complex (MHC) molecules plays a critical role in regulating cytotoxic T-cell response. While peptide-free MHC molecules are known to be highly unstable, the precise mechanisms underlying peptide-induced stabilization remain poorly understood.

**Materials and Methods:** Classical molecular dynamics simulations of human leukocyte antigen (HLA)-A\*02:01 in both peptide-free and peptide-bound states were performed. Each simulation was conducted in triplicate to ensure reproducibility. Protein energy networks were constructed using pairwise amino acid interaction energies computed from resulting trajectories. Network analysis was performed to reveal the roles of residues in protein stability.

**Results:** The analysis revealed that peptides with weak interactions at the F pocket failed to enhance connectivity at the HLA-β2m interface, thereby compromising the overall structural stability of peptide-loaded MHC (pMHC).

**Conclusion:** These findings shed light on the mechanisms by which peptides stabilize MHC molecules and modulate their dynamics, providing insights into T-cell receptor recognition and the regulation of immune responses.

**Keywords:** Major histocompatibility complex, protein stability, protein dynamics, immunogenicity, antigen presentation, molecular dynamics, structural bioinformatics, protein energy networks

## Introduction

The adaptive immune response is a critical component of the immune system, providing highly specific and long-lasting protection against pathogens. Cytotoxic T lymphocytes play a crucial role in this response by eliminating infected or cancerous cells (1,2). Cytotoxic T lymphocytes recognize and kill target cells through the interaction of their T cell receptors (TCRs) with peptide-loaded major histo-

### Correspondence

Onur Serçinoğlu

### E-mail

osercinoglu@gtu.edu.tr

### Received

February 25, 2025

### Accepted

July 18, 2025

### Published

December 4, 2025

### Suggested Citation

Serçinoğlu O. Understanding allosteric stabilization of pMHC by peptide ligands through molecular dynamics simulations. Turk J Immunol. 2025;13(3):132-45.

### DOI

10.36519/TJI.2025.576



This work is licensed under the Creative Commons Attribution-NonCommercial-Non-Derivatives 4.0 International License (CC BY-NC-ND 4.0).



compatibility complex (pMHC) molecules presented on the surface of antigen-presenting cells (APCs) (3). This interaction is highly specific, with the TCR recognizing both the peptide antigen and the MHC molecule, a phenomenon known as MHC restriction (4,5).

There are two classes of MHC molecules: MHC class I (MHC-I), which presents endogenously derived peptides to CD8<sup>+</sup> T cells, and MHC class II (MHC-II), which presents exogenously derived peptides to CD4<sup>+</sup> T cells (6). MHC-I molecules consist of a heavy chain, a light chain ( $\beta$ 2-microglobulin,  $\beta$ 2m), and a bound peptide. The heavy chain comprises three domains ( $\alpha$ 1,  $\alpha$ 2, and  $\alpha$ 3), with the  $\alpha$ 1 and  $\alpha$ 2 domains forming the peptide-binding groove. The peptide is anchored within this groove, while  $\beta$ 2m interacts with the binding groove and  $\alpha$ 3 domain of the heavy chain, stabilizing the overall structure (7,8).

Protein dynamics play a critical role in the interaction between TCRs and pMHC complexes (9). Both MHC and TCR molecules exhibit inherent flexibility, which is essential for their function (10,11). The dynamics of MHC-I molecules thus influence peptide binding, presentation, and T cell recognition. Once bound, the peptide ligand itself can also modulate the dynamics of pMHC, affecting its flexibility (12), with significant implications for TCR recognition and subsequent T cell activation (13).

The stability of pMHC complexes is also essential for efficient TCR recognition. Peptide ligands were shown to stabilize pMHC by interacting with specific pockets (A, B, C, D, E, and F) within the peptide-binding groove (14). Different peptides modulate the dynamics and flexibility of pMHC complexes in distinct ways, thereby altering the protein's energy landscape and influencing overall stability. Notably, pMHC stability has been positively correlated with its flexibility (15).

Furthermore,  $\beta$ 2m binding and dissociation have been used as accurate measures of pMHC stability, highlighting the importance of the human leukocyte antigen (HLA)- $\beta$ 2m interface (16,17). These findings suggest that peptides can allosterically affect the HLA- $\beta$ 2m interface, thereby influencing the stability of the pMHC complex. However, the exact mechanisms underlying this allosteric effect remain largely unknown.

Molecular dynamics (MD) simulations provide detailed insights into the conformational changes and interactions that govern pMHC stability and flexibility (18-22). Given

the potential of MD simulations to unravel the allosteric mechanisms by which peptides stabilize pMHC complexes, this study aimed to investigate these mechanisms using MD simulations and shed light on the complex interplay between peptide binding, pMHC dynamics, and TCR recognition.

## Materials and Methods

### Molecular Dynamics Simulations of Peptide-HLA\*02:01 Complexes

Explicit-solvent MD simulations were performed using GROMACS version 2023.4 (GROMACS Development Team, Stockholm, Sweden) (23). Hydrogen mass repartitioning was employed to enable a 4 fs integration time step (24). Each system was simulated three times, with each simulation covering a total time of 750 ns. The AMBER99SB-ILDN force field (25) was used in combination with the TIP3P water model (Jorgensen Laboratory, Yale University, New Haven, CT, USA).

Systems were neutralized with sodium/chloride ions to a final ionic strength of 0.15 M. Simulations were run in the isothermal-isobaric (NPT) ensemble with the pressure maintained at 1 bar and the temperature at 310 K. A non-bonded interaction cutoff of 12 Å was applied for van der Waals interactions. A conformation was saved every 5000 steps.

Initial protein structures were obtained from Protein Data Bank (PDB; Research Collaboratory for Structural Bioinformatics, Piscataway, NJ, USA) (26) with accession codes of 3UTQ, 5N1Y, and 5C0F (24). The peptide-free system was obtained by simply removing the peptide ligand from the MHC structure deposited in 3UTQ.

### Root Mean Square Deviation and Root Mean Square Fluctuation Analysis

Root mean square deviation (RMSD) was calculated for each simulation to assess the deviation of the molecular structure from its initial conformation over time. The calculation was based on alpha carbon coordinates, with the first frame of the trajectory as the reference. The equation used for RMSD calculation was as follows:

$$RMSD = \sqrt{\frac{1}{N} \sum_{i=1}^N (x_i - x_i^{ref})^2}$$

where  $N$  is the number of atoms,  $x_i$  is the position of atom  $i$  in the current frame, and  $x_i^{\text{ref}}$  is the position of atom  $i$  in the reference frame.

Root mean square fluctuation (RMSF) was computed to quantify the atomic flexibility around their average positions during the simulation. Root mean square fluctuation for each atom was calculated using the following equation:

$$RMSF_i = \sqrt{\frac{1}{T} \sum_{t=1}^T (x_{it} - \bar{x}_i)^2}$$

where  $T$  is the total number of frames,  $x_{it}$  is the position of atom  $i$  at time  $t$ , and  $\bar{x}_i$  is the average position of atom  $i$  over the entire simulation. Root mean square fluctuation was computed using only the final 500 ns of each trajectory.

### Essential Dynamics Analysis

Essential dynamics analysis (EDA), also known as principal component analysis (PCA), was performed to identify cooperative global motions of amino acids. First, a covariance matrix ( $C$ ) of alpha carbon coordinates was computed:

$$C = \langle (X - \langle X \rangle)(X - \langle X \rangle)^T \rangle$$

where  $X$  is the coordinates of all alpha carbon atoms, with a dimension of  $3N$  by  $3N$ .  $\langle X \rangle$  denotes the average position matrix over the equilibrium portion included in the RMSF analysis as well. This matrix is then diagonalized to identify its eigenvalues and eigenvectors:

$$\lambda = T^T C T$$

Here,  $\lambda$  is a diagonal matrix consisting of eigenvalues, and  $T$  denotes eigenvectors. The eigenvectors are principal components (or individual modes of motion) that describe the essential dynamics of the protein complex.

From each mode of motion, individual fluctuations of alpha carbons can thus be obtained. Using these fluctuations, elements of dynamic cross-correlation matrices (DCCMs) can be constructed using the following equation:

$$C_{ij} = \frac{\langle \Delta r_i \Delta r_j \rangle}{\langle \Delta r_i^2 \rangle^{1/2} \langle \Delta r_j^2 \rangle^{1/2}}$$

Here,  $C_{ij}$  is the cross-correlation value between residues  $i$  and  $j$ ,  $\Delta r_i$  and  $\Delta r_j$  represent the positional fluctuations of alpha carbons in the respective modes of motion. The values of  $C_{ij}$  range from -1 to 1, denoting the maximum levels of anti-correlation and correlation, respectively. To simplify the analysis and focus on the top global modes of motion that describe the majority of variance in motion,  $C$  matrices were computed for only the top 20 global modes of motion. A weighted average of these matrices was then computed using eigenvalues as weights to yield a single DCCM for each simulation trajectory.

Root mean square inner products (RMSIPs), also termed subspace overlaps, of two simulation trajectories were also computed to quantify the levels of (dis)similarities between them, using the following equation:

$$RMSIP = \sqrt{\frac{1}{20} \sum_{i=1}^{20} \sum_{j=1}^{20} (\eta_i \cdot \vartheta_j)^2}$$

Here,  $\eta_i$  and  $\vartheta_j$  are eigenvectors associated with modes  $i$  and  $j$ , respectively.

### Calculation of Pairwise Residue Interaction Energies

Non-bonded interaction energies between contacting amino acid pairs throughout the simulation trajectories were computed using a modified version of gRINN (get Residue Interaction eNergies and Networks) (28). First, a cutoff distance of 10 Å was used to identify pairs of amino acids to be included in the calculation, based on positions of their alpha carbons. Then, the “rerun” feature of gmx mdrun was used to compute non-bonded van der Waals and electrostatic interaction energies between these identified amino acid pairs. Energies were initially reported in kJ/mol by GROMACS and subsequently converted to kcal/mol before further analysis.

### Construction of Protein Energy Networks

Once interaction energies were computed, a protein energy network (PEN) was constructed by taking each amino acid as a node, each interaction as an edge, and van der Waals interaction energies as an edge weight. Edges were added between two residues if they were covalently-bound or interacted with each other in the respective conformation with a van der Waals interaction energy of at least 1 kcal/mol in magnitude (either  $\leq -1$  kcal/mol or  $\geq 1$  kcal/mol). Edge weights were given a value of 1 if the

two interacting pairs are covalently bound, and a value of  $X_{ij}$  if otherwise.  $X_{ij}$  was computed as follows:

$$x_{ij} = \begin{cases} \frac{|\varepsilon_{ij}|}{\max(\varepsilon_{att})}, & \text{if } \varepsilon_{if} < 0 \\ 0, & \text{otherwise} \end{cases}$$

Here,  $X_{ij}$  is the edge weight,  $\varepsilon_{ij}$  is the non-bonded van der Waals interaction energy, and  $\varepsilon_{att}$  is the array of negative interaction energies. Using this formula enables the assignment of higher weights to more negative (or more attractive) interactions. A PEN was constructed for each conformation in the simulation trajectory. Once a PEN was constructed, betweenness-centralities (BCs) of each node were computed using Brandes' algorithm (29), based on shortest paths identified using Dijkstra's algorithm (30).

### Statistical Analysis

Statistical significance was defined as  $p < 0.05$ . One-way analysis of variance (ANOVA) and Student's  $t$ -test were used as appropriate.

### Tools and Software Packages

All analyses were performed within a Python-based data analysis environment using the following packages: NumPy (31), Matplotlib (32), Seaborn, Pandas, and ProDy (33).

## Results

### Weaker Interactions with the F Pocket Lead to Lower pMHC Conformational Stability

Three peptides (ALW, MVW, and RQW) bound to HLA-A\*02:01 were studied using molecular dynamics simulations. Each system underwent three 750-ns simulations, including a peptide-free control as reference. The selection of these particular peptides was based on comprehensive experimental data reported by Hopkins et al. (31). This study is notable as it uniquely provides not only half-life measurements, indicative of thermal stability, but also detailed insights into the conformational flexibility of these pMHCs through high-pressure perturbation experiments. Such extensive experimental data, covering both stability and dynamic conformational responses, is uncommon in pMHC literature, where studies often report only affinity or thermal/cell surface stability, leaving the role of conformational flexibility less defined.

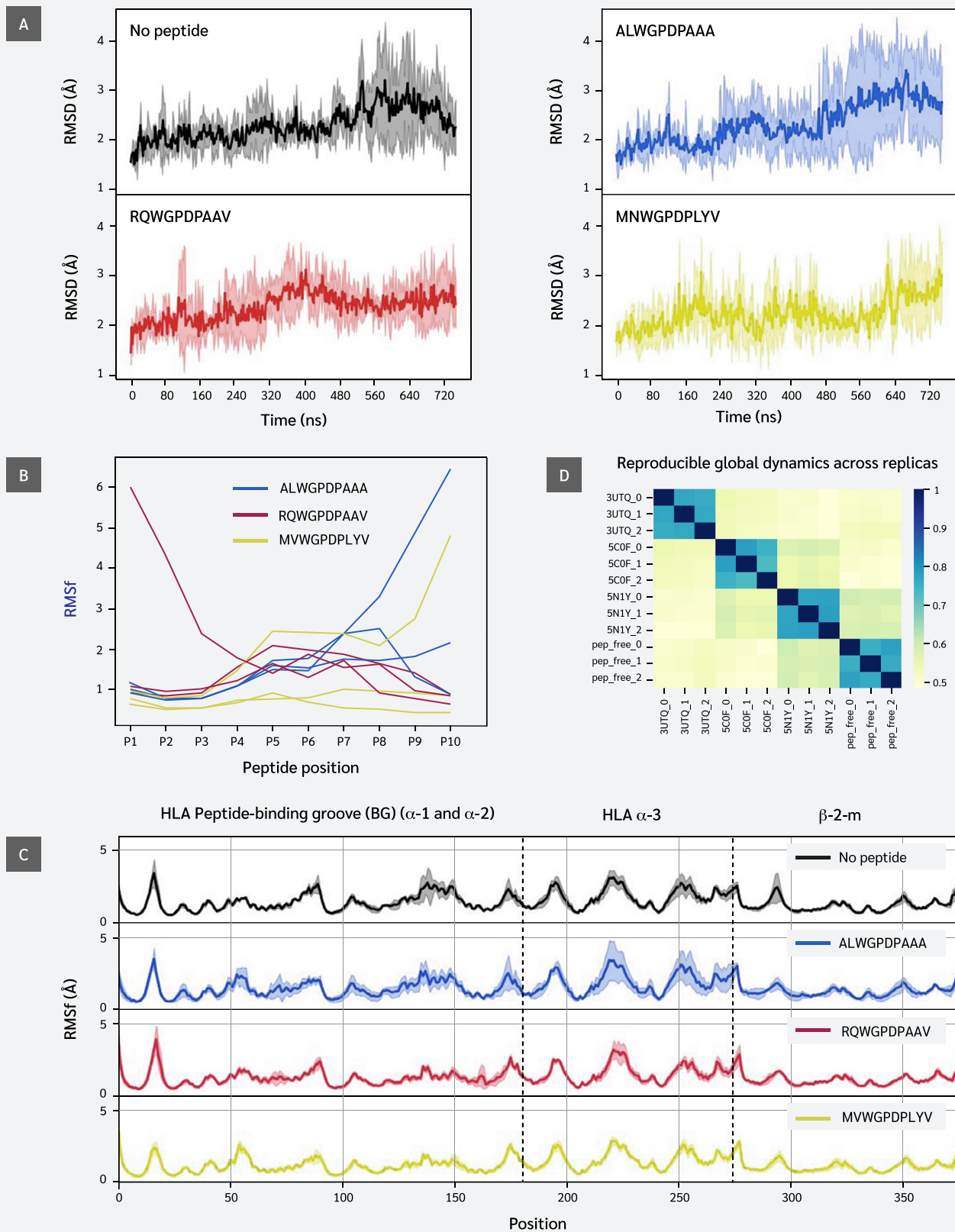
Given that all three pMHC systems (ALW, MVW, and RQW with HLA-A\*02:01) were found to behave differently in high-pressure or temperature perturbation experiments and previous molecular dynamics simulations (31), they serve as ideal benchmarks for a more granular investigation of the effect of peptide binding on the overall pMHC structure, as intended here. Notably, the experimental data from Hopkins et al. (31) highlighted distinct biophysical characteristics for these peptides; for instance, the ALW-HLA-A\*02:01 complex showed physicochemical indicators (a significantly higher  $\Delta C_p$ ) suggestive of greater conformational flexibility compared to the others. Furthermore, these peptides are valuable benchmarks due to observed discrepancies between their experimental stability and affinity data and those predicted by standard computational tools, underscoring the need for detailed mechanistic studies. A detailed description of the characteristics of these peptides can be found in [Supplementary Text](#).

Figure 1A shows stable fluctuations after equilibration, with the ALW peptide and peptide-free system displaying higher fluctuation levels. This suggests ALW's effect on pMHC dynamics is less significant than that of other peptides. The effect on stability of the whole complex is often directly linked to the binding stability of the peptide throughout the simulations. To probe the stability of each peptide residue, we next computed the RMSF values of each peptide residue (position) in each simulation.

This analysis revealed partial peptide detachment in one simulation of each system: at the C-terminus (F pocket) for ALW and MVW, and at the N-terminus (B pocket) for RQW. In peptide-free and ALW simulations, HLA and  $\beta 2m$  residues showed higher variation in positions 70-85 and 140-150, corresponding to  $\alpha$ -1 and  $\alpha$ -2 regions of the F pocket. Results indicate that strong peptide C-terminus-F-pocket interactions are crucial for conformational stability.

### Peptide Ligand Leads to Reproducible Global Dynamics Profiles

Our findings showed that peptide sequence and interactions affect fluctuations of peptide and HLA residues, and influence regions beyond the peptide binding groove. This is not clearly visible in the RMSF plot (Figure 1C), except in parts of the  $\alpha 3$  domain, possibly due to thermal fluctuations masking potential dynamic differences. We performed EDA of simulation trajectories to



**Figure 1.** Conformational stability and dynamic profiles of simulated peptide-loaded Major Histocompatibility Complex (pMHC) systems.

**A)** Root mean square deviation (RMSD) profiles over time for peptide-free and peptide-bound HLA-A02:01 systems. Darker lines represent the mean RMSD from three replicate simulations; shaded areas indicate standard deviation ranges.

**B)** Root mean square fluctuation (RMSF) profiles of individual peptides in each simulation. Each line corresponds to one replicate simulation.

**C)** Root mean square fluctuation profiles of HLA-A02:01 and  $\beta$ 2-microglobu-

lin ( $\beta$ 2m) residues. Darker lines indicate the average per-residue RMSF across three replicates; shaded areas denote the standard deviation.

**D)** Subspace overlap (Root Mean Square Inner Product, RMSIP) values between individual replicate simulations. An RMSIP of 1 denotes identical essential dynamics, while 0 indicates no similarity. Axis labels show PDB four-letter codes for each peptide-HLA-A\*02:01 complex, followed by the replicate number. 3UTQ corresponds to the ALW peptide, 5N1Y to the MVW peptide, and 5COF to the RQW peptide.



## Strong residue couplings = strong pocket interactions

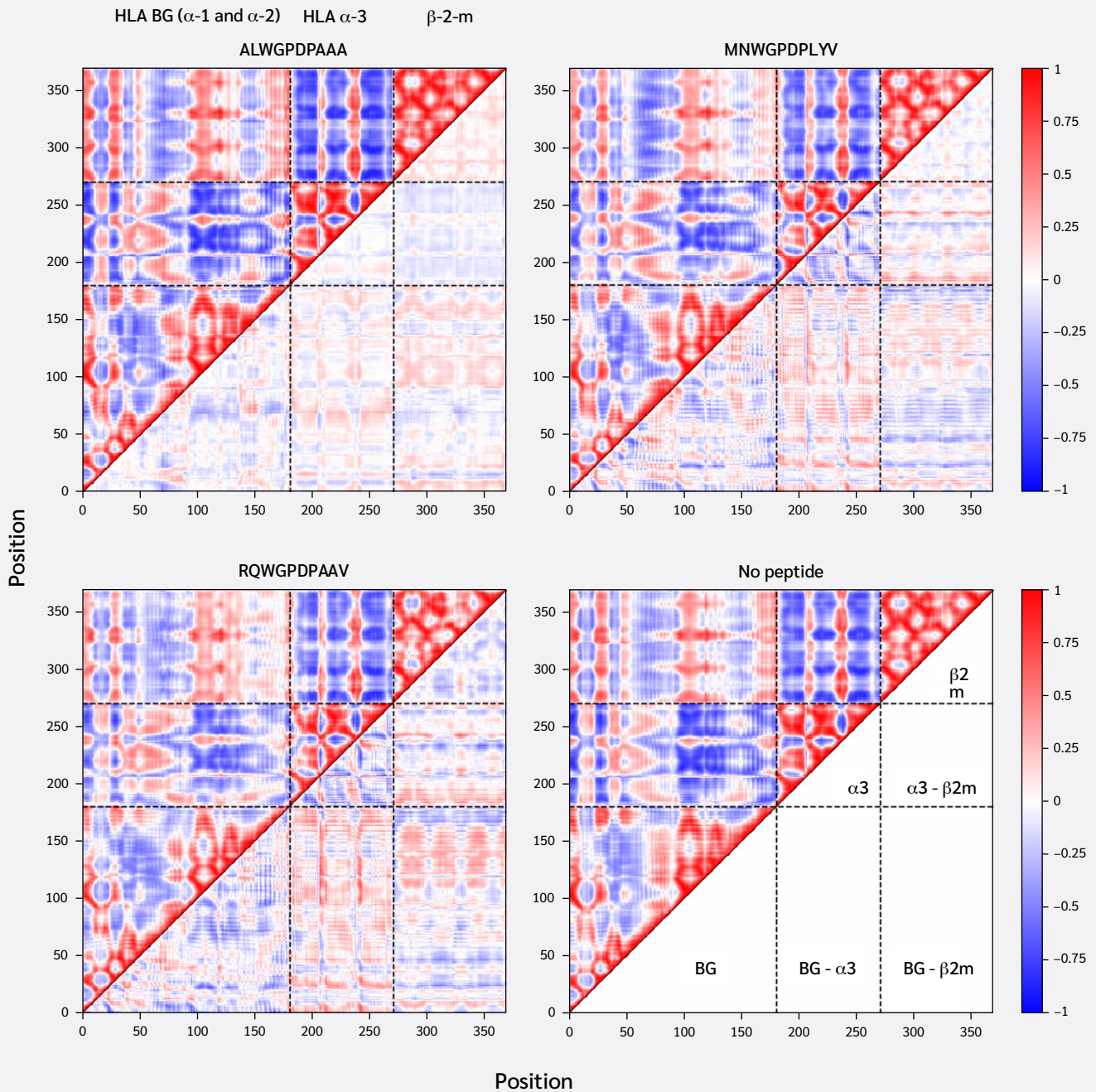


**Figure 2.** Residue coupling patterns and peptide-induced differences in residue coupling in HLA-A\*02:01 systems.

Dynamic cross-correlation matrices (DCCMs) and difference DCCMs ( $\Delta$ DCCMs) are shown for peptide-loaded and peptide-free systems.

**Top left:** DCCM (upper triangle) and  $\Delta$ DCCM (lower triangle) for the ALW peptide system.

**Top right:** DCCM (upper triangle) and  $\Delta$ DCCM (lower triangle) for the MVW peptide system.

**Bottom left:** DCCM (upper triangle) and  $\Delta$ DCCM (lower triangle) for the RQW peptide system.

**Bottom right:** Schematic legend defining intra- and inter-domain interaction regions on the DCCM heatmap. Domain labels indicate the peptide-binding groove (BG;  $\alpha 1$  and  $\alpha 2$  domains),  $\alpha 3$  domain,  $\alpha 2$ -microglobulin ( $\alpha 2m$ ), and inter-domain regions.



better understand similarities/differences between global dynamics profiles of different systems.

Essential dynamics analysis provides motional modes and their contributions to overall variance. We analyzed the top 20 motions describing global coordinated movements and calculated similarities between these modes using the RMSIP metric. Figure 1D shows that the replica simulations of each system exhibited the highest similarity, indicating strong reproducibility. This enables a reliable comparison between different systems. Subspace overlaps between different systems exhibit moderate similarity levels (0.5–0.6), indicating that while peptides do not create unique cooperative domain motions, they produce distinct motional profiles. RQW and MVW peptide simulations showed relatively higher similarities compared to others.

### Stronger Peptide Binding in F Pocket Leads to More Extensive Changes in Dynamic Residue Couplings

Having confirmed that replica simulations explored similar essential subspaces, we next investigated residue couplings, comparing peptide-loaded and peptide-free systems. For this, we generated average DCCMs for each system using the top 20 global motional modes. Subtracting the DCCM of the peptide-free system from each peptide-loaded system yielded difference DCCMs ( $\Delta$ DCCMs), visualizing changes in residue couplings upon peptide binding (Figure 2).

Consistent with similar RMSF profiles and RMSIP values above 0.5 (Figure 1D), the systems exhibited similar overall residue coupling profiles. However,  $\Delta$ DCCM plots also revealed subtle peptide-specific differences. ALW binding induced relatively smaller coupling changes, increasing both correlations and anti-correlations between the HLA binding groove and  $\alpha 3/\beta 2m$ . Notably, ALW binding showed minimal changes in intra- $\alpha 3$  couplings, with increased intra- $\beta 2m$  correlations but decreased  $\beta 2m-\alpha 3$  correlations.

Conversely, MVW and RQW exerted similar, but stronger, effects than ALW. They increased positive correlations between the HLA binding groove and  $\alpha 3/\beta 2m$ , shifted intra- $\alpha 3$  couplings toward anti-correlation, and increased  $\beta 2m-\alpha 3$  coupling. In summary, stronger F pocket peptide binding led to more extensive changes in MHC dynamic coupling, particularly an increase in the positive correlation between the peptide-binding groove and distal domains.

### Peptide Binding Induces Perturbations in Intra- and Inter-Chain Residue Interaction Energies

We identified "consistent pairs" that exhibited significantly similar interaction energies across replicas using one-way ANOVA. In other words, pairs whose interaction energies did not differ significantly ( $p > 0.05$ ) across replica simulations (defined as those with a  $p$ -value  $> 0.05$  from the ANOVA test) were identified (the full list of pairs and their corresponding  $p$  values can be found in [Supplementary Data](#) file under Tab "Consistent Pairs"). Finally, we identified pairs that showed statistically significant ( $p < 0.05$ , Student's  $t$ -test) energy shifts upon peptide binding, defined as those with a  $p$ -value  $< 0.05$  from a Student's  $t$ -test, and which also had with an absolute interaction energy difference of at least 2 kcal/mol upon peptide binding toward attractive or repulsive ranges (Figure 3) (the full list of pairs and their corresponding  $p$  values can be found in [Supplementary Data](#) file under Tab "Affected upon Peptide Binding").

Strikingly, ALW exhibited a smaller effect compared to the other peptides. ALW induced shifts toward attraction only within the binding groove, not extending to distal domains or the  $\beta 2m-\alpha 3$  interface. It also caused shifts toward repulsion in this interface, decreasing attraction between Val12(BG)-Ser34( $\beta 2m$ ) and Ile23(BG)-Phe63( $\beta 2m$ ). Conversely, MVW and RQW showed much more extensive effects, both within the binding groove and on interacting pairs between  $\beta 2m$  and  $\alpha 3$ , as well as at the bottom of the binding groove. Their effects were also highly similar, affecting the same pairs. Interactions becoming more attractive included Phe9(BG)-Phe57( $\beta 2m$ ), Ser11(BG)-Glu55( $\beta 2m$ ), and Tyr11( $\beta 2m$ )-Pro235( $\alpha 3$ ), while those becoming more repulsive included Val12(BG)-Ser34( $\beta 2m$ ), Thr10(BG)-Gly56( $\beta 2m$ ), and Val25(BG)-Gly56( $\beta 2m$ ).

### Stabilization of the F Pocket by Peptides Leads to Stabilized Interactions Near the Core of the MHC

Motivated by the differential effects of peptides on the pMHC protein-protein interface, we investigated how these changes translate to individual residue behavior. Since edge weights reflect interaction attractiveness or repulsiveness, PENs are useful for probing stability. We computed betweenness centrality (BC) values for each residue, representing the average number of shortest paths through that residue. Here, residues with optimized interactions (and thus predominantly negative/attractive

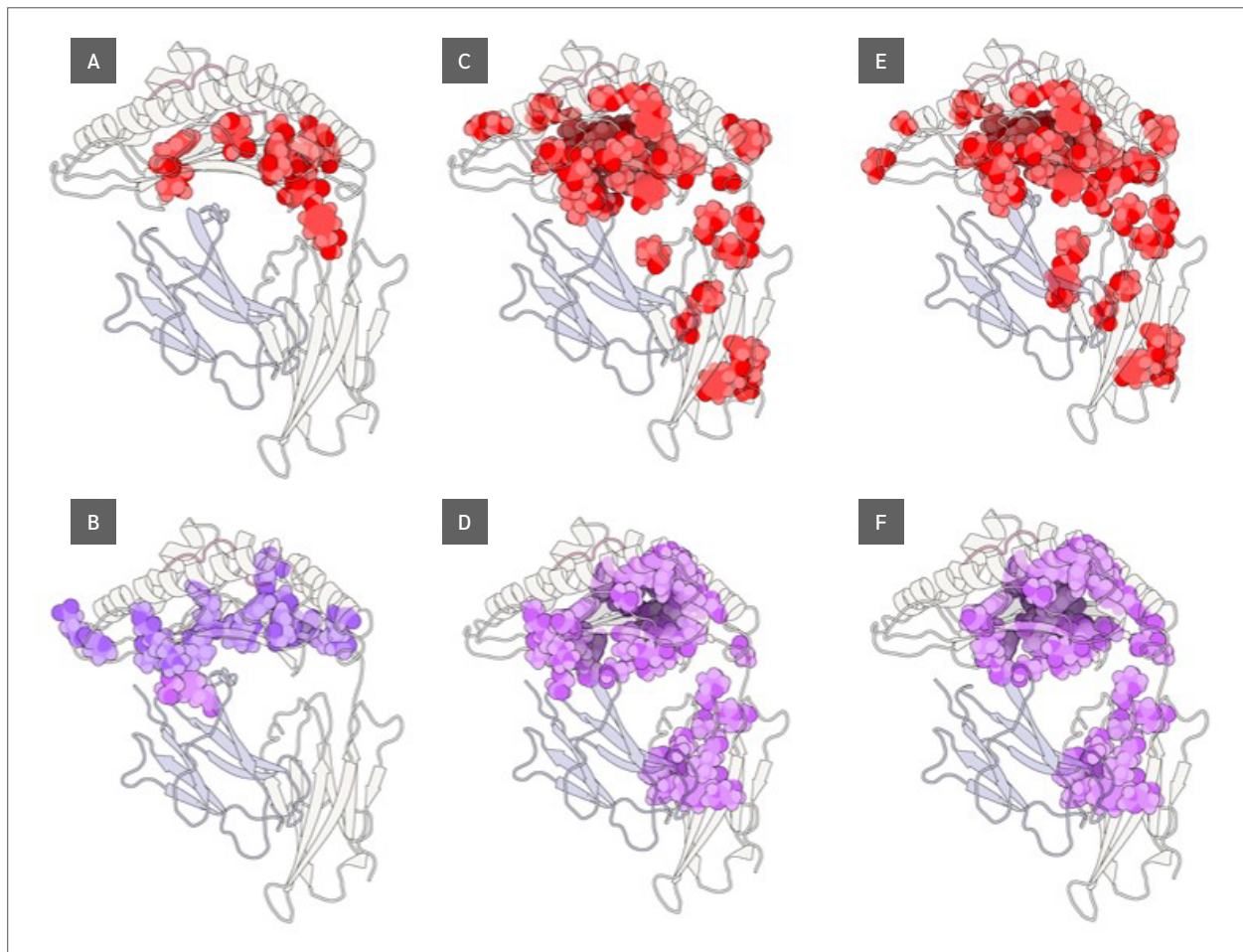


**Figure 3.** Residue pairs exhibiting significant shifts in interaction energies upon peptide binding.

Residue pairs that showed statistically significant shifts in nonbonded interaction energies upon binding of ALW, MVW, or RQW peptides are shown. (A, B) ALW-bound system; (C, D) MVW-bound system; (E, F) RQW-bound system.

Red spheres represent residue pairs with interactions shifted toward stronger attraction; purple spheres represent residue pairs with interactions shifted toward increased repulsion.

non-bonded interaction energies with their surroundings) have higher BC values.

These scores were subsequently compared to overall residue conservation scores obtained from the CONSURF database (35). A scatter plot of conservation scores versus mean BC levels is shown in Figure 4. A key takeaway from this plot is the high conservation levels of HLA residues with the highest BC levels. These include Pro235( $\alpha$ 3), Tyr209( $\alpha$ 3), Pro210( $\alpha$ 3), Trp244( $\alpha$ 3), Ala245( $\alpha$ 3), and Val28(BG).

Finally, we identified residues with statistically significant BC differences between systems, which were defined as those having a  $p$ -value  $< 0.05$  from a using one-way ANOVA test. From this group of significant residues, we ( $p < 0.05$ ) and selected the top 10 residues with the

largest BC increases or decreases upon peptide binding (Figure 5), based on median BC levels (the full list of residues with their corresponding  $p$  values can be found in [Supplementary Data](#) file under Tab “Betweenness Centralities”).

Two key findings emerged from this analysis. First, residues 64 B ( $\beta$ 2m threonine) and 235 A ( $\alpha$ 3 proline), both located in distal domains (Figure 6), showed the largest BC increases upon peptide binding. All peptides increased 64 B's betweenness, suggesting an allosteric effect near the  $\beta$ 2m/pMHC core, reinforcing surrounding interactions. However, 235 A's BC increase was observed only with RQW and MVW, not ALW.

The first finding leads to the second key finding: for most residues in Figure 4, BC patterns were shared between

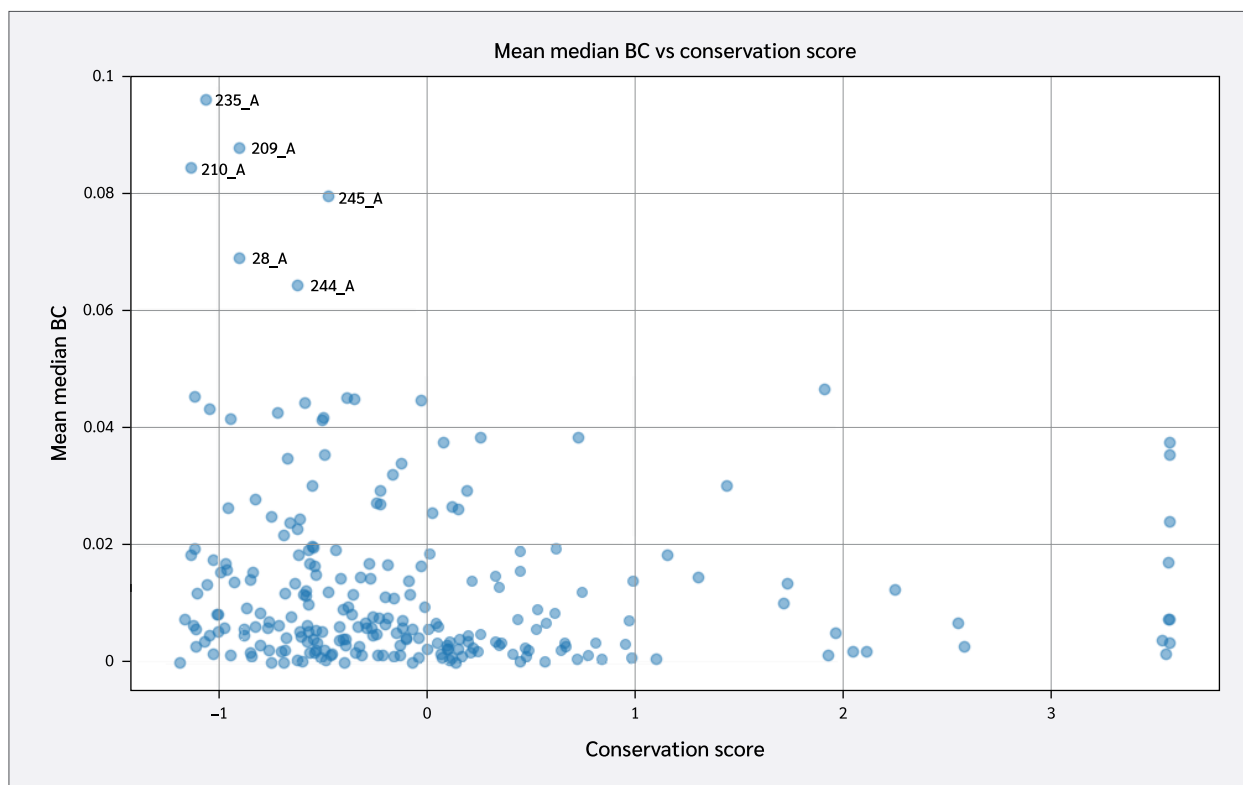


**Figure 4.** Relationship between residue betweenness centrality and evolutionary conservation.

Scatter plot of mean median betweenness centrality (BC) values for residues from peptide-bound simulations plotted against their conservation scores obtained from the **CONSURF** database (PDB ID: 5N1Y). Lower conservation

scores indicate higher evolutionary conservation. Chain identifiers following underscores denote the respective chains in the simulated complex; chain A corresponds to HLA-A\*02:01.

the ALW and peptide-free systems, as well as between the RQW and MVW peptides, consistent with the lack of structural effects upon ALW binding. Consequently, the behavior of Pro235( $\alpha 3$ ) is particularly noteworthy; its high mean BC as shown in Figure 4 underscores its general importance to the structural integrity of the complex, while its significant and selective increase in BC upon binding of the strongly stabilizing peptides RQW and MVW further pinpoints it as a key residue involved in mediating peptide-specific allosteric effects on pMHC stability.

## Discussion

This study investigated the influence of different peptide ligands on the structural dynamics and conformational stability of HLA-A\*02:01 using molecular dynamics simulations. Essential dynamics and protein energy network analyses provided insights into peptide-induced changes in MHC-I and the modulation of complex dynamics.

The stability of pMHC has long been recognized as a critical factor for immunogenicity (39,40). Consequently, characterization of pMHC stability is of great interest for immunotherapeutic applications (41). It is understood that peptide binding is not solely dictated by interactions within the peptide-binding groove. Instead, the entire MHC complex, including more distal domains, contributes to the binding event and the overall stability of the pMHC assembly (16,42). Indeed, previous simulation studies have shown the importance of regions beyond the canonical binding site in modulating peptide-MHC interactions (19,42).

Despite this broader understanding, a significant portion of computational studies aimed at predicting or characterizing pMHC stability has predominantly focused on the interactions within the peptide-binding groove. This focus is often a necessary simplification to enable predictions at larger scales (44–47). However, such a narrow perspective may overlook crucial contributions from other regions of the complex to its overall stability. To our knowledge, the present study is the first to employ mo-

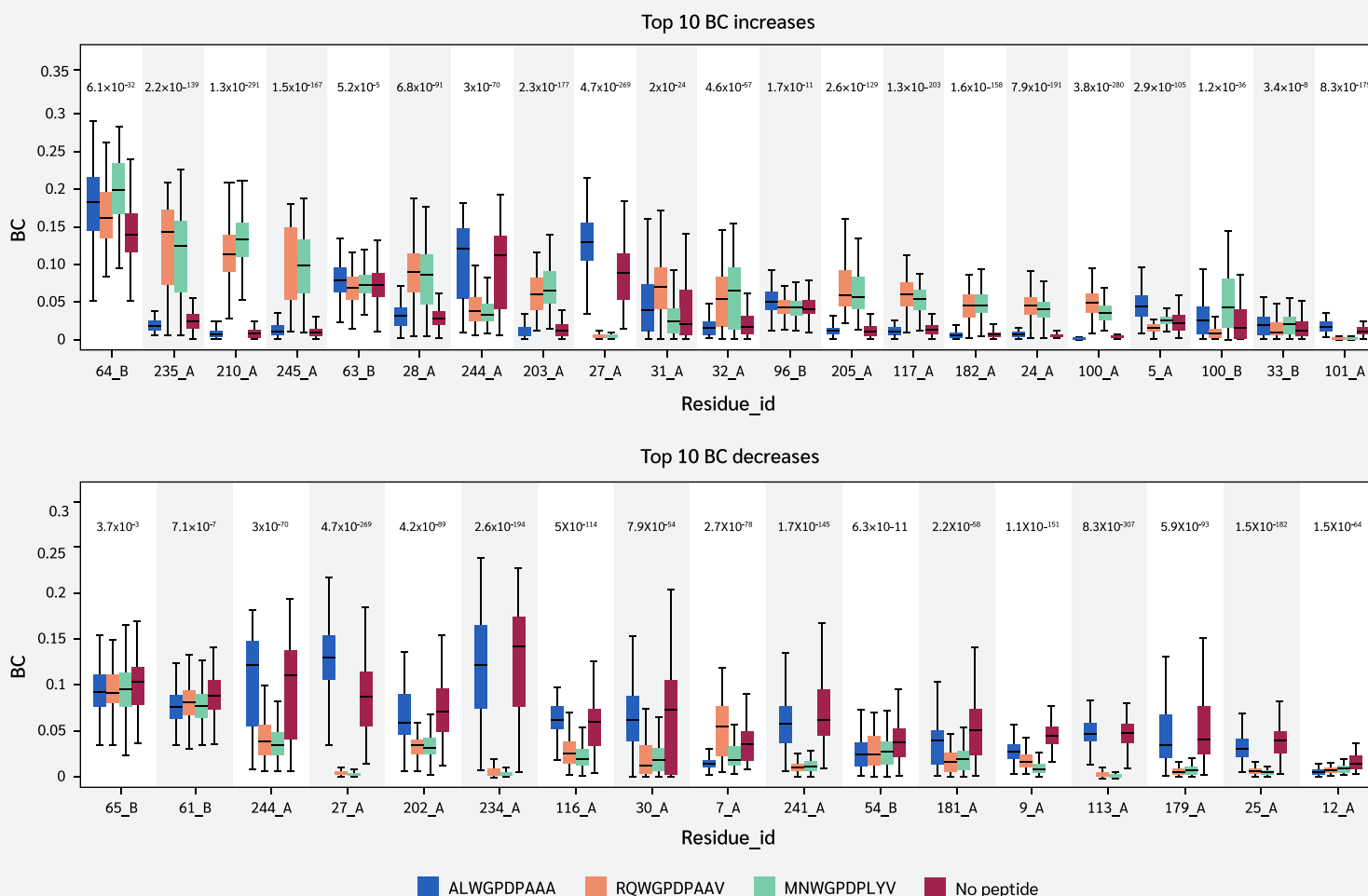


**Figure 5.** Residues with the highest peptide-induced changes in betweenness centrality.

Box plots show residues (Residue\_id) with the greatest increases (top) and decreases (bottom) in median betweenness centralities (BC) upon peptide binding. Data are presented for ALW, MVW, and RQW peptide-bound systems and the peptide-free control. Chain identifiers denote the respective chains:

chain A for HLA-A\*02:01 and chain B for  $\beta$ 2-microglobulin ( $\beta$ 2m). The p values denoting statistical significance of the BC differences per residue are denoted above each box plot.

lecular dynamics simulations to systematically evaluate pMHC stability with a specific focus on protein-protein interaction interfaces throughout the entire complex (e.g., the heavy chain- $\beta$ 2m interface and intramolecular domain contacts). This approach enabled the identification and characterization of allosteric mechanisms through which peptides differentially modulate stabilization across these distal interfaces, extending our understanding beyond direct peptide-groove interactions.

Our results are consistent with prior research that highlights the tight connection between peptide ligands and MHC-I. Peptides typically anchor deeply into the MHC-I binding groove, resulting in MHC-I stability and flexibility depending on the peptide cargo (49). Peptide-free MHC is known to be unstable (49), and peptide binding stabilizes and dampens complex dynamics, affecting distal  $\beta$ 2m and  $\alpha$ 3 domains. MHC conformational stability depends on peptide C-terminus interactions with the

F-pocket (50). Our findings offer new insights into this stabilization. We have shown that stable F-pocket binders (MVW and RQW) induce larger increases in positive correlations between the binding groove and  $\alpha$ 3, as well as in both positive and negative correlations between the binding groove and  $\beta$ 2m. This strengthens crosstalk between distal domains and the binding groove, potentially through increased attraction between HLA and  $\beta$ 2m, as revealed by our non-bonded interaction energy analysis. Weaker ALW binding even increased repulsiveness at the  $\beta$ 2m-HLA interface.

The highly polymorphic nature of MHC-I molecules has significant implications for their structural dynamics and stability (20,51-53). Certain MHC alleles are more dependent on the chaperone protein Tapasin for proper peptide loading compared to others (54-57). Micropolymorphisms within the F-pocket region of the peptide-binding groove may lead to differential dependencies on Tapasin

for binding of high-affinity peptides (57-60). These subtle sequence variations in the F-pocket can lead to distinct global conformational dynamics of the MHC complex, even in the peptide-free state. Specifically, some F-pocket polymorphisms may favor a more stable and rigid conformation of the MHC, while others may result in a more flexible and dynamic structure (61). This allele-specific behavior of the peptide-free MHC likely has consequences for the conformational stabilization induced by the binding of different peptide ligands, as observed in our findings. Future studies that explore the interplay among F-pocket polymorphisms, Tapasin dependency, global dynamics, and complex stability will provide valuable context for interpreting the conformational stabilization mechanisms revealed by our molecular dynamics' simulations.

Furthermore, major stability differences among HLA genes themselves may also imply differential behaviour to peptide binding. For instance, HLA-C alleles are known to exhibit lower cell surface expression and stability levels compared to HLA-A and HLA-B alleles (62,63). This reduced stability of HLA-C has also been associated with less efficient responses against viral infections (64). Our previous local frustration analysis of human MHC-I allele structures highlighted a less stable F pocket in HLA-C (65). Weaker interactions between the F pocket and peptide cargo may thus represent a general phenomenon in HLA-C, resulting in a failure to strengthen interactions with distal domains of the complex, as observed in the case of the ALW peptide in this study.

Finally, it is important to note that we did not observe a strong correlation between experimental or theoretical measures of thermal stability (i.e., melting temperature) or kinetic stability (i.e., half-time) and our findings related to conformational stability (see [Supplementary Text](#)). This may be explained by discrepancies between experimental measurements on the same peptide-HLA pair, or, more specifically, a lack of sufficient data points, which restricts the reliability of such comparisons. Alternatively, the thermal and conformational stability of MHC molecules may not be directly related, as is also the case for many other proteins (66,67). Previous work in this field has explored both kinetic (i.e., over time) and thermal stability of pMHC, and a positive correlation between these two types of stability metrics has been identified (68,69). It is also worth emphasizing that classical MD simulations in the isothermal-isobaric ensemble (i.e., at constant temperature and pressure) are inherently limited to mimic experimental conditions used in both types

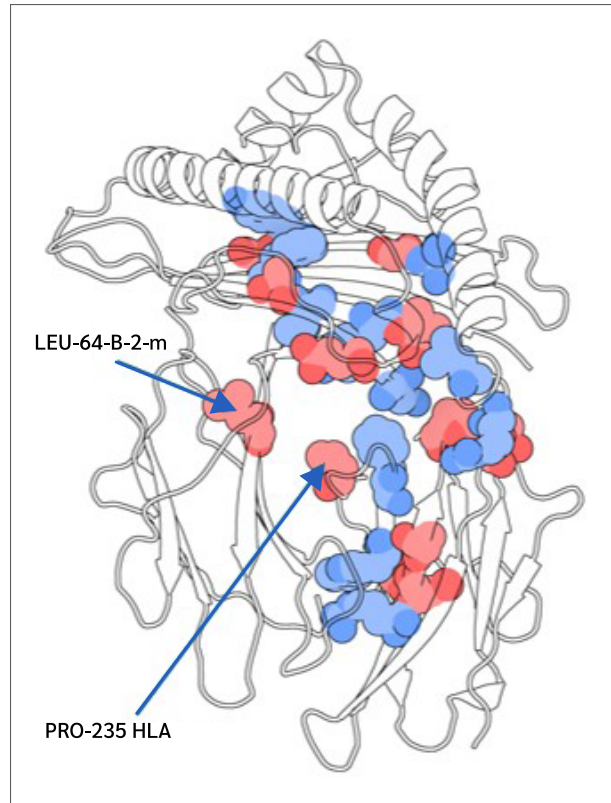


**Figure 6.** Spatial distribution of residues most affected by peptide binding based on betweenness centrality.

Residues corresponding to the top (red) and bottom (blue) ranked residues from Figure 5 are mapped onto the HLA-A\*02:01 structure. Red spheres denote residues with the largest BC increases; blue spheres indicate residues with the largest BC decreases upon peptide binding.

of stability measurements since simulations cover neither the full-time scale (often hours) nor the temperature ranges (increased over time) used in these experiments. To this end, predicting and evaluating MHC thermal stability alongside molecular simulation findings remains a challenge. Application of a similar computational strategy to a higher number of pMHC complexes with reliable experimental structures and both thermal and kinetic stability data may lead to more comprehensive insights into peptide-induced stabilization in this regard.

## Conclusion

In summary, this study highlights the intricate relationship between peptide ligands and the conformational dynamics of HLA-A\*02:01, emphasizing the crucial role of stable interactions within the F-pocket for achieving structural integrity and stability. The observed enhancements



in dynamic coupling and crosstalk between the peptide-binding groove and distal domains underscore the complexity of MHC-I-peptide interactions and their influence on overall protein behavior. These enhancements may result in a shift of attractive interactions towards the HLA- $\beta$ 2m interface, ultimately contributing to increased conformational stability of the whole complex. To this end, our findings also challenge the assumption that

thermal stability directly correlates with conformational stability, highlighting the need for further research to elucidate these relationships. The insights gained from our molecular dynamics simulations not only reinforce existing literature but also pave the way for future studies aimed at understanding the nuances of MHC-peptide interactions, which could ultimately inform therapeutic strategies in immunology and vaccine development.

**Ethical Approval:** N.A.

**Informed Consent:** N.A.

**Peer-review:** Externally peer-reviewed

**Author Contributions:** Concept – O.S.; Design – O.S.; Supervision – O.S.; Fundings – O.S.; Materials – O.S.; Data Collection and/or Processing – O.S.; Analysis and/or Interpretation – O.S.; Literature Review – O.S.; Writer – O.S.; Critical Reviews – O.S.

**Conflict of Interest:** The author declares no conflict of interest.

**Financial Disclosure:** The author declared that this study has received no financial support.

**Data Availability:** The data tables generated through analysis of MD simulation trajectories conducted, including all *p* values, can

be found at Zenodo at the following URL: <https://doi.org/10.5281/zenodo.14651951>. These data tables were used to generate figures presented in the manuscript.

**Declaration Regarding the Use of AI and AI-Assisted Technologies:** During the preparation of this work, the author utilized Jenni (jenni.ai) to create an initial draft of the introduction section. After carefully reviewing and editing the content as necessary, full responsibility for the publication's content is taken by the author. This incorporation of AI tool usage primarily impacted the flow of information and readability of the introduction section only.

**Acknowledgment:** The author would like to thank Malgorzata A. Garstka for her insightful comments on peptide-induced MHC stability and MHC-Tapasin interactions, which substantially improved the depth and clarity of the analyses presented in this study.








## References

- Hermens JM, Kesmir C. Role of T cells in severe COVID-19 disease, protection, and long term immunity. *Immunogenetics*. 2023;75(3):295-307. [\[CrossRef\]](#)
- Raskov H, Orhan A, Christensen JP, Gögenur I. Cytotoxic CD8+ T cells in cancer and cancer immunotherapy. *Br J Cancer*. 2021;124(2):359-67. [\[CrossRef\]](#)
- Amigorena S. Antigen presentation: from cell biology to physiology. *Immunol Rev*. 2016;272(1):5-7. [\[CrossRef\]](#)
- Parham P. Putting a face to MHC restriction. *J Immunol*. 2005;174(1):3-5. [\[CrossRef\]](#)
- Nesmiyanov PP. Antigen presentation and major histocompatibility complex. In: Rezaei N, editor. *Encyclopedia of Infection and Immunity*. 1st ed. Elsevier; 2022. p. 90-98. [\[CrossRef\]](#)
- Kotsias, F, Cebrian, I, Alloatti, A. Antigen processing and presentation. *International Review of Cell and Molecular Biology*. 2019;348:69-121. [\[CrossRef\]](#)
- Chiou, SJ, Chen, CH. Decipher  $\beta$ 2-microglobulin: gain- or loss-of-function (a mini-review). *Medical Science Monitor Basic Research*, 2013;19:271-3. [\[CrossRef\]](#)
- Solheim, JC. Class I MHC molecules: assembly and antigen presentation. *Immunological Review*. 1999;172:11-9. [\[Cross-Ref\]](#)
- Fodor J, Riley BT, Borg NA, Buckle AM. Previously hidden dynamics at the TCR-peptide-MHC interface revealed. *J Immunol*. 2018;200(12):4134-45. [\[CrossRef\]](#)
- Natarajan K, Jiang J, May NA, Mage MG, Boyd LF, McShan AC, et al. The role of molecular flexibility in antigen presentation and T cell receptor-mediated signaling. *Front Immunol*. 2018;9:1657. [\[CrossRef\]](#)
- Jantz-Naeem N, Springer S. Venus flytrap or pas de trois? The dynamics of MHC class I molecules. *Curr Opin Immunol*. 2021;70:82-9. [\[CrossRef\]](#)
- Ayres CM, Baker BM. Peptide-dependent tuning of major histocompatibility complex motional properties and the consequences for cellular immunity. *Curr Opin Immunol*. 2022;76:102184. [\[CrossRef\]](#)
- Borbulevych OY, Piepenbrink KH, Gloor BE, Scott DR, Somese RF, Cole DK, et al. T cell receptor cross-reactivity directed by antigen-dependent tuning of peptide-MHC molecular flexibility. *Immunity*. 2009;31(6):885-96. [\[CrossRef\]](#)
- Nguyen AT, Szeto C, Gras S. The pockets guide to HLA class I molecules. *Biochem Soc Trans*. 2021;49(5):2319-31. [\[CrossRef\]](#)
- Yanaka S, Ueno T, Shi Y, Qi J, Gao GF, Tsumoto K, et al. Peptide-dependent conformational fluctuation determines the

- stability of the human leukocyte antigen class I complex. *J Biol Chem.* 2014;289(35):24680-90. [\[CrossRef\]](#)
- 16 Dirscherl C, Löchte S, Hein Z, Kopicki JD, Harders AR, Linden N, et al. Dissociation of  $\beta$ 2m from MHC class I triggers formation of noncovalent transient heavy chain dimers. *J Cell Sci.* 2022;135(9):jcs259489. [\[CrossRef\]](#)
- 17 Harndahl M, Rasmussen M, Roder G, Buus S. Real-time, high-throughput measurements of peptide-MHC-I dissociation using a scintillation proximity assay. *J Immunol Methods.* 2011;374(1-2):5-12. [\[CrossRef\]](#)
- 18 Bingöl EN, Serçinoğlu O, Ozbek P. Unraveling the allosteric communication mechanisms in T-cell receptor-peptide-loaded major histocompatibility complex dynamics using molecular dynamics simulations: An approach based on dynamic cross correlation maps and residue interaction energy calculations. *J Chem Inf Model.* 2021;61(5):2444-53. [\[CrossRef\]](#)
- 19 Serçinoğlu O, Ozbek P. Computational characterization of residue couplings and micropolymerism-induced changes in the dynamics of two differentially disease-associated human MHC class-I alleles. *J Biomol Struct Dyn.* 2018;36(3):724-40. [\[CrossRef\]](#)
- 20 Amarajeewa AWP, Özcan A, Mukhtiar A, Ren X, Wang Q, Ozbek P, et al. Polymorphism in F pocket affects peptide selection and stability of type 1 diabetes-associated HLA-B39 allotypes. *Eur J Immunol.* 2024;54(6):e2350683. [\[CrossRef\]](#)
- 21 Knapp B, Demharter S, Esmailbeiki R, Deane CM. Current status and future challenges in T-cell receptor/peptide/MHC molecular dynamics simulations. *Brief Bioinform.* 2015;16(6):1035-44. [\[CrossRef\]](#)
- 22 Alba J, D'Abramo M. The full model of the pMHC-TCR-CD3 complex: A structural and dynamical characterization of bound and unbound states. *cells.* 2022;11(4):668. [\[CrossRef\]](#)
- 23 Abraham MJ, Murtola T, Schulz R, Páll S, Smith JC, Hess B, et al. GROMACS: high performance molecular simulations through multi-level parallelism from laptops to supercomputers. *SoftwareX.* 2015;1-2:19-25. [\[CrossRef\]](#)
- 24 Hopkins CW, Le Grand S, Walker RC, Roitberg AE. Long-time-step molecular dynamics through hydrogen mass repartitioning. *J Chem Theory Comput.* 2015;11(4):1864-74. [\[CrossRef\]](#)
- 25 Lindorff-Larsen K, Piana S, Palmo K, Maragakis P, Klepeis JL, Dror RO, et al. Improved side-chain torsion potentials for the Amber ff99SB protein force field. *Proteins.* 2010;78(8):1950-8. [\[CrossRef\]](#)
- 26 Berman HM, Westbrook J, Feng Z, Gilliland G, Bhat TN, Weissig H, et al. The protein data bank. *Nucleic Acids Res.* 2000;28(1):235-42. [\[CrossRef\]](#)
- 27 Bulek AM, Cole DK, Skowera A, Dolton G, Gras S, Madura F, et al. Structural basis for the killing of human beta cells by CD8(+) T cells in type 1 diabetes. *Nat Immunol.* 2012;13(3):283-9. [\[CrossRef\]](#)
- 28 Serçinoğlu O, Ozbek P. gRINN: a tool for calculation of residue interaction energies and protein energy network analysis of molecular dynamics simulations. *Nucleic Acids Res.* 2018;46(W1):W554-62. [\[CrossRef\]](#)
- 29 Brandes U. A faster algorithm for betweenness centrality. *J Math Sociol.* 2001;25(2):163-77. [\[CrossRef\]](#)
- 30 Dijkstra EW. A note on two problems in connexion with graphs. *Numer Math.* 1959;1(1):269-71. [\[CrossRef\]](#)
- 31 Harris CR, Millman KJ, van der Walt SJ, Gommers R, Virtanen P, Cournapeau D, et al. Array programming with NumPy. *Nature.* 2020;585(7825):357-62. [\[CrossRef\]](#)
- 32 Hunter JD. Matplotlib: a 2D graphics environment. *Comput Sci Eng.* 2007;9(3):90-5. [\[CrossRef\]](#)
- 33 Zhang S, Krieger JM, Zhang Y, Kaya C, Kaynak B, Mikulska-Ruminska K, et al. ProDy 2.0: increased scale and scope after 10 years of protein dynamics modelling with Python. *Bioinformatics.* 2021;37(20):3657-9. [\[CrossRef\]](#)
- 34 Hopkins JR, Crean RM, Catci DAM, Sewell AK, Arcus VL, Van der Kamp MW, et al. Peptide cargo tunes a network of correlated motions in human leucocyte antigens. *FEBS J.* 2020;287(17):3777-93. [\[CrossRef\]](#)
- 35 Vijayabaskar MS, Vishveshwara S. Interaction energy based protein structure networks. *Biophys J.* 2010;99(11):3704-15. [\[CrossRef\]](#)
- 36 Yan W, Sun M, Hu G, Zhou J, Zhang W, Chen J, et al. Amino acid contact energy networks impact protein structure and evolution. *J Theor Biol.* 2014;355:95-104. [\[CrossRef\]](#)
- 37 Yehorova D, Di Geronimo B, Robinson M, Kasson PM, Kamerlin SCL. Using residue interaction networks to understand protein function and evolution and to engineer new proteins. *Curr Opin Struct Biol.* 2024;89:102922. [\[CrossRef\]](#)
- 38 Ben Chorin A, Masrati G, Kessel A, Narunsky A, Sprinzak J, Lahav S, et al. ConSurf-DB: An accessible repository for the evolutionary conservation patterns of the majority of PDB proteins. *Protein Sci.* 2020;29(1):258-67. [\[CrossRef\]](#)
- 39 van der Burg SH, Visseren MJ, Brandt RM, Kast WM, Melief CJ. Immunogenicity of peptides bound to MHC class I molecules depends on the MHC-peptide complex stability. *J Immunol.* 1996;156(9):3308-14.
- 40 Harndahl M, Rasmussen M, Roder G, Dalgaard Pedersen I, Sørensen M, Nielsen M, et al. Peptide-MHC class I stability is a better predictor than peptide affinity of CTL immunogenicity. *Eur J Immunol.* 2012;42(6):1405-16. [\[CrossRef\]](#)
- 41 Jappe EC, Garde C, Ramarathinam SH, Passantino E, Illing PT, Mifsud NA, et al. Thermostability profiling of MHC-bound peptides: a new dimension in immunopeptidomics and aid for immunotherapy design. *Nat Commun.* 2020;11(1):6305. [\[CrossRef\]](#)
- 42 Omasits U, Knapp B, Neumann M, Steinhauser O, Stockinger H, Kobler R, et al. Analysis of key parameters for molecular dynamics of pMHC molecules. *Mol Simul.* 2008;34(8):781-93. [\[CrossRef\]](#)
- 43 Rasmussen M, Fenoy E, Harndahl M, Kristensen AB, Nielsen IK, Nielsen M, et al. Pan-specific prediction of peptide-MHC class I complex stability, a correlate of T cell immunogenicity. *J Immunol.* 2016;197(4):1517-24. [\[CrossRef\]](#)
- 44 Abella JR, Antunes DA, Clementi C, Kavraki LE. Large-scale structure-based prediction of stable peptide binding to class I HLAs using random forests. *Front Immunol.* 2020;11:1583. [\[CrossRef\]](#)

- 45 Chieochansin T, Sanachai K, Darai N, Chiraphappaiboon W, Choomee K, Yenchitsomanus PT, et al. *In silico* advancements in Peptide-MHC interaction: A molecular dynamics study of predicted glypican-3 peptides and HLA-A\*11:01. *Heliyon*. 2024;10(17):e36654. [\[CrossRef\]](#)
- 46 Rostamian M, Farasat A, Chegene Lorestan R, Nemati Zargar F, Ghadiri K, et al. Immunoinformatics and molecular dynamics studies to predict T-cell-specific epitopes of four *Klebsiella pneumoniae* fimbriae antigens. *J Biomol Struct Dyn*. 2022;40(1):166-76. [\[CrossRef\]](#)
- 47 Bunsuz A, Serçinoğlu O, Ozbek P. Computational investigation of peptide binding stabilities of HLA-B\*27 and HLA-B\*44 alleles. *Comput Biol Chem*. 2020;84:107195. [\[CrossRef\]](#)
- 48 Ayres CM, Abualrous ET, Bailey A, Abraham C, Hellman LM, Corcelli SA, et al. Dynamically driven allostery in MHC proteins: Peptide-dependent tuning of class I MHC global flexibility. *Front Immunol*. 2019;10:966. [\[CrossRef\]](#)
- 49 Theodossis A. On the trail of empty MHC class-I. *Mol Immunol*. 2013;55(2):131-4. [\[CrossRef\]](#)
- 50 Abualrous ET, Saini SK, Ramnarayan VR, Ilca FT, Zacharias M, Springer S. The carboxy terminus of the ligand peptide determines the stability of the MHC class I molecule H-2Kb: A combined molecular dynamics and experimental study. *PLoS One*. 2015;10(8):e0135421. [\[CrossRef\]](#)
- 51 Serçinoğlu O, Ozbek P. Sequence-structure-function relationships in class I MHC: A local frustration perspective. *PLoS One*. 2020;15(5):e0232849. [\[CrossRef\]](#)
- 52 Narzi D, Becker CM, Fiorillo MT, Uchanska-Ziegler B, Ziegler A, Böckmann RA. Dynamical characterization of two differentially disease associated MHC class I proteins in complex with viral and self-peptides. *J Mol Biol*. 2012;415(2):429-42. [\[CrossRef\]](#)
- 53 Bailey A, Dalchau N, Carter R, Emmott S, Phillips A, Werner JM, et al. Selector function of MHC I molecules is determined by protein plasticity. *Sci Rep*. 2015;5:14928. [\[CrossRef\]](#)
- 54 van Hateren A, Elliott T. The role of MHC I protein dynamics in tapasin and TAPBP-assisted immunopeptidome editing. *Curr Opin Immunol*. 2021;70:138-43. [\[CrossRef\]](#)
- 55 Badrinath S, Huyton T, Blasczyk R, Bade Doeding C, et al. HLA class I polymorphism and tapasin dependency. In: *HLA and Associated Important Diseases*. Rezaei N, editor. London: InTech; 2014. p. X Y. [\[CrossRef\]](#)
- 56 Aflalo A, Boyle LH. Polymorphisms in MHC class I molecules influence their interactions with components of the antigen processing and presentation pathway. *Int J Immunogenet*. 2021;48(4):317-25. [\[CrossRef\]](#)
- 57 Wieczorek M, Abualrous ET, Sticht J, Álvaro-Benito M, Stolzenberg S, Noé F, et al. Major histocompatibility complex (MHC) class I and MHC class II proteins: Conformational plasticity in antigen presentation. *Front Immunol*. 2017;8:292. [\[CrossRef\]](#)
- 58 Abualrous ET, Fritzsche S, Hein Z, Al-Balushi MS, Reinink P, Boyle LH, et al. F pocket flexibility influences the tapasin dependence of two differentially disease-associated MHC Class I proteins. *Eur J Immunol*. 2015;45(4):1248-57. [\[CrossRef\]](#)
- 59 Garstka MA, Fritzsche S, Lenart I, Hein Z, Jankevicius G, Boyle LH, et al. Tapasin dependence of major histocompatibility complex class I molecules correlates with their conformational flexibility. *FASEB J*. 2011;25(11):3989-98. [\[CrossRef\]](#)
- 60 Garstka MA, Fish A, Celie PH, Joosten RP, Janssen GM, Berlin I, et al. The first step of peptide selection in antigen presentation by MHC class I molecules. *Proc Natl Acad Sci U S A*. 2015;112(5):1505-10. [\[CrossRef\]](#)
- 61 Fisette O, Schröder GF, Schäfer LV. Atomistic structure and dynamics of the human MHC-I peptide-loading complex. *Proc Natl Acad Sci U S A*. 2020;117(34):20597-606. [\[CrossRef\]](#)
- 62 Neisig A, Melief CJ, Neefjes J. Reduced cell surface expression of HLA-C molecules correlates with restricted peptide binding and stable TAP interaction. *J Immunol*. 1998;160(1):171-9.
- 63 Kaur G, Gras S, Mobbs JI, Vivian JP, Cortes A, Barber T, et al. Structural and regulatory diversity shape HLA-C protein expression levels. *Nat Commun*. 2017;8:15924. [\[CrossRef\]](#)
- 64 Vigón L, Galán M, Torres M, Martín-Galiano AJ, Rodríguez-Mora S, Mateos E, et al; Multidisciplinary Group of Study of COVID-19 (MGS-COVID). Association between HLA-C alleles and COVID-19 severity in a pilot study with a Spanish Mediterranean Caucasian cohort. *PLoS One*. 2022;17(8):e0272867. [\[CrossRef\]](#)
- 65 Serçinoğlu O, Ozbek P. Sequence-structure-function relationships in class I MHC: A local frustration perspective. *PLoS One*. 2020;15(5):e0232849. [\[CrossRef\]](#)
- 66 Karshikoff A, Nilsson L, Ladenstein R. Rigidity versus flexibility: the dilemma of understanding protein thermal stability. *FEBS J*. 2015;282(20):3899-917. [\[CrossRef\]](#)
- 67 Hou XN, Song B, Zhao C, Chu WT, Ruan MX, Dong X, et al. Connecting protein millisecond conformational dynamics to protein thermal stability. *JACS Au*. 2024;4(8):3310-20. [\[CrossRef\]](#)
- 68 Jappe EC, Garde C, Ramarathnam SH, Passantino E, Illing PT, Mifsud NA, et al. Thermostability profiling of MHC-bound peptides: a new dimension in immunopeptidomics and aid for immunotherapy design. *Nat Commun*. 2020;11(1):6305. [\[CrossRef\]](#)
- 69 Blaha DT, Anderson SD, Yoakum DM, Hager MV, Zha Y, Gajewski TF, et al. High-throughput stability screening of neoantigen/HLA complexes improves immunogenicity predictions. *Cancer Immunol Res*. 2019;7(1):50-61. [\[CrossRef\]](#)

# Integrated Clinical and *In Silico* Analysis of Hypomorphic *DCLRE1C* Variants: Predicting Malignancy and Autoimmunity Risk

Serkan Küçüktürk<sup>1</sup> , Ali Şahin<sup>2</sup> , Mehmet Ali Karaselek<sup>3</sup> , Tuğçe Duran<sup>4</sup> , Şükrü Nail Güner<sup>3</sup> , Sevgi Keleş<sup>3</sup> , İsmail Reisli<sup>3</sup> 

<sup>1</sup>Karamanoğlu Mehmetbey University Faculty of Medicine, Department of Medical Biology, Karaman, Türkiye; <sup>2</sup>Selçuk University Faculty of Medicine, Konya, Türkiye; <sup>3</sup>Necmettin Erbakan University Faculty of Medicine, Department of Pediatric Immunology and Allergy, Konya, Türkiye; <sup>4</sup>KTO Karatay University Faculty of Medicine, Department of Medical Genetics, Konya, Türkiye

## Abstract

**Objectives:** Hypomorphic variants of *DNA cross-link repair 1C (DCLRE1C)* cause a spectrum of combined immunodeficiency phenotypes that range from mild autoimmunity to life-threatening malignancy. We aimed to integrate detailed clinical phenotyping with *in silico* pathogenicity metrics to improve the prediction of adverse outcomes in this rare disorder.

**Materials and Methods:** We compiled a descriptive cohort of 41 patients carrying one of 12 published hypomorphic *DCLRE1C* variants. Inferential analyses focused on the molecularly homogeneous subgroup of 25 individuals harboring three recurrent missense changes within the metallo- $\beta$ -lactamase/ $\beta$ -CASP domains—c.194C>T [p.Thr65Ile], c.500C>T [p.Thr167Met] and c.632G>T [p.Gly211Val]. Comprehensive clinical, immunological, and laboratory data were extracted. Pathogenicity was assessed with eight *in silico* algorithms,  $\Delta\Delta G$  stability modelling, and structural mapping. Logistic regression identified variables associated with malignancy and autoimmunity, and composite risk scores were generated.

**Results:** Median age at last follow-up was 9.4 years (range 0.5–27). Recurrent sinopulmonary infection (80%), chronic diarrhea (48%), and candidiasis (44%) were common across variants, while otitis media and growth retardation were confined to c-terminal changes. All three analyzed variants exceeded pathogenicity thresholds (mean Combined Annotation-Dependent Depletion [CADD]  $26.7 \pm 2.1$ ) and reduced predicted protein stability (mean  $\Delta\Delta G +1.8$  kcal/mol). A revised malignancy risk score (lymphadenopathy, immunoglobulin G [IgG] <400 mg/dL, diarrhea,  $\Delta\Delta G \geq 1$  kcal/mol, BayesDel >0.5, age > 60 months) > 4 achieved an area under the receiver operating characteristic curve (AUC) of 0.89 (95% confidence interval [CI] 0.57–1.00), with 75% sensitivity and 100% specificity. The analogous autoimmunity score (skin lesions, pulmonary infections, IgG low,  $\Delta\Delta G \geq 1$ , BayesDel > 0.5, CD19 low, age > 60 months) > 8 showed moderate discrimination (AUC 0.75; 95% CI, 0.54–0.97), with 83.3% sensitivity and 73.7% specificity.

**Conclusion:** Integration of domain-restricted *in silico* metrics with core clinical parameters modestly improves malignancy risk prediction in hypomorphic *DCLRE1C* deficiency. Prospective, multi-center validation and functional assays are required before clinical implementation.

**Keywords:** Artemis, leaky severe combined immunodeficiency, combined immune deficiency, *DCLRE1C*

## Correspondence

Serkan Küçüktürk

## E-mail

skuccukturk@kmu.edu.tr

## Received

June 17, 2025

## Accepted

October 2, 2025

## Published

December 4, 2025

## Suggested Citation

Küçüktürk S, Şahin A, Karaselek MA, Duran T, Güner ŞN, Keleş S, et al. Integrated clinical and *in silico* analysis of hypomorphic *DCLRE1C* variants: Predicting malignancy and autoimmunity risk. Turk J Immunol. 2025;13(3):146-57.

## DOI

10.36519/TJI.2025.734



This work is licensed under the Creative Commons Attribution-NonCommercial-Non-Derivatives 4.0 International License (CC BY-NC-ND 4.0).

## Introduction

The Artemis protein, encoded by the *DNA cross-link repair 1C* (*DCLRE1C*) gene, plays a critical role in variable, diversity, and joining [V(D)J] recombination and in the repair of non-homologous end joining (NHEJ) DNA double-strand breaks (1,2). Pathogenic variants in the *DCLRE1C* gene severely impair T and B-cell development, resulting in the clinical phenotype of severe combined immunodeficiency (SCID) (3). In contrast, hypomorphic *DCLRE1C* variants allow for partial protein expression, leading to a milder phenotype of combined immunodeficiency (CID) (4).

Patients with hypomorphic *DCLRE1C* variants, first identified in 2015 (5) may present at variable ages with diverse clinical manifestations (infections, granulomatous lesions, autoimmune disorders, malignancy) and laboratory findings. To date, only 16 hypomorphic variants in the *DCLRE1C* gene have been reported in 41 patients, resulting in a CID phenotype (Figure 1) (5-13). In addition to CID, these patients often develop malignancies and autoimmune diseases later in life (13), and predicting these conditions remains highly challenging. No large case series has been published regarding patients affected by the hypomorphic *DCLRE1C* gene variant, and the cases in the literature consist of studies with a small number of cases. Despite their clinical relevance, functional impacts of hypomorphic variants remain unclear. There is limited research investigating the correlation between hypomorphic *DCLRE1C* variants and clinical or laboratory parameters. Prior research has mainly focused on functional validations, creating a knowledge gap in the application of *in silico* tools for pathogenicity prediction in this context (14,15). Recently, *in silico* tools have emerged as promising approaches for predicting the pathogenicity of variants detected in patients (16-19).

Inborn errors of immunity (IEI) are rare diseases caused by mutations in over 550 genes (20,21), many of which are still classified as variants of uncertain significance (VUS), posing challenges for clinicians. However, pathogenicity analyses of variants identified as VUS through *in silico* analyses may lead to an increase in the number of new genes responsible for IEI, providing patients with the opportunity for early treatment. In IEI patients, variants identified as VUS have begun to be demonstrated as pathogenic through *in silico* analyses followed by functional studies (16-19).

From this perspective, our study aimed to correlate clinical and laboratory findings with data obtained through *in silico* analyses of hypomorphic *DCLRE1C* variants described in the literature. We further suggest that this approach may be applicable to similar analyses in other genes associated with IEI, especially when functional assays are unavailable.

## Materials and Methods

### Study Design

The study employed a two-tier design and was conducted at the Department of Paediatric Immunology and Allergy, Necmettin Erbakan University Faculty of Medicine.

We assembled a descriptive cohort of 41 patients (23 from the literature, 18 from our center) who harbor one of 12 hypomorphic *DCLRE1C* variants that have been reported to date (5-13). For genotype-phenotype comparisons, data from all available patients were included to provide a comprehensive descriptive overview. However, for laboratory-based *in silico* analyses, cases from the  $\beta$ -CASP domain were excluded due to substantial missing information. To maintain analytic homogeneity, these analyses were therefore restricted to 25 patients carrying missense variants in the metallo- $\beta$ -lactamase (MBL)/ $\beta$ -CASP domains (c.194C>T [p.Thr65Ile], c.500C>T [p.Thr167Met], and c.632G>T [p.Gly211Val]). Among these 25 patients, 18 originated from our institutional cohort and seven from the literature.

C-terminal variants were excluded from *in silico* analyses because they predominantly consist of large deletions, insertions, or duplications, which cannot be reliably evaluated using tools. These cases were nevertheless retained for descriptive clinical analyses.

### *In silico* Analysis of Commonly Observed Hypomorphic *DCLRE1C* Variants

A comprehensive literature review was conducted to identify pathogenic and potentially pathogenic variants associated with the Artemis protein, as shown in Figure 1. To assess the pathogenicity of these variants, we calculated multiple *in silico* prediction scores, including BayesDel addAF, BayesDel noAF, Combined Annotation-Dependent Depletion (CADD), Eigen, Eigen-PC, Functional Analysis through Hidden Markov Models (FATHMM)- Multiple Kernel Learning (MKL), FATHMM-

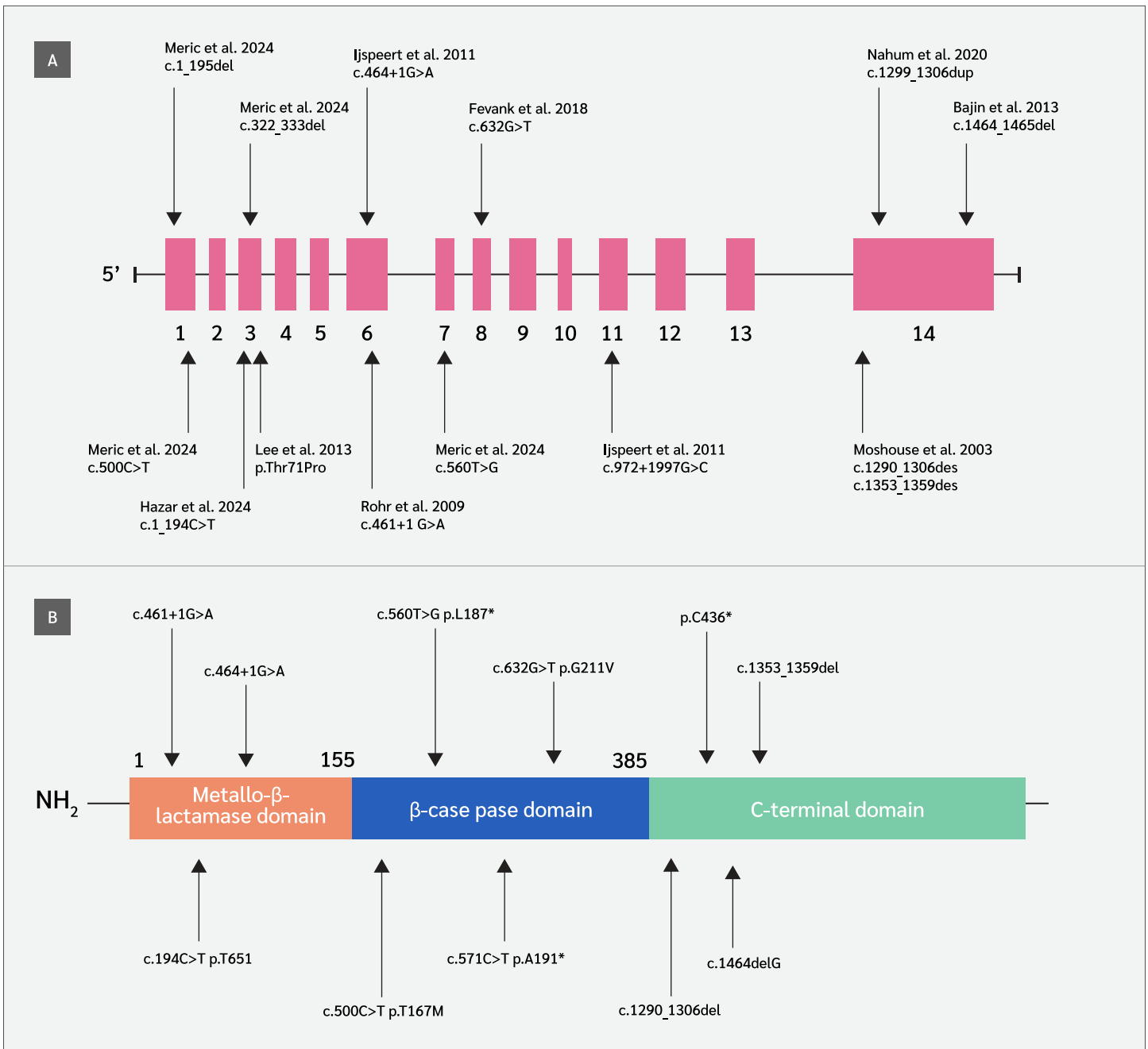


**Figure 1.** The genomic and protein localization of hypomorphic *DCLRE1C* variants described in the literature. (A) Genomic localizations of hypomorphic variants. (B) Localizations within the protein structure.

eXtended Features (XF), and Deleterious Annotation of Genetic Variants using Neural Networks (DANN) (22). These scores provide insights into the functional impact of the variants based on different computational models that integrate sequence conservation, protein structure, and functional annotations.

The three-dimensional (3D) structure of the Artemis protein was retrieved from the Research Collaboratory for Structural Bioinformatics Protein Data Bank (PDB ID: 6W00; <https://www.rcsb.org>). To evaluate the structural consequences of the identified variants, we utilized PremPS (Li Lab, Soochow University, China; <http://lilab.jysw.suda.edu.cn/research/PremPS/>), a tool designed to



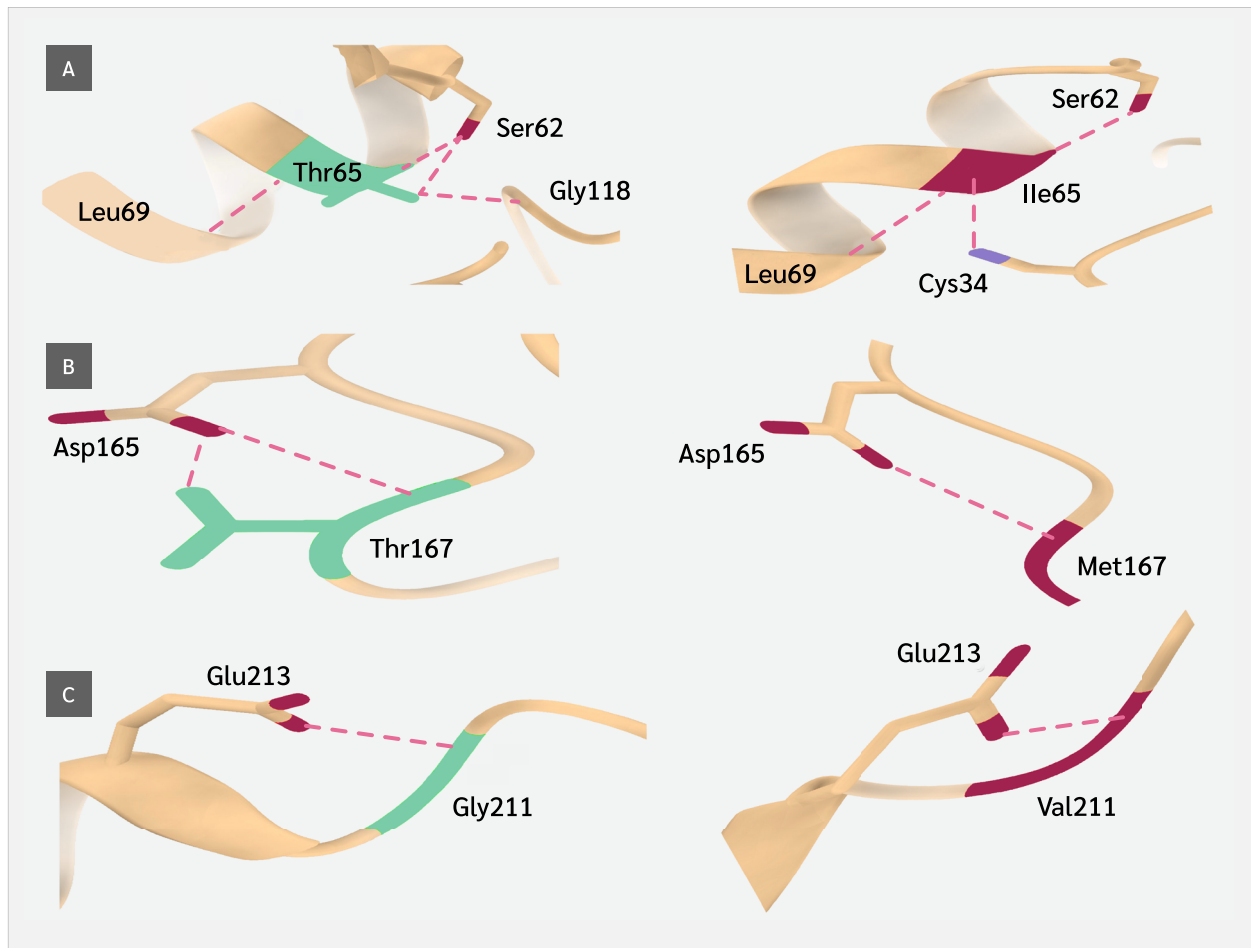


**Figure 2.** Schematic representation of the structural regions of the Artemis protein. Wild-type Artemis protein (left side of the panel). Mutant Artemis protein resulting from the variants and its interaction with other amino acids (right side of the panel). (A) c.194C>T, p.(Thr65Ile); (B) c.500C>T, p.(Thr167Met); (C) c.632G>T, p.(Gly211Val). Rose Pink dashed lines represent hydrogen bonds.

predict the impact of amino acid substitutions on protein stability (23). This analysis enabled us to determine the delta-delta G ( $\Delta\Delta G$ ) (kcal/mol) values, representing the predicted change in protein stability induced by each variant. A positive  $\Delta\Delta G$  value indicates destabilization, whereas a negative value suggests stabilization of the protein structure.

Wild-type and mutant structures were compared using UCSF ChimeraX (version 1.10.1; Resource for Biocomputing, Visualization, and Informatics, University of California, San Francisco, USA) (25). In addition to structural analyses, the evolutionary conservation of the affected residues was evaluated (Figure 2). Homologous protein sequences across multiple species were retrieved from the Ensembl database (release 115; European Bioinformatics Institute, Hinxton, UK), and multiple sequence

alignment (MSA) was performed using the Clustal $\Omega$  algorithm (version 2024; EMBL–EBI, Hinxton, Cambridge, UK) within the JalView platform (version 2.11.5.0; The Barton Group, University of Dundee, UK) (26). Conservation scores were analyzed to determine whether the substituted residues are located within highly conserved regions, as alterations in such positions are more likely to be functionally deleterious.

### Statistical Analysis

Categorical variables, including the presence of autoimmunity and malignancy, were compared across variant domain groups using the chi-square test of independence. Continuous variables were analyzed with the Mann-Whitney U test. Demographic data are presented as mean  $\pm$  standard deviation (SD). All statistical analyses were performed using Python software (version 3.11;

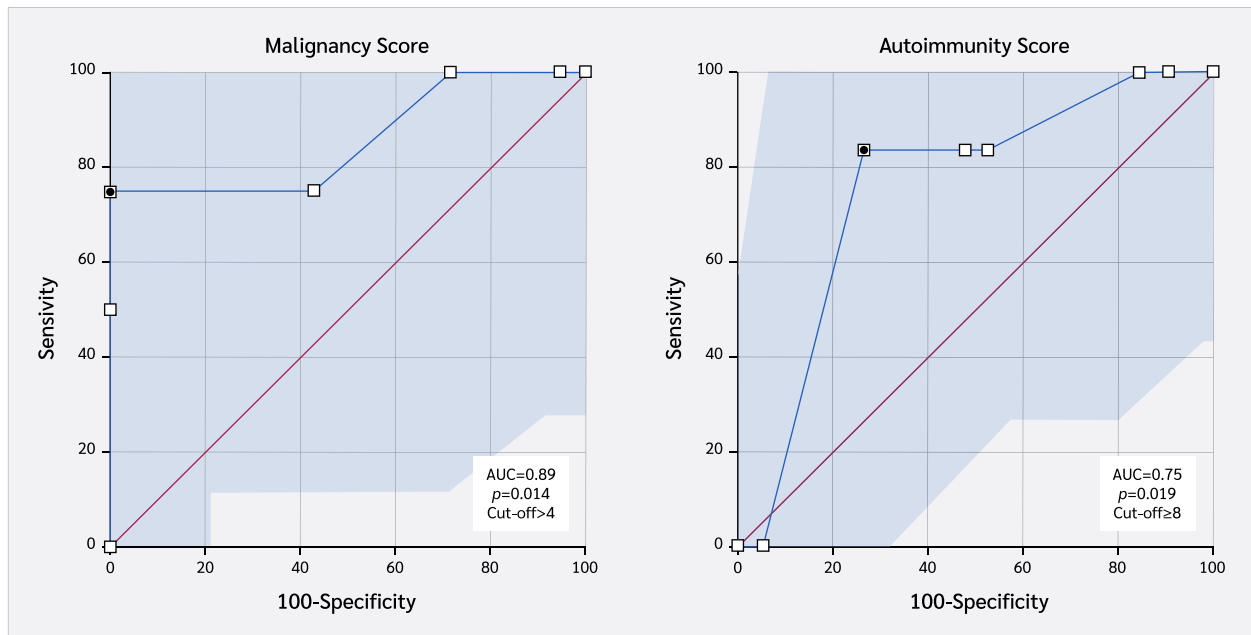


**Figure 3.** Schematic ROC curves for malignancy (AUC=0.89) and autoimmunity (AUC=0.75) risk scores based on combined clinical and *in silico* parameters.

Python Software Foundation, Wilmington, DE, USA) and GraphPad Prism (version 6.0; GraphPad Software, San Diego, CA, USA). A two-sided  $p$  value  $<0.05$  was considered statistically significant.

A composite risk scoring system was developed to predict the likelihood of malignancy and autoimmunity based on clinical, immunological, and *in silico* parameters. Variable selection was informed by univariate association, biological plausibility, and multicollinearity assessment. Each parameter was assigned a weighted score reflecting its relative contribution (Table 1). The total score ranges were optimized to 0–10 for malignancy and 0–12 for autoimmunity.

Predictive performance was evaluated using receiver operating characteristic (ROC) curve analysis (figure 3). The area under the ROC curve (AUC) was calculated, and 95% confidence intervals (CIs) were estimated using the method of DeLong et al. (24). To assess overfitting and provide optimism-corrected performance estimates, bias-corrected and accelerated (BCa) bootstrap CIs were computed with 1000 replications, using a fixed random seed (seed=978) to ensure reproducibility. Optimal cut-off values were determined using the Youden index. Sensitivity, specificity, positive predictive value (PPV), negative predictive value (NPV), and odds ratios (ORs) with

95% CIs were calculated using 2x2 contingency tables and Fisher's exact test where appropriate. For all estimated effect sizes, including odds ratios, 95% CIs were computed using exact or asymptotic methods as appropriate and are reported alongside  $p$ -values to reflect the precision of the estimates.

In this exploratory cohort, the predictive performance of the risk scores was evaluated in the context of a small sample size and clinical heterogeneity. Given the exploratory nature of this study and the rarity of hypomorphic *DCLRE1C* variants, AUC values exceeding 0.60 were considered to reflect potential discriminative ability in the context of preliminary risk stratification, with statistical significance ( $p<0.05$  vs. AUC=0.5) and internal validation via bootstrapping serving as key supportive criteria.

## Results

### Genomics, Clinical, and Laboratory Characteristics of Hypomorphic *DCLRE1C* Variants

In the initial phase of the study, a total of 41 patients with hypomorphic *DCLRE1C* variants were identified through literature review and institutional records. Domain-based

**Table 1.** Summary of variables and scoring weights used in the malignancy and autoimmunity risk models. Low IgG and low CD19 expression were defined according to age-adjusted reference intervals.

Variable	Condition	Malignancy score	Autoimmunity score
Pulmonary infections	Present	-	1
Lymphadenopathy	Present	2	-
Diarrhea	Present	1	-
Skin lesions	Present	1	1
Immunoglobulin G (IgG)	Low	2	3
Cluster of differentiation 19 (CD19)	Low	-	2
$\Delta\Delta G$ (kcal/mol)	$\geq 1.0$	1	2
BayesDel addAF	$> 0.5$	2	2
Age	$> 60$ months	1	1
Total score range		0–10	0–12

distribution and genotype associations were summarized as follows: Among them, 23 had mutations in the MBL domain, 15 in the C-terminal domain, and 3 in the  $\beta$ -CASP domain. Genotypic analysis revealed that 34 (82.9%) patients were homozygous, and 7 (17.1%) were compound heterozygous patients. No statistically significant differences were observed in the frequency of autoimmunity across variant domains ( $p=0.470$ ). Similarly, malignancy rates did not differ significantly among the domain groups ( $p=0.297$ ). In pairwise comparisons between genotypes, the prevalence of autoimmunity was similar between homozygous and compound heterozygous patients as was the occurrence of malignancy ( $p>0.05$ ). These findings suggest that neither the structural localization of the *DCLRE1C* variant nor genotype (homozygous vs compound heterozygous) significantly influences the risk of autoimmunity or malignancy in this cohort.

Among the clinical features examined, the frequency of pulmonary infections was significantly higher in patients with MBL domain variants (63.2%) compared to those with C-terminal domain variants ( $p=0.032$ ), whereas the difference between MBL and  $\beta$ -CASP domains was not statistically significant ( $p=0.236$ ), nor was the difference between  $\beta$ -CASP and C-terminal domains ( $p=0.502$ ). Several other clinical features showed statistically significant differences across domain groups, including diarrhea ( $p=0.028$ ), otitis ( $p=0.038$ ), fever ( $p<0.001$ ), growth retardation ( $p=0.007$ ), malignancy ( $p=0.048$ ), and mortality status ( $p=0.006$ ); however, skin lesions did not differ significantly. Notably, both otitis and growth

retardation were observed exclusively in the C-terminal domain group and were absent in the MBL and  $\beta$ -CASP groups. When clinical findings were evaluated by genotype, candidiasis was significantly more common among patients with compound heterozygous variants (3/7; 42.9%) than in those with homozygous mutations (1/34; 2.9%) ( $p=0.001$ ).

Statistically significant differences were found across domain groups for natural killer (NK) cells, CD25 activation, and naïve B-cell levels. Natural killer cells were low in 3/9 C-terminal cases (33%), but normal in 0/21 MBL and 6/7  $\beta$ -CASP cases ( $p=0.025$ ) (12). CD25 activation in T cells was markedly reduced in both C-terminal (88.9%) and MBL (90.5%) domain groups. Although these two domains showed comparable suppression rates ( $p=0.894$ ), the overall distribution reached statistical significance ( $p=0.030$ ), primarily due to the single  $\beta$ -CASP patient exhibiting normal CD25 activation. Naïve B-cell levels differed significantly across protein domains ( $\chi^2=7.843$ ,  $p=0.005$ ). Only patients with either decreased or normal naïve B-cell levels were included in the analysis due to the absence of elevated cases. The majority of patients with MBL domain variants exhibited decreased naïve B-cell counts (94.4%), whereas most patients with C-terminal domain variants showed normal counts (66.7%).

**In Silico Analysis Results**

Combined Annotation–Dependent Depletion scores were available for a subset of variants located within the MBL and  $\beta$ -CASP domains. All variants in both domains ex-

**Table 2.** Diagnostic performance of the malignancy and autoimmunity risk scores. Diagnostic performance of the two risk scoring systems applied to predict malignancy and autoimmunity. Sensitivity, specificity, predictive values, and odds ratio were calculated at the optimal cut-off value for each score using Youden's index.

Metric	Malignancy score (Cut-off >4)	95% CI	Autoimmunity score (Cut-off >8)	95% CI
AUC	0.89	0.573–1.00 ( $p=0.014$ )	0.75	0.542–0.967 ( $p=0.019$ )
Sensitivity (%)	75	19.4–99.4	83.3	35.9–99.6
Specificity (%)	100	83.9–100.0	73.7	48.8–90.9
PPV (%)	100	79.4–99.1	50	30.29–69.72
NPV (%)	95.5	79.4–99.1	93.3	69.64–98.84
OR	100	3.37–2988.99	14	1.29–150.89
Youden index (J)	0.75	0.25–1.00	0.57	0.18–0.84

**AUC:** Area under the receiver operating characteristic curve, **CI:** Confidence interval, **PPV:** Positive predictive value, **NPV:** Negative predictive value, **OR:** Odds ratio.

ceeded the commonly accepted pathogenicity threshold (CADD  $\geq 20$ ) (15), indicating a 100% predicted deleterious rate for these domains. No CADD scores were available for variants in the C-terminal domain, primarily due to the presence of large deletions and complex mutations not compatible with current CADD scoring models. According to BayesDel (addAF) scores, 50% of the variants in the MBL domain and 33.3% of those in the  $\beta$ -CASP domain were predicted to be deleterious (threshold  $> 0.5$ ). Based on Eigen scores, all evaluated variants in the MBL and  $\beta$ -CASP domains exhibited values greater than zero, which is indicative of potential deleteriousness. This corresponds to a 100% predicted pathogenicity rate in both groups. No Eigen scores were available for variants located in the C-terminal domain, primarily due to structural or complex variant types that are beyond the scope of this prediction tool. All evaluated variants within the MBL and  $\beta$ -CASP domains showed DANN scores above 0.9, indicating a predicted deleteriousness rate of 100% in both domains. Variants from the C-terminal domain could not be assessed due to unavailable scores. According to the FATHMM-MKL model, all variants in the MBL domain and 66.7% of those in the  $\beta$ -CASP domain were predicted to be deleterious (threshold  $> 0.5$ ). Using the FATHMM-XF model, deleterious predictions were observed in 50.0% and 66.7% of variants within the MBL and  $\beta$ -CASP domains, respectively. Based on protein stability predictions ( $\Delta\Delta G \geq 1.0$ ), 50.0% of the evaluated variants in the MBL domain were classified as destabilizing, whereas none of the variants in the  $\beta$ -CASP domain met this threshold.

### Association Between *in Silico* Deleteriousness Scores and Clinical Features

To explore the association between *in silico* pathogenicity metrics and clinical phenotypes, we developed two separate minimal predictive scoring systems tailored for malignancy and autoimmunity. Each scoring system combined selected clinical and immunological features with *in silico* deleterious parameters.

For malignancy risk stratification, the scoring model included lymphadenopathy, diarrhea, skin lesions, low IgG levels,  $\Delta\Delta G \geq 1.0$ , BayesDel addAF  $> 0.5$ , and age  $> 60$  months. Each variable contributed one or two points depending on presumed clinical relevance, with a total possible score of 11. Receiver operating characteristic analysis in our cohort ( $n=25$ ) revealed an AUC of 0.89. At an optimal cut-off of  $> 4$  points, determined by Youden's index, the model achieved 75% sensitivity and 100% specificity, with a PPV of 100%, NPV of 95.5%, and an odds ratio of 100 (Table 2). These findings support the utility of this score in identifying patients at elevated risk of malignancy while minimizing false positives.

For autoimmunity prediction, a separate composite score was optimized using  $\Delta\Delta G \geq 1.0$ , BayesDel addAF  $> 0.5$ , low IgG, low CD19 expression, and the presence of skin lesions and pulmonary infections. At a cut-off of  $> 8$  points, the model demonstrated 83.3% sensitivity and 73.7% specificity, with a PPV of 50%, NPV of 93.14%, odds ratio of 14, and an AUC of 0.75 (Table 2). Although the discriminatory power was limited, this score may

serve as a high-sensitivity screening tool for identifying patients at risk of autoimmune manifestations.

Both scoring systems integrate clinical and computational evidence, offering a practical framework for early risk stratification in patients harboring hypomorphic *DCLRE1C* mutations.

## Discussion

This study represents one of the most comprehensive evaluations of patients with hypomorphic *DCLRE1C* mutations under study to date, integrating clinical, immunological, and bioinformatic data. While previous reports have described these variants in small patient cohorts, our findings further highlight the significant phenotypic heterogeneity associated with hypomorphic mutations in the *DCLRE1C* gene. Affected individuals presented with a wide clinical spectrum, ranging from recurrent infections and autoimmune manifestations to malignancies, whereas some patients exhibited only mild features of immune deficiency. This variability suggests that *DCLRE1C* mutations alone may not fully account for disease expression, and that additional genetic, environmental, or epigenetic modifiers likely play a role. Furthermore, the increasing application of *in silico* tools provides valuable insights into the functional consequences of these variants, supporting their utility in clinical diagnostics and variant interpretation.

The pronounced phenotypic variability observed among patients with similar *DCLRE1C* variants suggests that additional modifying factors likely contribute to disease expression. These may include genetic background, epigenetic regulation, or environmental influences such as infectious exposures and treatment differences. Similar modifying effects have been described in other inborn errors of immunity, where host genetics, epigenetic programming, and external triggers modulate clinical severity beyond the primary causal mutation (20,21). A deeper exploration of these modifiers—through multi-omic approaches and longitudinal environmental monitoring—will be essential to fully understand disease heterogeneity in hypomorphic *DCLRE1C* deficiency.

Our analysis revealed no statistically significant association between the localization of these variants within functional Artemis domains and the occurrence of au-

toimmunity or malignancy. Similarly, genotype distribution (homozygous vs. compound heterozygous) did not predict clinical severity with respect to these outcomes. These results align with previous reports documenting phenotypic variability among patients with structurally similar mutations (5,9,13). Moshous et al. (3,4) also noted that patients with identical or similar mutations may exhibit widely differing clinical courses, suggesting the involvement of additional modifying genetic or environmental factors. Hence, while domain-based classification offers structural insights, it appears insufficient for predicting disease progression or associated complications. These findings underscore the need for integrative approaches beyond sequence localization—incorporating immune profiling, environmental exposures, and multi-omic analyses—to better predict clinical outcomes in Artemis deficiency.

Previous studies have highlighted the susceptibility to recurrent respiratory and fungal infections in patients with hypomorphic variants, though the correlation between clinical features and mutation localization has remained largely unexplored. For instance, Volk et al. (5) and Hazar et al. (13) reported recurrent sinopulmonary infections and candidiasis as common manifestations, particularly in early-onset cases. In our study, a statistically significant association was observed between C-terminal domain mutations and a higher frequency of pulmonary infections. This may reflect the functional role of the C-terminal region in facilitating nuclear localization signals and protein stability, suggesting that alterations in this domain impair mucosal immune defense more severely than mutations in catalytic regions. In addition to these findings, other clinical manifestations such as diarrhea, otitis, fever, growth retardation, malignancy, and survival status also differed significantly across domain groups. Otitis and growth retardation, notably, were observed only in patients with C-terminal domain mutations, further supporting domain-specific clinical vulnerability. Moreover, candidiasis was significantly more frequent in patients with compound heterozygous variants compared to homozygous individuals (42.9% vs. 2.9%,  $p=0.001$ ), indicating that allelic diversity may exacerbate susceptibility independently of domain localization. Although candidiasis has been described in Artemis-deficient individuals (10), our data indicate that allelic diversity may exacerbate susceptibility, potentially through additive or synergistic loss of function (9). This observation warrants further investigation in functional assays and may have implications

for early clinical monitoring in compound heterozygous patients.

Immunological analyses revealed domain-specific alterations in lymphocyte subsets and immune function. Notably, NK cells were reduced exclusively in patients with C-terminal domain mutations (33.3%; 3/9), while they remained normal in patients harboring variants in the MBL or  $\beta$ -CASP domains ( $p=0.028$ ). Although no major NK cell abnormalities have been consistently reported in patients with the hypomorphic *DCLRE1C* variant, this finding may reflect subtle defects in hematopoietic regulation or lineage development in the context of structurally disruptive variants. Previous studies, such as Moshous et al. (4), have reported variable T- and B-cell abnormalities, but NK cell dysregulation has not been systematically analyzed. Similarly, CD25 activation, which reflects T cell proliferative capacity, decreased in most patients across domains. This aligns with findings by Rohr et al. (6) and Ijspeert et al. (7), who demonstrated impaired T cell responses in patients with splicing or deletional *DCLRE1C* variants. These data support the notion that even hypomorphic variants can lead to functional T cell compromise despite partial V(D)J recombination activity. These immunophenotypic differences across domains may have important clinical implications. The selective reduction of NK cells in patients with C-terminal variants could suggest a role for this region in hematopoietic lineage stability or NK cell development, potentially contributing to increased susceptibility to viral infections or malignancy. Similarly, the consistent decrease in CD25 activation across MBL and C-terminal variants reflects impaired T-cell proliferative capacity, which may compromise immune surveillance and predispose to autoimmunity or lymphoproliferation. The depletion of naïve B cells in MBL variants highlights the catalytic domain's importance for B-cell maturation and bone marrow output, consistent with impaired V(D)J recombination activity. Taken together, these findings support the concept that distinct structural regions of Artemis differentially influence lymphocyte subsets, providing mechanistic clues to the heterogeneous clinical outcomes observed in hypomorphic *DCLRE1C* deficiency.

The most striking immunological finding was the depletion of naïve B-cells. All patients with MBL domain mutations exhibited reduced naïve B-cells (100%), whereas those with C-terminal or  $\beta$ -CASP variants displayed mixed patterns. Since naïve B-cells are a critical mark-

er of bone marrow output and immune reconstitution, this domain-specific depletion suggests that catalytic domain integrity may be particularly essential for B cell development. These results expand upon prior observations by Volk et al. (5) and highlight the diagnostic value of detailed immunophenotyping in Artemis-deficient cohorts.

Our *in silico* analysis demonstrated consistently high pathogenicity scores for missense variants located in the MBL and  $\beta$ -CASP domains, with all assessed mutations surpassing deleteriousness thresholds for CADD, DANN, and Eigen scores. This is consistent with the catalytic importance of these regions, where even subtle amino acid substitutions may severely impair Artemis function. In contrast, variants located in the C-terminal domain were not amenable to assessment using most computational models, largely due to their complex nature (e.g., large deletions or splice-disrupting mutations). This highlights a technical limitation of current *in silico* tools, which remain optimized for simple missense changes rather than structural alterations or non-coding variants (14,15).

Protein stability analysis using  $\Delta\Delta G$  values (PremPS) further reinforced these findings: half of the variants in the MBL domain were predicted to destabilize the protein structure ( $\Delta\Delta G \geq 1.0$ ), whereas no such destabilization was observed in  $\beta$ -CASP domain variants. This discrepancy underscores that not all high-scoring *in silico* predictors necessarily translate into structural damage, reaffirming the importance of integrating multiple tools and domains of evidence. Similar approaches have recently been validated in other primary immunodeficiencies, such as ISG15 and ZBTB24-related ICF (immunodeficiency, centromeric instability, and facial anomalies) syndromes (16,18), supporting the broader utility of *in silico*-guided pathogenicity frameworks in rare immune disorders.

The incorporation of *in silico* predictors into the model is particularly noteworthy, as these tools are increasingly being used to reclassify VUS in primary immunodeficiencies (16,17). Building on this trend, our study introduces a novel composite scoring system tailored to Artemis deficiency. To our knowledge, no comparable composite scoring system has been proposed in the context. Existing studies tend to describe qualitative associations or focus solely on molecular characterization (5,13), without integrating predictive algorithms into patient management strategies.



To improve clinical risk stratification in hypomorphic *DCLRE1C* variant carriers, we developed a minimal predictive score incorporating both clinical and *in silico* variables. Although preliminary, the model demonstrated modest discriminatory power for malignancy and autoimmunity, with particularly high sensitivity for malignancy at a threshold of >4 points. Although specificity was limited, the high sensitivity suggests that the score may be useful as a screening tool for early risk stratification. In interpreting these results, it is important to note that variable weightings were intentionally guided by presumed clinical relevance rather than purely statistical optimization. Features such as lymphadenopathy and hypogammaglobulinemia were prioritized, given their established links with immunodeficiency-associated malignancy, whereas *in silico* parameters were assigned lower weights reflecting their exploratory role. Likewise, the malignancy cut-off of >4 points was chosen not only by statistical optimization (Youden index) but also because it represents the co-occurrence of several clinically meaningful abnormalities. This dual rationale strengthens the interpretability of the proposed score despite its exploratory nature.

### Study Limitations

Although this study offers a detailed picture of the clinical impact of hypomorphic *DCLRE1C* variants, several constraints must be acknowledged. First, the sample size is relatively small, and a substantial proportion of cases were extracted from the literature, introducing potential publication bias and inter-center diagnostic heterogeneity. This limitation must also be considered in light of the exceptional rarity of hypomorphic *DCLRE1C* deficiency: to date, only 16 hypomorphic variants have been reported in 41 patients worldwide. Consequently, while our findings provide a useful preliminary framework, the limited cohort size reduces statistical power and precludes external validation. Future prospective, multi-center collaborations will therefore be indispensable to confirm and refine the predictive models.

Second, the inclusion of both institutional and literature-derived cases may still introduce heterogeneity in clinical assessments. However, to mitigate this effect, we applied strict inclusion criteria, excluded literature cases

with substantial missing data, and restricted inferential analyses to a genetically homogeneous subgroup. Despite these steps, residual heterogeneity remains a potential source of bias.

Third, the *in silico* pathogenicity and protein stability predictions incorporated into our analysis have not yet been validated by functional assays such as DNA repair activity or V(D)J recombination studies. Although prior reports have demonstrated functional impairment in hypomorphic *DCLRE1C* variants, our predictive models remain inferential until corroborated by direct experimental validation.

In addition, this study may be subject to selection bias, as literature-derived cases were included based on available data quality, which may not fully represent the entire spectrum of hypomorphic *DCLRE1C* deficiency. Missing data for certain clinical and immunological parameters further limited statistical power and comparability across groups. Finally, the retrospective design inherently introduces heterogeneity in diagnostic assessments and follow-up practices across centers, which should be considered when interpreting the results.

### Conclusion

Hypomorphic *DCLRE1C* variants exhibit broad clinical variability, and current structural or genotypic classifications alone appear insufficient for precise risk stratification. Integrating domain-restricted *in silico* metrics with clinical parameters modestly improves the prediction of malignancy risk and may also provide insight into overall disease severity. Our findings suggest that combining computational predictions with clinical parameters can facilitate the earlier identification of high-risk patients and guide therapeutic decision-making—particularly in resource-limited settings where functional assays are unavailable. Nonetheless, prospective, multi-center validation and functional studies are essential before these approaches can be implemented in clinical practice.

**Ethical Approval:** The study was approved by the Necmettin Erbakan University Clinical Research Ethics Committee on May 23, 2025, with the decision number 5789.

**Informed Consent:** N.A.

**Peer-review:** Externally peer-reviewed

**Author Contributions:** Concept – S.K., M.A.K., İ.R.; Design – S.K., M.A.K., A.Ş.; Supervision – İ.R., S.Ke., Ş.N.G.; Data Collection and/or Processing – S.K., M.A.K., A.Ş., T.D., Ş.N.G., S.Ke.; Analysis and/or Interpretation – S.K., M.A.K., A.Ş., T.D.; Literature Review – S.K., M.A.K., T.D.; Writer – S.K., M.A.K., A.Ş., T.D.; Critical Reviews – M.A.K., Ş.N.G., S.Ke., İ.R.

**Conflict of Interest:** The authors declare no conflict of interest.

**Financial Disclosure:** The authors declared that this study has received no financial support.

**Acknowledgment:** The authors have no acknowledgments to declare.









**Scientific Presentation:** The preliminary data of this study were presented as an abstract at the 11th Clinical Immunology Congress, held in Antalya, Türkiye, on April 9–12, 2025, where the study received the third prize for oral presentation.

## References

- 1 de Villartay, J. P. Congenital defects in V(D)J recombination. *Br Med Bull.* 2015;114(1):157-67. [\[CrossRef\]](#)
- 2 Buckley RH, Schiff RI, Schiff SE, Markert ML, Williams LW, Harville TO, et al. Human severe combined immunodeficiency: genetic, phenotypic, and functional diversity in one hundred eight infants. *J Pediatr.* 1997;130(3):378-87. [\[CrossRef\]](#)
- 3 Moshous D, Callebaut I, de Chasseval R, Corneo B, Cavazana-Calvo M, Le Deist F, et al. Artemis, a novel DNA double-strand break repair/V(D)J recombination protein, is mutated in human severe combined immune deficiency. *Cell.* 2001;105(2):177-86. [\[CrossRef\]](#)
- 4 Moshous D, Pannetier C, Chasseval Rd Rd, Deist Fl Fl, Cavazana-Calvo M, Romana S, et al. Partial T and B lymphocyte immunodeficiency and predisposition to lymphoma in patients with hypomorphic mutations in Artemis. *J Clin Invest.* 2003;111(3):381-7. [\[CrossRef\]](#)
- 5 Volk T, Pannicke U, Reisli I, Bulashevskaya A, Ritter J, Björkman A, et al. *DCLRE1C* (ARTEMIS) mutations causing phenotypes ranging from atypical severe combined immunodeficiency to mere antibody deficiency. *Hum Mol Genet.* 2015;24(25):7361-72. [\[CrossRef\]](#)
- 6 Rohr J, Pannicke U, Döring M, Schmitt-Graeff A, Wiech E, Busch A, et al. Chronic inflammatory bowel disease as key manifestation of atypical ARTEMIS deficiency. *J Clin Immunol.* 2010;30(2):314-20. [\[CrossRef\]](#)
- 7 Ijspeert H, Lankester AC, van den Berg JM, Wiegant W, van Zelm MC, Weemaes CM, et al. Artemis splice defects cause atypical SCID and can be restored *in vitro* by an antisense oligonucleotide. *Genes Immun.* 2011;12(6):434-44. [\[CrossRef\]](#)
- 8 Bajin İY, Ayvaz DÇ, Ünal S, Özgür TT, Çetin M, Gümrük F, et al. Atypical combined immunodeficiency due to Artemis defect: a case presenting as hyperimmunoglobulin M syndrome and with LGLL. *Mol Immunol.* 2013;56(4):354-7. [\[CrossRef\]](#)
- 9 Lee PP, Woodbine L, Gilmour KC, Bibi S, Cale CM, Amrolia PJ, et al. The many faces of Artemis-deficient combined immunodeficiency - Two patients with *DCLRE1C* mutations and a systematic literature review of genotype-phenotype correlation. *Clin Immunol.* 2013;149(3):464-74. [\[CrossRef\]](#)
- 10 Fevang B, Fagerli UM, Sorte H, Aarset H, Hov H, Langmyr M, et al. Runaway train: a leaky radiosensitive SCID with skin lesions and multiple lymphomas. *Case Reports Immunol.* 2018;2053716. [\[CrossRef\]](#)
- 11 Nahum A, Somech R, Shubinsky G, Levy J, Broides A. Unusual phenotype in patients with a hypomorphic mutation in the *DCLRE1C* gene: IgG hypergammaglobulinemia with IgA and IgE deficiency. *Clin Immunol.* 2020;213:108366. [\[CrossRef\]](#)
- 12 Meric Z, Gemici Karaaslan B, Yalcin Gungoren E, Bektas Hortoglu M, Cavas T, Aydemir S, et al. Artemis deficiency: A large cohort including a novel variant with increased radiosensitivity. *Pediatr Allergy Immunol.* 2024;35(6):e14171. [\[CrossRef\]](#)
- 13 Hazar E, Karaselek MA, Kapakli H, Dogar O, Kuccuk Turk S, Uygun V, et al. Variable clinical presentation of hypomorphic *DCLRE1C* deficiency from childhood to adulthood. *Pediatr Allergy Immunol.* 2024;35(10):e14260. [\[CrossRef\]](#)
- 14 Tavtigian SV, Greenblatt MS, Lesueur F, Byrnes GB; IARC Unclassified Genetic Variants Working Group. In silico analysis of missense substitutions using sequence-alignment based methods. *Hum Mutat.* 2008;29(11):1327-36. [\[CrossRef\]](#)
- 15 Kircher M, Witten DM, Jain P, O'Roak BJ, Cooper GM, Shendure J. A general framework for estimating the relative pathogenicity of human genetic variants. *Nat Genet.* 2014;46(3):310-5. [\[CrossRef\]](#)
- 16 Napoleao SMDs, Salgado RC, Ferreira JFS, de Barros Dorna M, de Moura TCL, França TT, et al. First Brazilian case report of unrelated patients with identical ISG15 mutation. *J Clin Immunol.* 2024;45(1):21. [\[CrossRef\]](#)
- 17 Vorsteveld EE, Van der Made CI, Smeekens SP, Schuur-Hoeijmakers JH, Astuti G, Diepstra H, et al. Clinical exome sequencing data from patients with inborn errors of immunity: Cohort level diagnostic yield and the benefit of systematic reanalysis. *Clin Immunol.* 2024;268:110375. [\[CrossRef\]](#)
- 18 Duran T, Karaselek MA, Kuccuk Turk S, Gul Y, Sahin A, Guner SN, et al. Investigation of transcription factor and cytokine gene expression levels in helper T cell subsets among Turkish patients diagnosed with ICF2 (novel ZBTB24 gene

- variant) and ICF3 (CDCA7 variant) syndrome. *J Clin Immunol.* 2024;45(1):16. [\[CrossRef\]](#)
- 19 Jenni R, Klaa H, Khamessi O, Chikhaoui A, Najjar D, Ghedira K, et al. Clinical and genetic spectrum of Ataxia Telangiectasia Tunisian patients: Bioinformatic analysis unveil mechanisms of ATM variants pathogenicity. *Int J Biol Macromol.* 2024;278(Pt 1):134444. [\[CrossRef\]](#)
- 20 Poli MC, Aksentijevich I, Bousfiha AA, Cunningham-Rundles C, Hambleton S, Klein C, et al. Human inborn errors of immunity: 2024 update on the classification from the International Union of Immunological Societies Expert Committee. *J Hum Immun.* 2025;1(1):e20250003. [\[CrossRef\]](#)
- 21 IJspeert H, Edwards ESJ, O'Hehir RE, Dalm VASH, van Zelm MC. Update on inborn errors of immunity. *J Allergy Clin Immunol.* 2025;155(3):740-51. [\[CrossRef\]](#)
- 22 Schubach M, Maass T, Nazaretyan L, Röner S, Kircher M. CADD v1.7: using protein language models, regulatory CNNs and other nucleotide-level scores to improve genome-wide variant predictions. *Nucleic Acids Res.* 2024;52(D1):D1143-54. [\[CrossRef\]](#)
- 23 Chen Y, Lu H, Zhang N, Zhu Z, Wang S, Li M. PremPS: Predicting the impact of missense mutations on protein stability. *PLoS Comput Biol.* 2020;16(12):e1008543. [\[CrossRef\]](#)
- 24 DeLong ER, DeLong DM, Clarke-Pearson DL. Comparing the areas under two or more correlated receiver operating characteristic curves: a nonparametric approach. *Biometrics.* 1988;44(3):837-45. [\[CrossRef\]](#)
- 25 Meng EC, Goddard TD, Pettersen EF, Couch GS, Pearson ZJ, Morris JH, et al. UCSF ChimeraX: tools for structure building and analysis. *Protein Sci.* 2023;32(11):e4792. [\[CrossRef\]](#)
- 26 Clamp M, Cuff J, Searle SM, Barton GJ. The Jalview Java alignment editor. *Bioinformatics.* 2004;20(3):426-7. [\[CrossRef\]](#)
-

# Dose-Dependent Effects of Maternal Vitamin D<sub>3</sub> on Offspring IL-6 and IL-1 $\beta$ in a Rat Model

Kurnia Maidarmi Handayani<sup>1</sup> , Widia Sari<sup>2</sup> , Ghaniyyatul Khudri<sup>3</sup> , Alief Dhuha<sup>2</sup> , Rifkind Malik<sup>1</sup> , Melya Susanti<sup>2</sup> , Laura Zeffira<sup>4</sup> , Annisa Lidra Maribeth<sup>5</sup> 

<sup>1</sup>Universitas Baiturrahmah Faculty of Medicine, Department of Biochemistry and Nutrition, Padang, Indonesia; <sup>2</sup>Universitas Baiturrahmah Faculty of Medicine, Department of Anatomy, Physiology, and Radiology, Padang, Indonesia; <sup>3</sup>Universitas Baiturrahmah Faculty of Medicine, Department of Histology and Immunology, Padang, Indonesia; <sup>4</sup>Universitas Baiturrahmah Faculty of Medicine, Department of Pediatrics, Padang, Indonesia; <sup>5</sup>Universitas Baiturrahmah Faculty of Medicine, Department of Public Health, Padang, Indonesia

## Abstract

**Objective:** Vitamin D<sub>3</sub> is increasingly recognized for its role in immune regulation, particularly in modulating proinflammatory cytokines during early development. This study aimed to investigate the dose-dependent effects of maternal vitamin D<sub>3</sub> supplementation during pregnancy and lactation on offspring inflammatory cytokine levels, focusing on interleukin-1 beta (IL-1 $\beta$ ) and interleukin-6 (IL-6).

**Materials and Methods:** Twelve pregnant Sprague-Dawley rats were randomly assigned to four groups: one control and three treatment groups receiving vitamin D<sub>3</sub> at 62, 415 and 663 IU/kg body weight/day, respectively. Supplementation was administered orally from gestation day 1 to postnatal day 23. Offspring were subjected to an acute inflammatory challenge via lipopolysaccharide injection, after which induration size was measured. Serum levels of vitamin D<sub>3</sub>, IL-1 $\beta$  and IL-6 in six offspring per group were quantified using enzyme-linked immunosorbent assay (ELISA). Data were analyzed by one-way analysis of variance (ANOVA) followed by the least significant difference (LSD) post hoc test.

**Results:** No significant difference was observed in post-injection induration size between groups ( $p>0.05$ ). However, the group receiving 663 IU/kg/day vitamin D<sub>3</sub> exhibited significantly higher serum vitamin D<sub>3</sub> levels ( $21.15 \pm 15.8$  ng/mL) compared with controls ( $3.56 \pm 3.20$  ng/mL,  $p=0.023$ ), along with significantly lower IL-1 $\beta$  level ( $33.5 \pm 25.44$  pg/mL,  $p<0.001$ ). IL-6 levels showed a similar decreasing trend. Serum vitamin D<sub>3</sub> was moderately and inversely correlated with IL-1 $\beta$  ( $r = -0.43$ ,  $p=0.042$ ).

**Conclusion:** Maternal vitamin D<sub>3</sub> supplementation during gestation and lactation elevated serum vitamin D<sub>3</sub> and suppressed IL-1 $\beta$  and IL-6 levels in offspring, suggesting a dose-dependent immunomodulatory effect. These findings highlight the potential of maternal vitamin D<sub>3</sub> status to influence inflammatory responses during early life.

**Keywords:** Inflammation, IL-1 $\beta$  and IL-6, maternal supplementation, vitamin D<sub>3</sub>

## Correspondence

Widia Sari

## E-mail

widia\_sari@fk.unbrah.ac.id

## Received

June 17, 2025

## Accepted

October 2, 2025

## Published

November 19, 2025

## Suggested Citation

Handayani KM, Sari W, Khudri G, Dhuha A, Malik R, Susanti M, et al. Dose-dependent effects of maternal vitamin D<sub>3</sub> on offspring IL-6 and IL-1 $\beta$  in a rat model. Turk J Immunol. 2025;13(3):158-68.

## DOI

10.36519/TJI.2025.761



This work is licensed under the Creative Commons Attribution-NonCommercial-Non-Derivatives 4.0 International License (CC BY-NC-ND 4.0).

## Introduction

Vitamin D<sub>3</sub> deficiency is a significant health concern during pregnancy and lactation due to its potential long-term effects on both maternal and neonatal health (1,2). Vitamin D<sub>3</sub> supports calcium homeostasis, immune development, and inflammation regulation (3). Low maternal vitamin D<sub>3</sub> levels are associated with an increased risk of pregnancy complications, including preeclampsia and gestational diabetes, and studies have shown higher rates of neonatal asphyxia and immune dysregulation in infants born to vitamin D<sub>3</sub>-deficient mothers (4). Boskabadi et al. (5) reported a higher prevalence of respiratory complications in premature infants of vitamin D<sub>3</sub>-deficient mothers, highlighting the link between maternal vitamin D<sub>3</sub> status and neonatal outcomes (5). Furthermore, maternal deficiency reduces neonatal vitamin D<sub>3</sub> levels, increasing susceptibility to immune dysregulation and excessive inflammation (6,7).

During pregnancy and lactation, vitamin D<sub>3</sub> is transferred to the fetus and infant through the placenta and breast milk. It contributes to modulating immune responses by balancing cytokine production, thereby reducing the risk of allergies, chronic inflammation, and other immune-mediated conditions in early life (8). Studies have demonstrated that adequate maternal vitamin D<sub>3</sub> levels during pregnancy decrease the risk of chronic inflammation in infants and promote immune balance, thereby lowering the likelihood of allergic diseases and asthma (9,10). Notably, vitamin D<sub>3</sub> supplementation during pregnancy and lactation has been shown to promote immune homeostasis and reduce inflammation in offspring (9,11).

Vitamin D<sub>3</sub> deficiency has been associated with increased levels of pro-inflammatory cytokines, particularly interleukin-6 (IL-6) and interleukin-1 beta (IL-1 $\beta$ ), which are implicated in the development of inflammatory disorders in children (12). Although vitamin D<sub>3</sub> is widely recognized for its role in immune modulation, limited research has explored its dose-dependent impact during both pregnancy and lactation on offspring cytokine responses to acute inflammatory stimuli (13). To address this gap, the present study investigated the immunomodulatory effects of varying doses of maternal vitamin D<sub>3</sub> supplementation administered throughout gestation and lactation, with a focus on IL-6 and IL-1 $\beta$  expression in the offspring. A rat model is used to simulate maternal and offspring interactions and to support the development of early prevention strategies for inflammatory diseases.

No preclinical study has simultaneously implemented prenatal (gestational & lactational) vitamin D<sub>3</sub> supplementation, followed by acute lipopolysaccharide (LPS)-induced inflammation in offspring, with serum measurement of IL-6 and IL-1 $\beta$  at the 3-hour post-injection timepoint. Prior studies have focused on single markers (e.g., tumor necrosis factor alpha [TNF- $\alpha$ ] without LPS challenge), organ-specific inflammation, or descriptive immune modulation without acute challenge. Our design fills this critical knowledge gap by targeting downstream cytokine responses in a time-sensitive, systemic inflammatory context.

## Materials and Methods

### Experimental Animals

Female founder (F0) *Rattus norvegicus* (Sprague-Dawley strain) rats were used as experimental animals. The animals were housed in a controlled environment at a temperature of 22  $\pm$  2°C, with a relative humidity of 40–70% and a 12/12-hour light/dark cycle. They had unrestricted access to water and were provided with standard feed (30 grams/day) *ad libitum*. The study was conducted at the Experimental Animal Laboratory, Faculty of Medicine, Universitas Baiturrahmah, West Sumatra, Indonesia, in accordance with the ARRIVE (Animal Research: Reporting *In Vivo* Experiments) guidelines. All experimental procedures were approved by the Research Ethics Committee of the Faculty of Medicine, Universitas Baiturrahmah, West Sumatra, Indonesia (Approval No. 040/ETIK-FKUNBRAH/03/07/2024).

### Study Design

This experimental *in vivo* study included 12 female Sprague Dawley rats (150–200 g, 8–12 weeks old). The schematic flow of the study is shown in Figure 1. All founder rats underwent a 14-day acclimatization phase before any intervention. After a 14-day acclimatization, founder rats (F0) were paired with males (1 male: 2 females per cage). Pregnancy was confirmed by the presence of a vaginal plug, marking gestational day 1, after which pregnant rats were housed individually (14).

Pregnant rats were randomly assigned to four groups. Three groups received standard feed diet combined with vitamin D<sub>3</sub> (Cat. No. 020734; SUPRA FERBINDO FARMA®, Jakarta, Indonesia) supplementation administered orally via gavage, with each group assigned to a specific supplementation dose ([Supplement 1](#)). Group A received



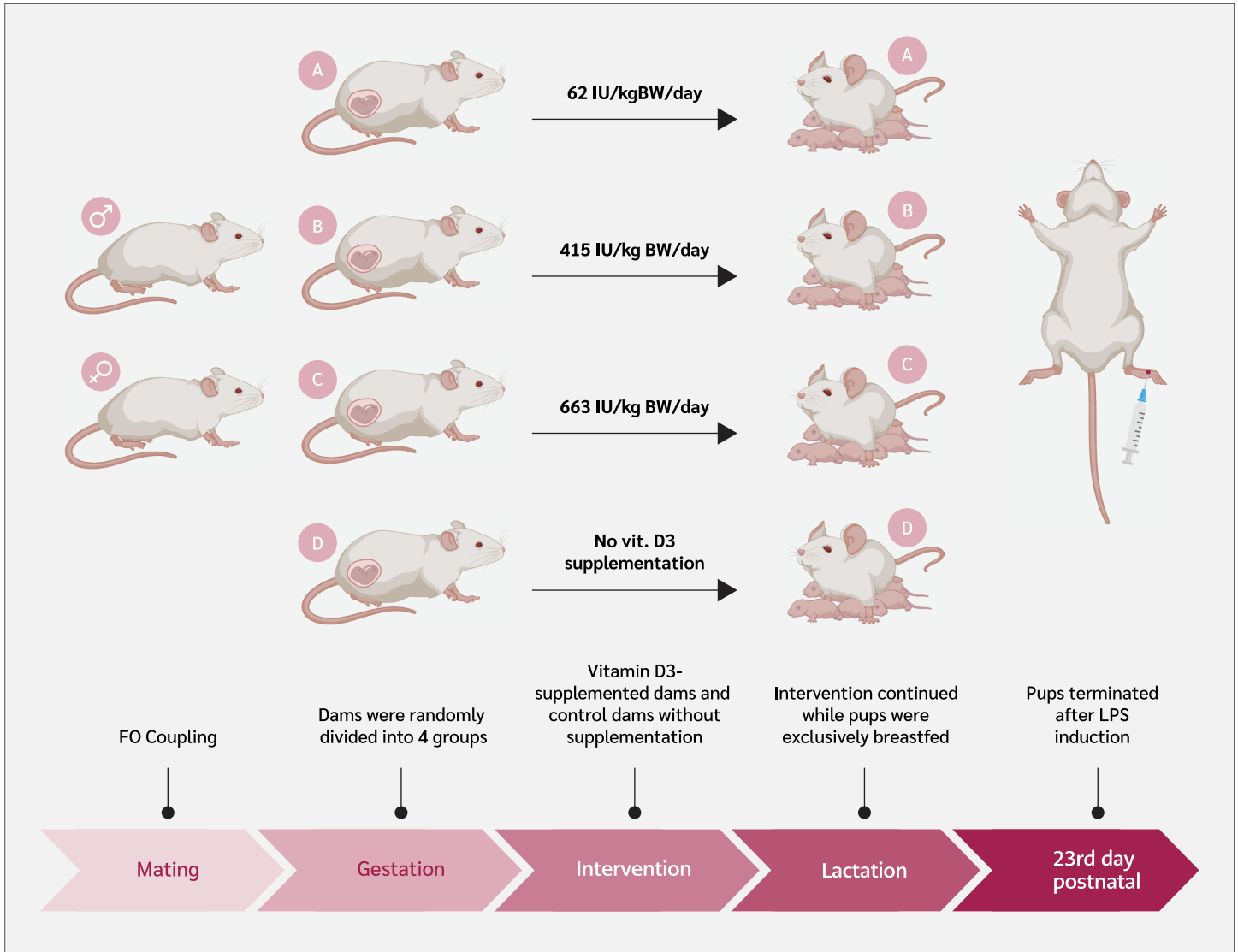


**Figure 1.** Vitamin D<sub>3</sub> supplementation and experimental intervention design (created with BioRender®, Canada; n=6 per group)

62 IU/kg body weight (BW)/day of vitamin D<sub>3</sub>, Group B received 415 IU/kg BW/day of vitamin D<sub>3</sub>, and Group C received 663 IU/kg BW/day of vitamin D<sub>3</sub>. The vitamin D supplementation was provided separately from the standard diet to ensure accurate dosage administration. Group D served as the control and received no vitamin D<sub>3</sub> supplementation.

The supplementation doses were adjusted to experimental requirements using the Animal Equivalent Dose (AED) conversion formula based on the Km ratio. The human-to-rat dose conversion formula was:

$$\text{AED (mg/kg)} = \text{Human dose (mg/kg)} \times \text{Km ratio},$$

Where the Km value for rats is 6.2, and then the results are converted to IU/kg BW. Accordingly, 62 IU/kg BW/day in rats corresponds to 600 IU/day in humans, 415 IU/kg BW/day corresponds to 4000 IU/day, and 663 IU/kg BW/day corresponds to 6400 IU/day. These adjustments ensured the administered doses were physiologically relevant across species.

Rats received 30 grams of feed daily *ad libitum* and vitamin D<sub>3</sub> administered by oral gavage from gestational day 1 to postnatal day 23. Daily feed intake was measured, including spilled pellets collected from the sawdust. Before weaning on postnatal day 23, six offspring (according to Federer's formula) with similar body weights

per group were selected randomly, regardless of sex, for analysis of serum vitamin D<sub>3</sub> levels, acute inflammation response, edema, and serum IL-1 $\beta$  and IL-6 levels.

### Inflammation Induction

On postnatal day 23, inflammation was induced in each offspring with a 100  $\mu$ g/100  $\mu$ L LPS (Cat. No. L2630-10MG; Sigma-Aldrich®, Darmstadt, Germany) injection into the paw (0.1 mL). The inflammatory response was assessed by measuring induration 3 hours post-injection, as described by Vajja (15), who found that pro-inflammatory cytokines, such as IL-6 and IL-1 $\beta$ , increased at 3 hours post-LPS injection.

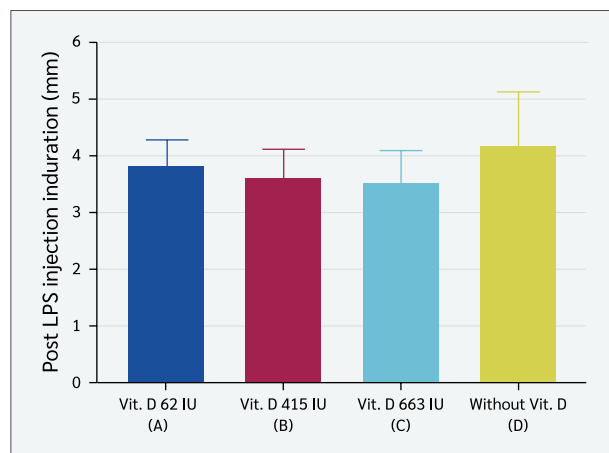


**Figure 2.** Mean induration diameter (mm) of offspring after lipopolysacchride (LPS) induction (3 hours) (one-way ANOVA,  $p=0.37$ ;  $n=6$  per group).

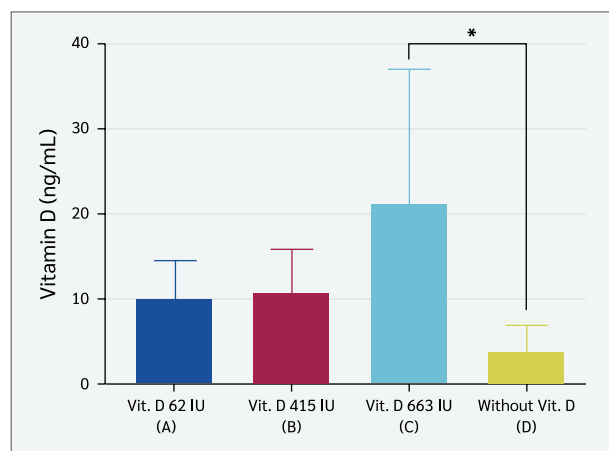


**Figure 3.** Serum vitamin D<sub>3</sub> levels (ng/mL) in offspring across the four treatment groups (one-way ANOVA,  $p=0.031$ ).

\*Data are presented as mean  $\pm$  SD ( $n=6$  per group).  $p=0.023$  compared with the control group.

### Sample Collection and Biochemical Analysis

Blood samples were collected from the left ventricle. Approximately 2 mL of blood was collected directly from the heart following euthanasia, which was performed using intraperitoneal administration of ketamine at a dose of 100 mg/kg BW. The collected blood was centrifuged at 5000 rpm for 10 minutes to separate the serum. The supernatant was transferred to a new tube and stored at  $-20^{\circ}\text{C}$ . Serum vitamin D<sub>3</sub> concentrations were measured using the competitive enzyme-linked immunosorbent assay (ELISA) kit (Cat. No. E-EL-0014; Elabscience®, USA). The detection limit for vitamin D<sub>3</sub> was 0.94 ng/mL, and the intra-assay coefficients were  $<10\%$ . IL-1 $\beta$  and IL-6 concentrations were assessed using sandwich ELISA kits (Cat. No. E-EL-R0012; Elabscience®, Houston, TX, USA for IL-1 $\beta$  and Cat. No. E-EL-R0015; Elabscience®, Houston, TX, USA for IL-6). The intra-assay coefficients of variation for IL-1 $\beta$  were  $<10\%$  with a sensitivity of 18.75 pg/mL, while for IL-6, the intra-assay coefficients of variation were  $<10\%$  with a sensitivity of 7.5 pg/mL.

### Statistical Analysis

Data were analyzed using IBM SPSS Statistics for Windows, version 26.0 (IBM Corp., Armonk, NY, USA). The Shapiro-Wilk test was used to assess data normality, and Levene's test was used to evaluate homogeneity of variances. For normally distributed data, two-way analysis of variance (ANOVA) followed by least significant difference (LSD) post hoc testing was performed. For non-normally distributed data, the Kruskal-Wallis test followed by the Mann-Whitney post hoc test was applied. Correlations between variables were examined using Pearson's correlation coefficient. All results were expressed as mean  $\pm$  standard deviation (SD), and statistical significance was set as  $p<0.05$ .

## Results

### Post-LPS Induction Induration Response

Inflammatory induction was performed by injecting LPS subcutaneously into the plantar surface of the offspring's paw, and induration was measured 3 hours post-injection. The induration measurements (mm) are presented in the graph below (Figure 2). No significant differences in induration diameter were observed among the groups following LPS injection (one-way ANOVA,  $p>0.05$ ).

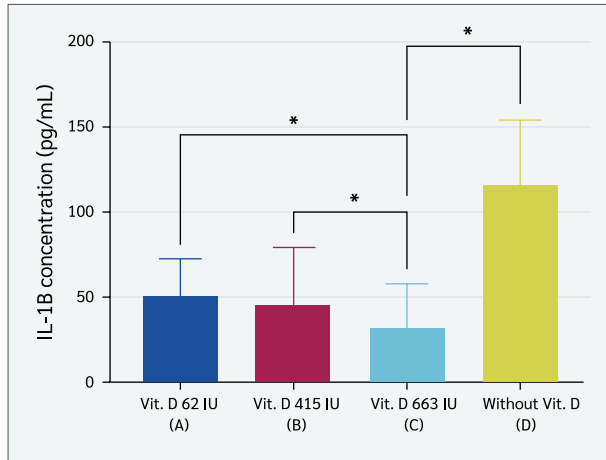


**Figure 4.** Serum interleukin-1 $\beta$  (IL-1 $\beta$ ) levels (pg/mL) in the four offspring groups (one-way ANOVA,  $p<0.001$ ; post hoc LSD test,  $p=0.03$ ;  $p=0.02$ ;  $p<0.001$ ).

\*Data are presented as mean  $\pm$  SD (n=6 per group).  $p\leq 0.05$  compared with the control group.

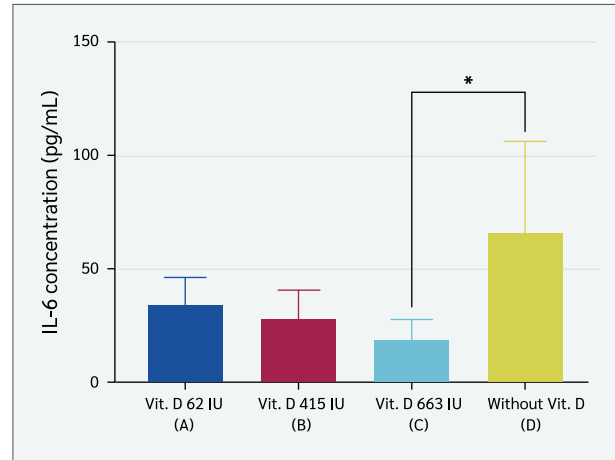


**Figure 5.** Serum interleukin-6 (IL-6) levels (pg/mL) in the four offspring groups (Kruskal-Wallis test,  $p=0.037$ ).

\*Data are presented as mean  $\pm$  SD (n=6 per group).  $p=0.023$  compared with the control group.

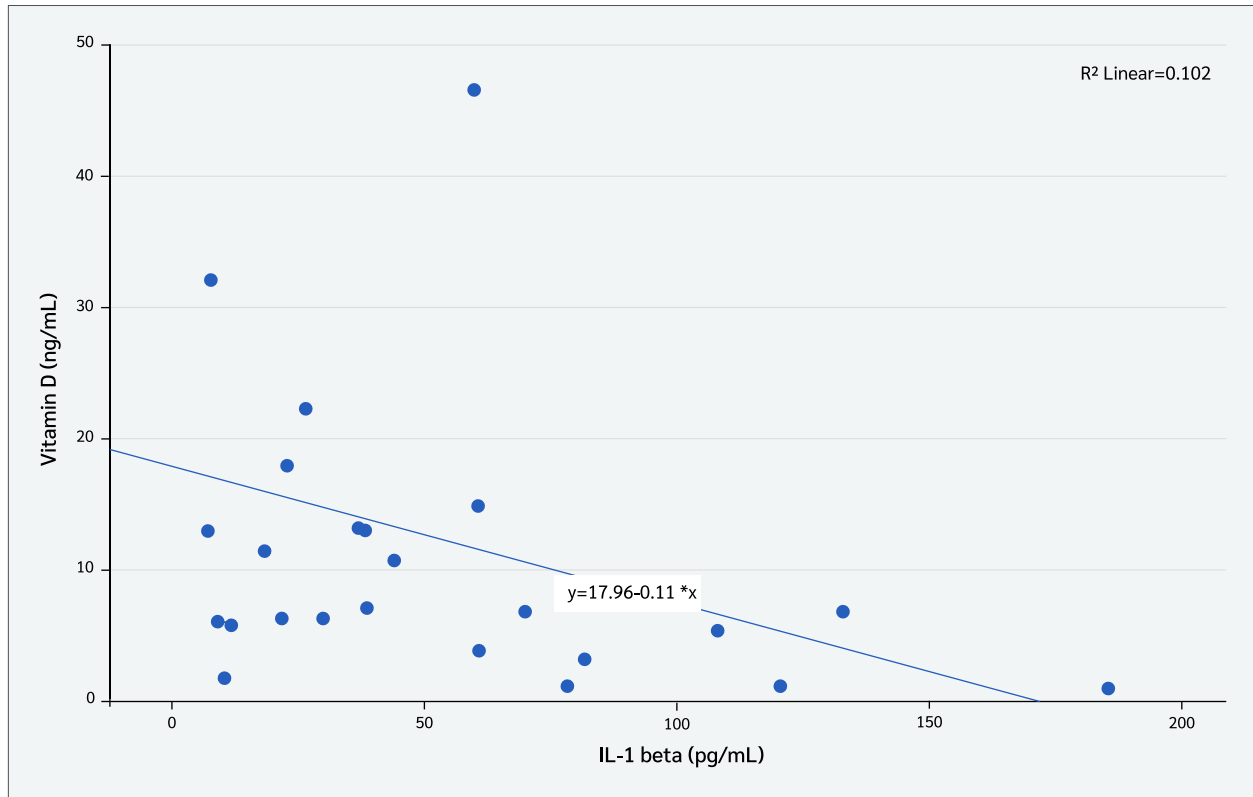


**Figure 6.** Correlation between serum vitamin D<sub>3</sub> levels (ng/mL) and serum interleukin-1 $\beta$  (IL-1 $\beta$ ) concentrations (pg/mL) (Pearson's correlation,  $r=-0.43$ ,  $p=0.042$ ; n=24)

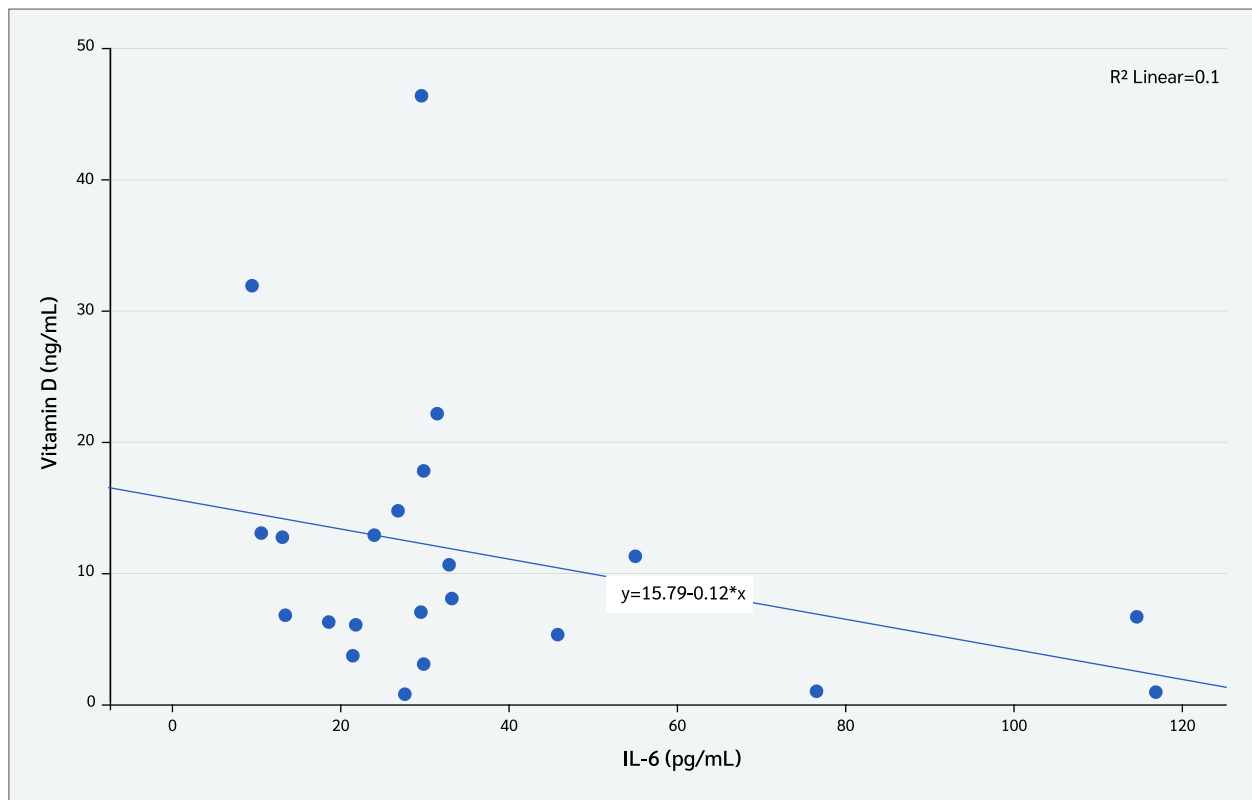


**Figure 7.** Correlation between serum vitamin D<sub>3</sub> levels (ng/mL) and serum interleukin-6 (IL-6) concentrations (pg/mL) (Pearson's correlation,  $r=-0.31$ ,  $p=0.153$ ;  $n=24$ ).

### Serum Vitamin D<sub>3</sub> Levels

Serum vitamin D<sub>3</sub> levels (ng/mL) in the four groups were assessed on day 23 after LPS induction. This study showed a significant difference in the mean levels (Figure 3) between the group of rats receiving 663 IU/kg BW of vitamin D<sub>3</sub> ( $21.15 \pm 15.8$  ng/mL) and the group that did not receive vitamin D<sub>3</sub> ( $3.56 \pm 3.20$  ng/mL) (one-way ANOVA, post hoc LSD,  $p=0.023$ ).

### Serum IL-1 $\beta$ level

Group C exhibited the lowest serum IL-1 $\beta$  levels, with a mean concentration of  $33.5 \pm 25.44$  pg/mL (Figure 4). Statistical analysis (one-way ANOVA,  $p<0.001$ ) showed IL-1 $\beta$  levels were significantly higher in low-dose vitamin D<sub>3</sub> groups (62 IU and 415 IU) than in the 663 IU group (LSD post hoc,  $p=0.03$ ;  $p=0.02$ ). The non-supplemented group also showed higher IL-1 $\beta$  levels than the 663 IU group ( $p<0.001$ ), suggesting a modulatory effect of higher vitamin D<sub>3</sub> doses on inflammation.

### Serum IL-6 Level

Serum IL-6 levels were lowest in Group C, with a mean of  $19.64 \pm 9.05$  pg/mL (Figure 5). Kruskal-Wallis analysis

showed a significant difference among groups ( $p=0.037$ ), with post hoc LSD revealing lower IL-6 levels in Group C than the non-supplemented group ( $p=0.023$ ).

### Correlation Between Serum Vitamin D<sub>3</sub> Levels and Interleukin Levels

Correlation analyses were conducted to examine the relationship between serum vitamin D<sub>3</sub> levels (pg/mL) and interleukin levels. As shown in Figure 6, serum vitamin D<sub>3</sub> levels exhibited a moderate negative correlation with serum IL-1 $\beta$  concentrations (Pearson's correlation,  $r=-0.43$ ,  $p=0.042$ ). In contrast, no statistically significant correlation was observed between serum vitamin D<sub>3</sub> levels (pg/mL) and serum IL-6 concentrations (Pearson's correlation,  $r=-0.031$ ,  $p=0.153$ ) (Figure 7).

## Discussion

The dosage selection in this study was based on previous research and established recommendations (16,17). A dose of 600 IU/day for humans, equivalent to 63 IU/kg BW in rats, was derived from the Institute of Medi-

cine (IOM) guidelines recommending 400–600 IU/day during pregnancy and lactation. However, studies have shown that this level is insufficient to maintain adequate vitamin D<sub>3</sub> status. The maximum dose of 6400 IU/day in humans (663 IU/kg BW in rats) was chosen because evidence indicates it meets maternal requirements during breastfeeding without adverse effects (16). An intermediate dose of 4000 IU/day (415 IU/kg BW in rats) was also included, as previous findings demonstrated its effectiveness in meeting vitamin D needs in lactating mothers (17).

This study investigated the effects of maternal vitamin D<sub>3</sub> supplementation on the offspring's inflammatory response to LPS, assessing induration diameter as a marker of local inflammation. The results showed no significant differences between groups, suggesting that maternal vitamin D<sub>3</sub> supplementation may not directly influence acute local inflammatory responses.

The physiological mechanism underlying LPS-induced induration involves TLR4-dependent activation of innate immune cells and release of pro-inflammatory cytokines—TNF- $\alpha$ , IL-1 $\beta$ , and IL-6—which drive endothelial activation, chemokine production, leukocyte infiltration, and localized swelling/induration (18,19). Although vitamin D<sub>3</sub> is known to downregulate these cytokines and enhance the production of anti-inflammatory cytokines such as IL-10 (20), its modulatory effects appear to be more prominent in chronic or systemic inflammation rather than in acute, localized immune responses (21). We selected IL-6 and IL-1 $\beta$  as primary pro-inflammatory readouts at 3 hours post-LPS. We did not assay TNF- $\alpha$  because its serum levels are known to peak much earlier (often within 1–2 hours post-stimulation) and rapidly decline, making detection at 3 hours susceptible to false negatives. In contrast, IL-6 and IL-1 $\beta$  have more sustained serum profiles and reliably reflect downstream inflammatory amplification (15,22).

Vitamin D<sub>3</sub> primarily modulates systemic inflammation, with studies linking high doses to reduced serum IL-1 $\beta$  and IL-6, but not localized inflammation (23). Additionally, the neonatal immune system is more tolerogenic. A study by Hughes and Norton (24) highlighted that neonatal immune responses tend to suppress excessive inflammation as a developmental adaptation, which may further limit induration diameter in offspring after maternal vitamin D<sub>3</sub> supplementation (25).

Maternal D<sub>3</sub> supplementation significantly altered the serum vitamin D<sub>3</sub> levels of offspring. Offspring from dams receiving 663 IU/kg BW exhibited markedly higher vitamin D<sub>3</sub> levels compared to the non-supplemented group ( $p=0.023$ ), consistent with findings by Chien et al. (26), who reported that maternal intake exceeding 400 IU/day was associated with improved maternal and offspring outcomes. A clear dose-dependent response was observed, as the 663 IU/kg BW group showed substantially higher levels than controls ( $21.15 \pm 15.8$  ng/mL vs.  $3.56 \pm 3.20$  ng/mL), whereas the 62 IU/kg BW group did not differ significantly from controls, suggesting that low doses are insufficient. This aligns with Hollis et al. (16), who noted that low-dose maternal supplementation fails to raise vitamin D<sub>3</sub> concentrations in breast milk, thereby increasing the risk of neonatal deficiency (27).

Maternal vitamin D<sub>3</sub> supplementation enhances the vitamin D<sub>3</sub> status of offspring through both placental transfer and breast milk, with higher maternal levels directly increasing neonatal vitamin D<sub>3</sub> concentrations (28,29). Hollis et al. (16) further emphasized the critical role of adequate maternal vitamin D<sub>3</sub> in optimal fetal development, underscoring the importance of supplementation during pregnancy (27). Additionally, the placental expression of vitamin D<sub>3</sub> metabolic enzymes, such as CYP24A1 and CYP27B1, is regulated, facilitating the transfer of vitamin D<sub>3</sub> to the fetus (30).

Postnatally, breast milk is a key source of vitamin D<sub>3</sub> for exclusively breastfed infants, and its vitamin D content is strongly dependent on maternal intake; high-dose maternal supplementation ( $\approx 6000$ – $6400$  IU/day) increases milk vitamin D<sub>3</sub> and achieves infant vitamin D sufficiency comparable to direct infant supplementation, thereby lowering the risk of neonatal deficiency (16,31). Adequate maternal supplementation increases milk vitamin D<sub>3</sub> levels, thereby reducing the risk of neonatal deficiency (32,33). Conversely, exclusive breastfeeding without sufficient maternal vitamin D<sub>3</sub> may result in infant deficiency (33). Clinical studies further emphasize the importance of maternal supplementation in maintaining adequate vitamin D<sub>3</sub> levels in infants (34).

Maternal vitamin D<sub>3</sub> supplementation significantly attenuated offspring inflammatory responses, reflected by lower serum IL-1 $\beta$  and IL-6 levels following LPS-induced inflammation. The highest dose of supplementation (663 IU/kg) produced the most pronounced effect, yielding the lowest IL-1 $\beta$  concentration and indicating



a dose-dependent anti-inflammatory effect ( $p < 0.001$ ). In contrast, offspring from dams receiving lower doses (62 IU and 415 IU) and the non-supplemented displayed markedly higher IL-1 $\beta$  levels. These findings support the notion that higher maternal vitamin D<sub>3</sub> intake more effectively mitigates inflammation and are consistent with a previous report describing the immunomodulatory capacity of vitamin D<sub>3</sub> in downregulating pro-inflammatory cytokines and limiting excessive immune activation (35).

IL-1 $\beta$  is a pivotal mediator of systemic inflammation, produced predominantly by monocytes and macrophages in response to pathogens or endotoxins (36). It amplifies inflammatory signaling by upregulating inducible nitric oxide synthase (iNOS) and cyclooxygenase-2 (COX-2) (23,37), while simultaneously promoting the release of IL-6 and TNF- $\alpha$ , thereby sustaining inflammatory cascades and contributing to chronic inflammatory diseases (38-41). In this study, offspring from dams supplemented with 663 IU/kg vitamin D<sub>3</sub> exhibited the lowest IL-1 $\beta$  levels which were significantly lower than those of the non-supplemented group. These results indicate that maternal vitamin D<sub>3</sub> supplementation at higher doses is capable of suppressing acute inflammatory responses by downregulating IL-1 $\beta$  production. Mechanistically, vitamin D<sub>3</sub> exerts these effects by inhibiting NLRP3 inflammasome activation, reducing caspase-1-mediated IL-1 $\beta$  maturation, and promoting macrophage polarization toward the M2 phenotype, which enhances IL-10 secretion while suppressing pro-inflammatory cytokines (42-45). Furthermore, vitamin D<sub>3</sub> downregulates Toll-like receptor 4 (TLR4) and nuclear factor kappa B (NF- $\kappa$ B) signaling, key pathways in LPS-induced IL-1 $\beta$  expression, and restrains Th17 differentiation, thereby controlling IL-17-driven inflammation (46-48).

In addition to IL-1 $\beta$ , maternal vitamin D<sub>3</sub> supplementation also reduced serum IL-6 concentrations in offspring. The lowest IL-6 level was observed in the 663 IU/kg group, which was significantly different from the non-supplemented group. IL-6 is a pleiotropic cytokine secreted by macrophages, dendritic cells, T lymphocytes, and fibroblasts in response to infection or tissue injury (49). It regulates immune cell activation, antibody production, and acute-phase responses, and persistent elevation is linked to chronic inflammatory conditions such as type 2 diabetes, autoimmune diseases, and atherosclerosis (37,40,41). Lipopolysaccharide, the main component of Gram negative bacterial cell walls, stimulates IL-6 production by binding TLR4 and activating NF- $\kappa$ B signaling,

which also drives the release of IL-1 $\beta$  and TNF- $\alpha$  (38-41). By suppressing NF- $\kappa$ B activation and preventing its nuclear translocation, vitamin D<sub>3</sub> downregulates IL-6 expression (39,49). Vitamin D<sub>3</sub> also reprograms macrophages from a pro-inflammatory M1 state to an anti-inflammatory M2 state, reduces IL-6 while increasing IL-10 secretion, and inhibits Th17 cells that normally amplify IL-6 production, while supporting regulatory T cells that maintain immune tolerance (23, 50-52). These findings are in line with research by Gatera et al. (52), which reported that vitamin D<sub>3</sub> reduces LPS-induced IL-6 synthesis by interfering with NF- $\kappa$ B signaling. Collectively, these mechanisms demonstrate the capacity of vitamin D<sub>3</sub> to modulate LPS-triggered inflammation through coordinated suppression of both IL-1 $\beta$  and IL-6.

Correlation analyses further confirmed the anti-inflammatory role of vitamin D<sub>3</sub>. A moderate negative correlation was observed between serum vitamin D<sub>3</sub> and IL-1 $\beta$  levels, whereas no significant relationship was detected with IL-6. These findings aligned with earlier studies demonstrating that higher vitamin D<sub>3</sub> status was associated with lower IL-1 $\beta$  levels (54,55), and may indicate that IL-1 $\beta$  is a more sensitive biomarker of immunomodulatory effects of vitamin D<sub>3</sub> in acute inflammation. Additional evidence suggests that vitamin D<sub>3</sub> supplementation suppresses both IL-1 $\beta$  and IL-6 by modulating mitogen-activated protein kinase (MAPK) phosphatase-1, thereby alleviating LPS-induced inflammatory responses (39). Taken together, these results provide compelling evidence that maternal vitamin D<sub>3</sub> supplementation not only reduces pro-inflammatory cytokine production in offspring but also enhances immune regulation, supporting its potential role as a preventive strategy against excessive inflammatory activation in early life (56,57).

## Conclusion

Maternal vitamin D<sub>3</sub> supplementation during pregnancy and lactation increased offspring serum vitamin D<sub>3</sub> levels and reduced IL-6 and IL-1 $\beta$  concentrations, demonstrating a dose-dependent role in regulating systemic inflammation. The negative correlation between vitamin D<sub>3</sub> and IL-1 $\beta$  highlights its potential as an immunomodulatory agent, promoting immune homeostasis in the offspring.

**Ethical Approval:** The study was approved by the Research Ethics Committee of the Faculty of Medicine, Universitas Baiturrahmah, on July 3, 2024, with decision number 040/ETIK-FKUN-BRAH/03/07/2024.

**Informed Consent:** N.A.

**Peer-review:** Externally peer-reviewed

**Author Contributions:** Concept – K.M.H., W.S., G.K., A.D., L.Z., A.L.M.; Design – K.M.H., W.S., A.D., R.M., M.S.; Supervision – K.M.H., W.S., A.D., R.M.; Fundings – K.M.H., W.S.; Materials – K.M.H., W.S., G.K., A.D., M.S., R.M.; Data Collection and/or Processing – K.M.H.,

W.S., G.K., A.D., M.S.; Analysis and/or Interpretation – K.M.H., W.S., G.K., A.L.M.; Literature Review – K.M.H., W.S., G.K., L.Z.; Writer – K.M.H., W.S., G.K., A.D., R.M., M.S., L.Z., A.L.M.; Critical Reviews – K.M.H., W.S., G.K., A.D., R.M., M.S., L.Z., A.L.M.

**Conflict of Interest:** The authors declare no conflict of interest.

**Financial Disclosure:** This study was supported by the PDP KEMDIK-BUDRISTEK funding scheme (Grant No. 0459/E5/PG.02.00/2024).

**Scientific Presentation:** Part of this study was presented at the 31st FAOBMB International Conference, May 22, 2025, Busan, South Korea.

## References

- 1 Aghajafari F, Nagulesapillai T, Ronksley PE, Tough S C, O'Beirne M, Rabi D M, et al. Association between maternal serum 25-hydroxyvitamin D level and pregnancy and neonatal outcomes: systematic review and meta-analysis of observational studies. *BMJ*. 2013;346:f1169 [CrossRef]
- 2 Lindqvist PG, Silva AT, Gustafsson SA, Gidlöf S. Maternal vitamin D deficiency and fetal distress/birth asphyxia: a population-based nested case-control study. *BMJ Open*. 2016 Sep 22;6(9):e009733. [CrossRef]
- 3 Milajerdi A, Abbasi F, Mousavi SM, Esmailzadeh A. Maternal vitamin D status and risk of gestational diabetes mellitus: A systematic review and meta-analysis of prospective cohort studies. *Clin Nutr*. 2021;40(5):2576-86. [CrossRef]
- 4 Butola LK, Vagga A, Ambad R, Kanyal D, Jankar J. A systematic review of association between vitamin D levels and pre-eclampsia in pregnant women—an old problem revisited. *Int J Res Pharm Sci*. 2020;11(SPL4):2910-20. [CrossRef]
- 5 Boskabadi H, Zakerihamidi M, Mehrad-Majd H, Ghoflchi S. Evaluation of vitamin D in the diagnosis of infants with respiratory distress, the clinical value: A systematic review and meta-analysis. *Paediatr Respir Rev*. 2025;53:44-54. [CrossRef]
- 6 Cyprian F, Lefkou E, Varoudi K, Girardi G. Immunomodulatory effects of vitamin D in pregnancy and beyond. *Front Immunol*. 2019;10:2739. [CrossRef]
- 7 Karras SN, Fakhoury H, Muscogiuri G, Grant WB, van den Ouweland JM, Colao AM, et al. Maternal vitamin D levels during pregnancy and neonatal health: evidence to date and clinical implications. *Ther Adv Musculoskelet Dis*. 2016;8(4):124-35. [CrossRef]
- 8 Khudri G, Sukmawati D. Exploring hematopoietic stem cell population in human milk and its benefits for infants: A scoping review. *Asian Pac J Reprod*. 2024;13(3):107-14. [CrossRef]
- 9 Ao T, Kikuta J, Ishii M. The effects of vitamin D on immune system and inflammatory diseases. *Biomolecules*. 2021;11(11):1624. [CrossRef]
- 10 Cashman KD, Ritz C, Kiely M, Odin Collaborators. Improved dietary guidelines for vitamin D: Application of individual participant data (IPD)-Level meta-regression analyses. *Nutrients*. 2017;9(5):469. [CrossRef]
- 11 Rizkia CP. Vitamin D and its role in modulating immune system: a narrative literature review. *Open Access Indonesian J Med Rev*. 2023;3(1):356-61. [CrossRef]
- 12 Goldsmith JR. Vitamin D as an immunomodulator: Risks with deficiencies and benefits of supplementation. *Healthcare (Basel)*. 2015;3(2):219-32. [CrossRef]
- 13 Chen WJ, Hou XJ, Yang SF, Yin XH, Ren L. Effect of vitamin D supplementation during pregnancy on the Th1/Th2 cell balance of rat offspring. *Pharmazie*. 2014;69(5):385-90.
- 14 Voipio H-M, Nevalainen T. Improved method for vaginal plug detection in rats. *Scand J Lab Anim Sci*. 1998;25(1). [Cross-Ref]
- 15 Vajja BN, Juluri S, Kumari M, Kole L, Chakrabarti R, Joshi VD. Lipopolysaccharide-induced paw edema model for detection of cytokine modulating anti-inflammatory agents. *Int Immunopharmacol*. 2004;4(7):901-9. [CrossRef]
- 16 Hollis BW, Wagner CL, Howard CR, Ebeling M, Shary JR, Smith PG, et al. Maternal versus infant vitamin d supplementation during lactation: A randomized controlled trial. *Pediatrics*. 2015;136(4):625-34. Erratum in: *Pediatrics*. 2019;144(1):e20191063. [CrossRef]
- 17 DePender S, Russell MM, DeJager J, Comstock SS. Impact of maternal vitamin D supplementation during breastfeeding on infant serum vitamin D levels: A narrative review of the recent evidence. *Children (Basel)*. 2022;9(12):1863. [CrossRef]
- 18 Buters TP, Hameeteman PW, Jansen IME, van Hindevoort FC, Ten Voorde W, Florencia E, et al. Intradermal lipopolysaccharide challenge as an acute in vivo inflammatory model in healthy volunteers. *Br J Clin Pharmacol*. 2022;88(2):680-90. [CrossRef]
- 19 Patil KR, Mahajan UB, Unger BS, Goyal SN, Belemkar S, Surana SJ, et al. Animal models of inflammation for screening of anti-inflammatory drugs: implications for the discovery and development of phytopharmaceuticals. *Int J Mol Sci*. 2019;20(18):4367. [CrossRef]
- 20 Willis KS, Smith DT, Broughton KS, Larson-Meyer DE. Vitamin D status and biomarkers of inflammation in runners. *Open Access J Sports Med*. 2012;3:35-42. [CrossRef]

- 21 Guan J, Karsy M, Brock AA, Eli IM, Ledyard HK, Hawryluk GWJ, et al. A prospective analysis of hypovitaminosis D and mortality in 400 patients in the neurocritical care setting. *J Neurosurg.* 2017;127(1):1-7. [\[CrossRef\]](#)
- 22 Held F, Hoppe E, Cvijovic M, Jirstrand M, Gabrielsson J. Challenge model of TNF $\alpha$  turnover at varying LPS and drug provocations. *J Pharmacokinet Pharmacodyn.* 2019;46(3):223-40. [\[CrossRef\]](#)
- 23 Rai V, Agrawal DK. Immunomodulation of IL-33 and IL-37 with vitamin D in the neointima of coronary artery: A comparative study between balloon angioplasty and stent in hyperlipidemic microswine. *Int J Mol Sci.* 2021;22(16):8824. [\[CrossRef\]](#)
- 24 Hughes DA, Norton R. Vitamin D and respiratory health. *Clin Exp Immunol.* 2009;158(1):20-5. [\[CrossRef\]](#)
- 25 Castillo EC, Hernandez-Cueto MA, Vega-Lopez MA, Lavallo C, Kouri JB, Ortiz-Navarrete V. Effects of vitamin D supplementation during the induction and progression of osteoarthritis in a rat model. *Evid Based Complement Alternat Med.* 2012;2012:156563. [\[CrossRef\]](#)
- 26 Chien MC, Huang CY, Wang JH, Shih CL, Wu P. Effects of vitamin D in pregnancy on maternal and offspring health-related outcomes: An umbrella review of systematic review and meta-analyses. *Nutr Diabetes.* 2024;14(1):35. [\[CrossRef\]](#)
- 27 Liu PT, Stenger S, Li H, Wenzel L, Tan BH, Krutzik SR, et al. Toll-like receptor triggering of a vitamin D-mediated human antimicrobial response. *Science.* 2006;311(5768):1770-3. [\[CrossRef\]](#)
- 28 Al-Rubaye WEL, Al-Saeedy BAT, Al-Sattam ZMJ. Vitamin D deficiency/insufficiency and some of its related factors in a sample of Iraqi pregnant women and their neonates at Al-Elwiya Maternity Teaching Hospital during 2019. *Al-Kindy Coll Med J.* 2021;17(1):35-40. [\[CrossRef\]](#)
- 29 Agarwal N, Tandon P. Incidence of vitamin D levels in cord blood of newborns and correlation with maternal vitamin D. *Int J Health Sci (Qassim).* 2021;5(S1):687-92. [\[CrossRef\]](#)
- 30 Ashley B, Simner C, Manousopoulou A, Jenkinson C, Hey F, Frost JM, et al. Placental uptake and metabolism of 25(OH) vitamin D determine its activity within the fetoplacental unit. *Elife.* 2022;11:e71094. [\[CrossRef\]](#)
- 31 Dawodu A, Salameh KM, Al-Janahi NS, Bener A, Elcum N. The effect of high-dose postpartum maternal vitamin D supplementation alone compared with maternal plus infant vitamin D supplementation in breastfeeding infants in a high-risk population. A randomized controlled trial. *Nutrients.* 2019;11(7):1632. [\[CrossRef\]](#)
- 32 Qin LL, Lu FG, Yang SH, Xu HL, Luo BA. Does maternal vitamin D deficiency increase the risk of preterm birth: A meta-analysis of observational studies. *Nutrients.* 2016;8(5):301. [\[CrossRef\]](#)
- 33 Mallick AK, Yadav RK, Sannalli K, Bewal NM. Maternal hypovitaminosis D presenting as late-onset hypocalcemic seizure in a term neonate: a case report. *Egyptian Pediatric Association Gazette.* 2023;71(1):15. [\[CrossRef\]](#)
- 34 Hutabarat M, Wibowo N, Obermayer-Pietsch B, Huppertz B. Impact of vitamin D and vitamin D receptor on the trophoblast survival capacity in preeclampsia. *PLoS One.* 2018;13(11):e0206725. [\[CrossRef\]](#)
- 35 Hoe E, Nathanielsz J, Toh ZQ, Spry L, Marimla R, Balloch A, et al. Anti-inflammatory effects of vitamin D on human immune cells in the context of bacterial infection. *Nutrients.* 2016;8(12):806. [\[CrossRef\]](#)
- 36 Dinarello CA. Overview of the IL-1 family in innate inflammation and acquired immunity. *Immunol Rev.* 2018;281(1):8-27. [\[CrossRef\]](#)
- 37 Rodriguez AJ, Mousa A, Ebeling PR, Scott D, de Courten B. Effects of vitamin D supplementation on inflammatory markers in heart failure: a systematic review and meta-analysis of randomized controlled trials. *Sci Rep.* 2018;8(1):1169. [\[CrossRef\]](#)
- 38 Benedetti G, Miossec P. Interleukin 17 contributes to the chronicity of inflammatory diseases such as rheumatoid arthritis. *Eur J Immunol.* 2014;44(2):339-47. [\[CrossRef\]](#)
- 39 Zhang Y, Leung DY, Richers BN, Liu Y, Remigio LK, Riches DW, et al. Vitamin D inhibits monocyte/macrophage proinflammatory cytokine production by targeting MAPK phosphatase-1. *J Immunol.* 2012;188(5):2127-35. [\[CrossRef\]](#)
- 40 Pasupuleti P, Suchitra MM, Bitla AR, Sachan A. Attenuation of oxidative stress, interleukin-6, high-sensitivity C-reactive protein, plasminogen activator inhibitor-1, and fibrinogen with oral vitamin D supplementation in patients with T2DM having vitamin D deficiency. *J Lab Physicians.* 2021;14(2):190-6. [\[CrossRef\]](#)
- 41 Mansournia MA, Ostadmohammadi V, Doosti-Irani A, Ghayour-Mobarhan M, Ferns G, Akbari H, et al. The effects of vitamin D supplementation on biomarkers of inflammation and oxidative stress in diabetic patients: A systematic review and meta-analysis of randomized controlled trials. *Horm Metab Res.* 2018;50(6):429-40. [\[CrossRef\]](#)
- 42 Rao Z, Chen X, Wu J, Xiao M, Zhang J, Wang B, et al. Vitamin D Receptor Inhibits NLRP3 Activation by Impeding Its BRCC3-Mediated Deubiquitination. *Front Immunol.* 2019;10:2783. [\[CrossRef\]](#)
- 43 Cao R, Ma Y, Li S, Shen D, Yang S, Wang X, et al. 1,25(OH)<sub>2</sub>D<sub>3</sub> alleviates DSS-induced ulcerative colitis via inhibiting NLRP3 inflammasome activation. *J Leukoc Biol.* 2020;108(1):283-95. [\[CrossRef\]](#)
- 44 Lowe DW, Hollis BW, Wagner CL, Bass T, Kaufman DA, Horgan MJ, et al. Vitamin D insufficiency in neonatal hypoxic-ischemic encephalopathy. *Pediatr Res.* 2017;82(1):55-62. [\[CrossRef\]](#)
- 45 Agak GW, Qin M, Nobe J, Kim MH, Krutzik SR, Tristan GR, et al. *Propionibacterium acnes* Induces an IL-17 response in acne vulgaris that is regulated by vitamin A and vitamin D. *J Invest Dermatol.* 2014;134(2):366-73. [\[CrossRef\]](#)
- 46 Ben-Zvi I, Aranow C, Mackay M, Stanevsky A, Kamen DL, Marinescu LM, et al. The impact of vitamin D on dendritic cell function in patients with systemic lupus erythematosus. *PLoS One.* 2010;5(2):e9193. [\[CrossRef\]](#)
- 47 Jiang LJ, Rong ZH, Zhang HF. The changes of Treg and Th17 cells relate to serum 25(OH)D in patients with initial-onset childhood systemic lupus erythematosus. *Front Pediatr.* 2023;11:1228112. [\[CrossRef\]](#)
- 48 Dankers W, Davelaar N, van Hamburg JP, van de Peppel J, Colin EM, Lubberts E. Human memory Th17 cell populations change into anti-inflammatory cells with regulatory capacity upon

- exposure to active vitamin D. *Front Immunol.* 2019;10:1504. [\[CrossRef\]](#)
- 49 Tanaka T, Narazaki M, Kishimoto T. IL-6 in inflammation, immunity, and disease. *Cold Spring Harb Perspect Biol.* 2014;6(10):a016295. [\[CrossRef\]](#)
- 50 Gunasekar P, Swier VJ, Fleegel JP, Boosani CS, Radwan MM, Agrawal DK. Vitamin D and macrophage polarization in epicardial adipose tissue of atherosclerotic swine. *PLoS One.* 2018;13(10):e0199411. [\[CrossRef\]](#)
- 51 Fabri M, Stenger S, Shin DM, Yuk JM, Liu PT, Realegeno S, et al. Vitamin D is required for IFN-gamma-mediated antimicrobial activity of human macrophages. *Sci Transl Med.* 2011;3(104):104ra102. [\[CrossRef\]](#)
- 52 Chen L, Eapen MS, Zosky GR. Vitamin D both facilitates and attenuates the cellular response to lipopolysaccharide. *Sci Rep.* 2017;7:45172. [\[CrossRef\]](#)
- 53 Gatera VA, Lesmana R, Musfiroh I, Judistiani RTD, Setiabudiawan B, Abdulah R. Vitamin D inhibits lipopolysaccharide (LPS)-induced inflammation in A549 cells by downregulating inflammatory cytokines. *Med Sci Monit Basic Res.* 2021;27:e931481. [\[CrossRef\]](#)
- 54 Li G, Lin L, Wang YL, Yang H. 1,25(OH)2D3 protects trophoblasts against insulin resistance and inflammation via suppressing mTOR signaling. *Reprod Sci.* 2019;26(2):223-32. [\[CrossRef\]](#)
- 55 Sun J, Zhong W, Gu Y, Groome LJ, Wang Y. 1,25(OH)2D3 suppresses COX-2 up-regulation and thromboxane production in placental trophoblast cells in response to hypoxic stimulation. *Placenta.* 2014;35(2):143-5. [\[CrossRef\]](#)
- 56 Ma R, Gu Y, Zhao S, Sun J, Groome LJ, Wang Y. Expressions of vitamin D metabolic components VDBP, CYP2R1, CYP27B1, CYP24A1, and VDR in placentas from normal and preeclamptic pregnancies. *Am J Physiol Endocrinol Metab.* 2012;303(7):E928-35. [\[CrossRef\]](#)
- 57 Vestergaard AL, Andersen MK, Olesen RV, Bor P, Larsen A. High-dose vitamin D supplementation significantly affects the placental transcriptome. *Nutrients.* 2023;15(24):5032. [\[Cross-Ref\]](#)

# Effects of Typeable and Non-typeable *Haemophilus influenzae* on Human CD4<sup>+</sup> T Cell Proliferation and Production of Th1 and Th2 Cytokines

Abdel-Rahman Youssef<sup>1</sup> 

<sup>1</sup>Umm Al-Qura University College of Dental Medicine, Department of Basic and Clinical Oral Sciences, Division of Basic Medical Sciences, Makkah, Saudi Arabia

## Abstract

**Objective:** *Haemophilus influenzae* is a Gram-negative bacterium that commonly colonizes and infects the respiratory tract. The bacterial infection may modulate host immune responses. However, the T cell responses to *H. influenzae* remain unclear. This study aimed to investigate the CD4<sup>+</sup> T cell responses to live strains of typeable *H. influenzae* (THi) and non-typeable *H. influenzae* (NTHi) *in vitro*.

**Materials and Methods:** CD4<sup>+</sup> T cells were isolated from healthy individuals and infected with live variants of a single strain of THi (132b<sup>+</sup>, 132b<sup>-</sup>, 132b<sup>-</sup>p5<sup>-</sup>) and NTHi (A950002, A950002p5<sup>-</sup>, A850052, d1, d3). The CD4<sup>+</sup> T cell responses to *H. influenzae* were investigated *in vitro* by evaluating the cell proliferation using a [<sup>3</sup>H]-thymidine incorporation assay and measuring the levels of T helper-1 (Th1) cytokines (interferon-gamma [IFN- $\gamma$ ], tumor necrosis factor-alpha [TNF- $\alpha$ ]) and Th2 cytokines (interleukin-5 [IL-5], interleukin-10 [IL-10]) using a human Th1/Th2 cytokine cytometric bead array (CBA).

**Results:** Both NTHi strains and THi are bound to CD4<sup>+</sup> T cells to variable degrees, and the presence of the P5 protein in *H. influenzae* P5<sup>+</sup> strains increased the binding to CD4<sup>+</sup> T cells significantly compared to P5-deficient strains (132b<sup>-</sup> vs. 132b<sup>-</sup>p5<sup>-</sup> [ $p=0.0009$ ], A950002 vs. A950002p5<sup>-</sup> [ $p=0.0039$ ], d1 vs. d3 [ $p=0.0014$ ]). THi (132b<sup>-</sup>, 132b<sup>-</sup>p5<sup>-</sup>) and NTHi strains (A850052, d1, d3) caused marked inhibition of CD4<sup>+</sup> T cell proliferation ( $p<0.0001$ ). NTHi strains (A850052, d1, d3) significantly suppressed IFN- $\gamma$ , TNF- $\alpha$ , IL-5, and IL-10 production ( $p<0.0001$ ). THi strains 132b<sup>-</sup> and 132b<sup>-</sup>p5<sup>-</sup> markedly suppressed IFN- $\gamma$  production ( $p<0.0001$ ). TNF- $\alpha$  production was significantly inhibited by 132b<sup>-</sup> strain ( $p=0.0002$ ), and A950002 strain ( $p=0.01$ ). IL-5 production was reduced by all THi and NTHi strains ( $p<0.0001$ ), while all THi and some NTHi strains (A850052, d1, d3) decreased IL-10 production ( $p<0.0001$ ).

**Conclusion:** These results suggest that the immunosuppressive effects of certain strains of *H. influenzae* may represent a mechanism by which the bacterium evades the adaptive immune response, facilitating the establishment of respiratory colonization and persistence of the infection.

**Keywords:** *Haemophilus influenzae*, CD4 T cell proliferation, Th1 and Th2 cytokines

## Correspondence

Abdel-Rahman Youssef

## E-mail

amyoussef@uqu.edu.sa

## Received

July 31, 2025

## Accepted

September 16, 2025

## Published

November 14, 2025

## Suggested Citation

Youssef AR. Effects of typeable and non-typeable *Haemophilus influenzae* on human CD4<sup>+</sup> T cell proliferation and production of Th1 and Th2 cytokines. Turk J Immunol. 2025;13(3):169-76.

## DOI

10.36519/TJI.2025.793



This work is licensed under the Creative Commons Attribution-NonCommercial-Non-Derivatives 4.0 International License (CC BY-NC-ND 4.0).



## Introduction

*Haemophilus influenzae* bacterium inhabits the upper respiratory tract and may cause local and systemic diseases (1). *Haemophilus influenzae* strains are classified into capsulate or typeable *H. influenzae* (THi) and acapsulate or non-typeable *H. influenzae* (NTHi) based on the expression of a polysaccharide capsule (1). Typeable *H. influenzae* strains include six serotypes (a–f), with type b being the most virulent of them all (2). Typeable *H. influenzae* strains can cause severe diseases, including septicemia and meningitis (3,4). Non-typeable *H. influenzae* strains are characterized by the absence of a polysaccharide capsule, which distinguishes them from typeable strains (5). These strains may colonize the respiratory tract and are often implicated in exacerbation of chronic obstructive pulmonary disease (COPD). Non-typeable *H. influenzae* is the most prevalent bacterial cause of recurrent otitis media during childhood (6) and COPD exacerbations in humans (7) and mice (8). Furthermore, NTHi promote biofilm formation and exhibit a strong resistance to the immune system's antimicrobial defenses, which enables them to survive in the COPD lung and cause persistent infections that recur (9).

The initial step in bacterial colonization is attaching to specific receptors on human mucosal epithelial cells. Outer membrane proteins (OMPs) P2 and P5 are involved in the binding of NTHi to mucin, whereas binding to mucosal epithelial cells is mediated by pili (10), high-molecular-weight surface proteins (HMW1 and HMW2) (11), *H. influenzae* adhesin (12), *Haemophilus* adhesion and penetration (Hap) protein (13), OMP P5 (14), and the opacity-associated (Opa) protein A (15).

Bacterial colonization may induce host damage and trigger specific immune responses that can eradicate the bacteria. T lymphocytes detect microbial antigens in conjunction with major histocompatibility complex molecules. In the presence of costimulatory signals, T cells become activated and produce cytokines that regulate immune responses. T helper-1 (Th1) cells are generated by T-bet expression through STAT1 and STAT4 upon T cell receptor (TCR) stimulation in the presence of interferon-gamma (IFN- $\gamma$ ) and interleukin-12 (IL-12), respectively. T helper-2 cells are stimulated by activation of TCR-stimulated T cell factor 1 and IL-2 and IL-4 signaling (16).

Mucosal CD4<sup>+</sup> T cell priming occurs in mucosa-associated lymphoid tissue following bacterial invasion, leading

to the production of effector and memory T cells (17). Activated CD4<sup>+</sup> T cells produce both Th1 cytokines, such as TNF- $\alpha$  and IFN- $\gamma$ , and Th2 cytokines, including IL-5 and IL-10. Th1 cytokines activate cell-mediated immunity, whereas Th2 cytokines stimulate humoral immunity (18,19). The sequel of infectious diseases is largely dependent on the balance between Th1 and Th2 cytokines (20).

Bacteria can inhibit lymphocyte proliferation and cytokine production, while others can stimulate the production of pro-inflammatory cytokines. Failure to evoke a strong proinflammatory response from immune cells might impair host clearance of pathogens and prolong colonization. *Haemophilus influenzae* utilizes capsular polysaccharide for immune evasion, resulting in a deficiency of co-stimulatory signals that impairs robust lymphocyte activation and proliferation (21). Also, it can directly trigger programmed cell death in lymphocytes, effectively shutting down the adaptive immune response before it can fully develop (22).

Previous studies highlighted the importance of lymphocyte responses in the pathogenesis of NTHi infection. The incidence of COPD exacerbations due to NTHi suggests that the immunological defense mechanisms against these bacteria are hindered. It has been demonstrated that exacerbations of COPD are associated with a decrease in the proliferation of T cells in response to the outer membrane lipoprotein P6 of NTHi (23). Additionally, CD4<sup>+</sup> memory T cells specific for NTHi were present at low rates in the peripheral blood of COPD patients and healthy controls (24). Furthermore, COPD due to NTHi was associated with Th2 cytokines and decreased expression of CD40 ligand (1). However, the immune responses of CD4<sup>+</sup> T cells to *H. influenzae* are not clearly characterized. This study aimed to investigate the effects of live variants of single NTHi and THi strains on CD4<sup>+</sup> T cell proliferation and production of Th1 and Th2 cytokines *in vitro*.

## Materials and Methods

### Bacterial Strains

Variants of a single strains of THi (132b<sup>+</sup>, 132b<sup>-</sup>, 132b<sup>-</sup>p5<sup>-</sup>) and NTHi (A950002, A950002p5<sup>-</sup>, A850052, d1, d3) were used in this study. Bacterial strains 132b<sup>-</sup>, A950002, and d1 express P5 protein whereas P5 deficient strains include 132b<sup>-</sup>p5<sup>-</sup>, A950002p5<sup>-</sup>, and d3. *Haemophilus*

*influenzae* strains were cultivated on brain heart infusion agar enriched with 5% blood.

### Isolation of Primary CD4<sup>+</sup> T Cells

Peripheral blood (18 mL) was collected from healthy individuals and placed in a Falcon tube containing 2 mL sodium citrate as an anticoagulant. The blood was carefully layered over 20 mL of Histopaque®-1077 (Sigma-Aldrich, Dorset, UK) in 50 mL conical tubes. Following centrifugation, peripheral blood mononuclear cells (PBMCs) were extracted from the buffy coat layer. CD4<sup>+</sup> T cells were then isolated from the PBMCs using negative selection, adhering to the protocol provided with the immunomagnetic CD4<sup>+</sup> T cell isolation kit (Miltenyi Biotec, Surrey, UK). The cells were subsequently cultured in RPMI 1640 medium (Sigma Aldrich, Dorset, UK), enriched with 10% inactivated fetal bovine serum, 20 mM HEPES buffer (Sigma-Aldrich, Dorset, UK), 1% L-glutamine (Sigma-Aldrich, Dorset, UK). Cell culture was kept in a humidified incubator at 37°C with 5% CO<sub>2</sub>. For adhesion, cell proliferation, and cytokines assays, the T cells were infected with live strains of *H. influenzae* at a multiplicity of infection (MOI) of 100:1. This MOI was chosen based on a previously published study (25).

### Bacterial Adhesion Assay

To upregulate carcinoembryonic antigen-related cell adhesion molecule 1 (CEACAM1) on the surface of CD4<sup>+</sup> T cells, IL-2 (200 U/mL) was added to the cell cultures for 48 hours. After washing, the cells were infected with live strains of THi and NTHi at MOI of 100:1 and incubated for 3 hours at 37°C in a humidified atmosphere of 5% CO<sub>2</sub>. Cells and bacteria were transferred to a 5 µm Transwell filter (Costar, Corning, NY, USA). To remove nonadherent bacteria, the filters were washed six times with Hanks' balanced salt solution (HBSS; Sigma-Aldrich, Dorset, UK). The filters were then transferred to new wells, and 200 µL of 1% saponin was added per filter for 30 minutes to release cell-associated bacteria. These bacteria were harvested by four 200 µL washes with HBSS, and suspensions of bacteria were plated after appropriate dilutions to estimate the colony-forming units (CFU). The bacterial adhesion assay was conducted in duplicate, and adhesion was quantified by counting the number of bacterial CFUs attached to the CD4<sup>+</sup> T cells, as previously described (25).

### T Cell Proliferation Assay and Th1/Th2 Cytokine Analysis

To evaluate the impact of live bacteria on CD4<sup>+</sup> T cell proliferation, cells were seeded at a density of  $2 \times 10^5$

cells/well in 24-well plates pre-coated with anti-CD3 antibody (OKT3) at 1 µg/mL. Simultaneously, the cells were infected with bacteria at MOI of 100:1. Gentamicin (50 µg/mL) was added 3 hours post-infection and maintained throughout the experiment to stop bacterial overgrowth. On day 3, cell proliferation was evaluated by determining the [<sup>3</sup>H]-thymidine incorporation, as outlined in prior studies (26). Briefly, 100 µL aliquots of each CD4<sup>+</sup> T cell culture were added in triplicate to a 96-well plate, pulsed with [<sup>3</sup>H]-thymidine (1 µCi/well), and incubated for 6 hours in a humidified atmosphere of 5% CO<sub>2</sub> at 37°C. Radioactivity was quantified by a liquid scintillation beta counter (1450 Microbeta; LKB Wallac, Turku, Finland). The results were expressed as the average counts per minute (CPM) of duplicate cultures. Additionally, 50 µL samples of cell supernatants were collected in duplicate on day 3 for cytokine analysis. The levels of IFN-γ, TNF-α, IL-5, and IL-10 were measured using a human Th1/Th2 cytokine cytometric bead array (CBA) kit (BD Biosciences, Oxford, UK), following the manufacturer's guidelines. Cytokine concentrations were determined based on fluorescent intensities (FL2), and average values were computed using CBA software (BD Biosciences, Oxford, UK). The Th1/Th2 CBA assay is a reliable and sensitive method for simultaneously quantifying multiple cytokines (27).

### Statistical Analysis

All data were analyzed using GraphPad Prism version 8 (GraphPad Software, San Diego, CA, USA). Results are presented as mean ± standard error of the mean (SEM). Statistical comparisons were performed using one-way analysis of variance (ANOVA) with Tukey's and Dunnett's multiple comparison tests, and unpaired t-tests. The statistical significance was set as  $p < 0.05$ . In figures, significance is indicated as follows: \* =  $p \leq 0.05$ , \*\* =  $p \leq 0.01$ , \*\*\* =  $p \leq 0.001$ , \*\*\*\* =  $p \leq 0.0001$ , ns =  $p > 0.05$ .

## Results

### Adhesion of *Haemophilus influenzae* to CD4<sup>+</sup> T Cells

Variants of single strains of THi and NTHi were used to assess the adhesion of *H. influenzae* to CD4<sup>+</sup> T cells. Carcinoembryonic antigen-related cell adhesion molecule 1 was upregulated on CD4<sup>+</sup> T cells by stimulation with IL-2 before infection with bacteria. As shown in Figure 1, both THi and NTHi strains are bound to CD4<sup>+</sup> T cells to varying degrees. Typeable *H. influenzae* (132b<sup>+</sup> and 132b<sup>-</sup>)

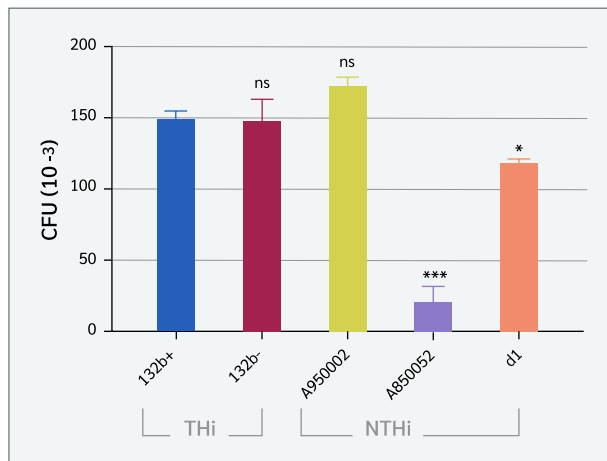


**Figure 1.** Quantitative analysis of the binding of typeable Hi (THi) and non-typeable Hi (NTHi) to CD4<sup>+</sup> T cells. The CD4<sup>+</sup> T cells were infected with live single strains of THi (132b<sup>+</sup>, 132b<sup>-</sup>) and NTHi (A950002, A850052, d1) at a multiplicity of MOI of 100:1. The bacterial binding was assessed by viable count assays. Data are representative of at least two independent experiments. A one-way ANOVA followed by Tukey's multiple comparisons test was used to compare NTHi and NTHi. THi (132b<sup>+</sup> and 132b<sup>-</sup>) vs NTHi A850052 ( $p=0.0004$ ) and THi (132b<sup>+</sup> and 132b<sup>-</sup>) vs d1 ( $p=0.0196$  and  $0.0219$ ) respectively. THi (132b<sup>+</sup> or 132b<sup>-</sup>) vs NTHi A950002 ( $p=0.3812$  and  $0.3325$ ), respectively.

bind more to CD4<sup>+</sup> T cells compared to NTHi A850052 ( $p=0.0004$ ) and d1 ( $p=0.0196$  and  $0.0219$ ), respectively. However, there was no significant difference between THi (132b<sup>+</sup> or 132b<sup>-</sup>) and NTHi A950002 ( $p=0.3812$  and  $0.3325$ ), respectively.

As shown in Figure 2, the presence of P5 protein in P5<sup>+</sup> strains (132b<sup>-</sup>, A950002, and d1) increased the binding to CD4<sup>+</sup> T cells significantly compared to P5-deficient strains (132b<sup>-</sup>p5<sup>-</sup>, A950002p5<sup>-</sup>, and d3), with  $p$  value less than 0.05 [132b<sup>-</sup> vs. 132b<sup>-</sup>p5<sup>-</sup> ( $p=0.0009$ ), A950002 vs. A950002p5<sup>-</sup> ( $p=0.0039$ ), d1 vs. d3 ( $p=0.0014$ )]. However, P5-deficient strains can still bind to T cells. These findings suggest that the P5 protein contributes to *H. influenzae* binding to T cells in a significant but non-essential way.

### Effect of *Haemophilus influenzae* on CD4<sup>+</sup> T Cell Proliferation

CD4<sup>+</sup> T cells were stimulated by immobilized anti-CD3 (iCD3) antibody. The cells were infected with live THi or NTHi strains in the presence of iCD3 antibody. Figure 3 shows that THi (132b<sup>-</sup>, 132b<sup>-</sup>p5<sup>-</sup>) and NTHi strains (A850052, d1, d3) caused marked inhibition of CD4<sup>+</sup> T cell proliferation ( $p<0.0001$ ), whereas THi strain 132b<sup>+</sup>

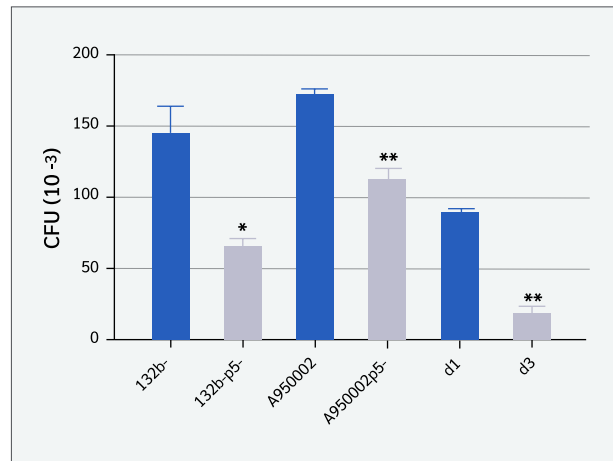


**Figure 2.** Quantitative analysis of the binding of P5<sup>+</sup> or P5<sup>-</sup> *H. influenzae* to active CD4<sup>+</sup> T cells. Black bars represent P5<sup>+</sup> strains (132b<sup>-</sup>, A950002, d1) and grey represent P5 deficient strains (132b<sup>-</sup>p5<sup>-</sup>, A950002p5<sup>-</sup> and d3). The bacterial binding was assessed by viable count assays. Data are representative of at least two independent experiments.  $p=0.0009$  for 132b<sup>-</sup> vs. 132b<sup>-</sup>p5<sup>-</sup>,  $p=0.0039$  for A950002 vs. A950002p5<sup>-</sup>,  $p=0.0014$  for d1 vs. d3.

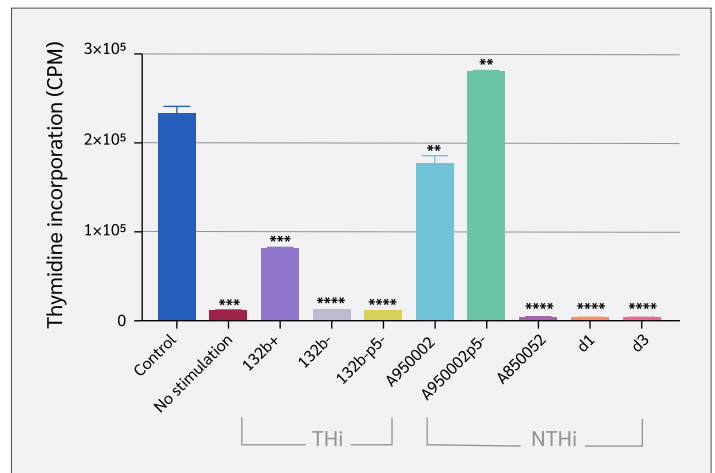


**Figure 3.** Effect of *H. influenzae* on CD4<sup>+</sup> T cell proliferation. The cells were stimulated with anti-CD3 antibody and then either left uninfected (control) or infected with THi (132b<sup>+</sup>, 132b<sup>-</sup>, 132b<sup>-</sup>p5<sup>-</sup>) or NTHi (A950002, A950002p5<sup>-</sup>, d1, d3) at MOI of 100:1. The unstimulated cells were cultured without iCD3 or bacteria. CD4 proliferation was determined by [<sup>3</sup>H]-thymidine incorporation on day 3. Results are represented as the means of duplicate samples. Data are representative of at least two independent experiments. A one-way ANOVA followed by Dunnett's multiple comparisons test was used to compare all *H. influenzae* strains with the control. THi strains (132b<sup>-</sup>, 132b<sup>-</sup>p5<sup>-</sup>) and NTHi strains (A850052, d1, d3) inhibit CD4<sup>+</sup> T cell proliferation markedly ( $p<0.0001$ ). THi strain 132b<sup>+</sup> and NTHi strain A950002 induced moderate inhibition ( $p=0.0004$ ,  $p=0.0079$ ), respectively. NTHi strain A950002p5<sup>-</sup> increased proliferation slightly ( $p=0.0064$ ).

and NTHi strain A950002 induced moderate inhibition compared to uninfected controls ( $p=0.0004$ ,  $p=0.0079$ ),

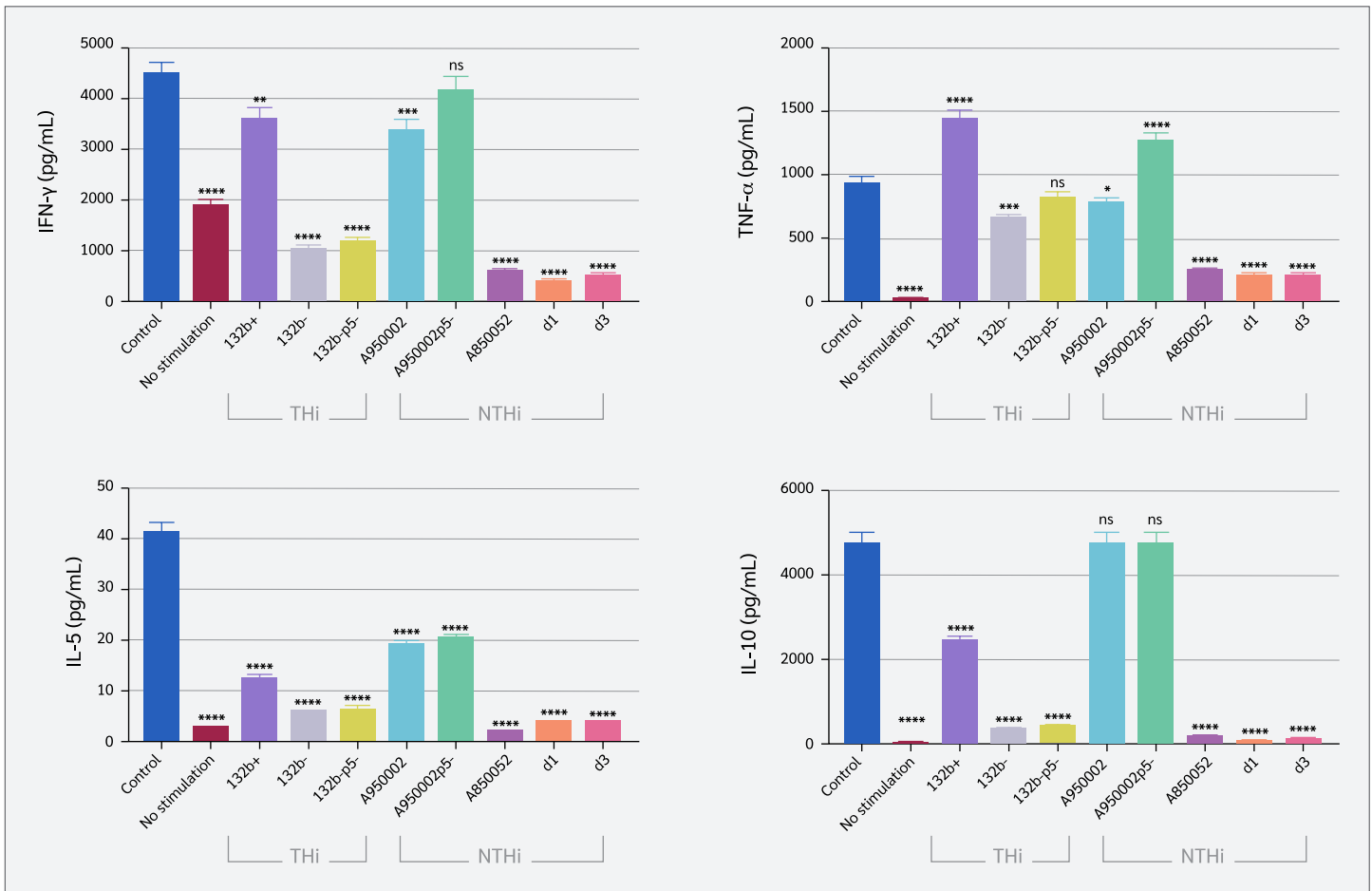


**Figure 4.** Effects of *H. influenzae* on the production of Th1 cytokines (IFN- $\gamma$  and TNF- $\alpha$ ) and Th2 cytokines (IL-5 and IL-10) by CD4<sup>+</sup> T cells. The cells were stimulated with anti-CD3 antibody and then either left uninfected (control) or infected with THi (132b<sup>+</sup>, 132b<sup>-</sup>, 132b-p5<sup>-</sup>) or NTHi (A950002, A950002p5<sup>-</sup>, d1, d3) at MOI of 100:1. The unstimulated cells were cultured without anti-CD3 or bacteria. The cell supernatants were analyzed on day 3 for Th1 and Th2 cytokines by cytometric bead array, and the average of the calculated cytokine values was calculated by CBA software. One-way ANOVA Dunnett's multiple comparisons test was used to compare all *H. influenzae* strains with the control. \* $p=0.0101$ , \*\* $p=0.0016$ , \*\*\* $p=0.0001$  and  $0.0002$ , \*\*\*\* $p<0.0001$ .

respectively. In contrast, NTHi strain A950002p5<sup>-</sup> increased proliferation slightly ( $p=0.0064$ ). The overall pattern of CD4<sup>+</sup> T cell proliferation was not significantly influenced by the P5 protein.

### Effect of *Haemophilus influenzae* on Th1 and Th2 Cytokine Production

The production of Th1 (IFN- $\gamma$  and TNF- $\alpha$ ) and Th2 (IL-5, and IL-10) cytokines by CD4<sup>+</sup> T cells were assessed using a cytometric bead array to assess Th1 and Th2 immunological responses to *H. influenzae* infection (Figure 4). IFN- $\gamma$  production was significantly inhibited by both THi and NTHi strains (except A950002p5<sup>-</sup> strain), with marked suppression observed for NTHi strains (A850052, d1, d3) and the THi strains 132b<sup>-</sup> and 132b-p5<sup>-</sup> ( $p<0.0001$ ). TNF- $\alpha$  production was significantly inhibit-

ed by 132b<sup>-</sup> strain ( $p=0.0002$ ), A950002 strain ( $p=0.01$ ), A850052, d1 and d3 strains ( $p<0.0001$ ). In contrast, THi strain 132b<sup>+</sup> and NTHi strain A950002p5<sup>-</sup> significantly increased TNF- $\alpha$  production ( $p<0.0001$ ). IL-5 production was reduced by all THi and NTHi strains ( $p<0.0001$ ), while all THi and NTHi (A850052, d1, d3) decreased IL-10 production ( $p<0.0001$ ).

## Discussion

This study demonstrates that both THi and NTHi strains of *H. influenzae* bind to CD4<sup>+</sup> T cells at varying degrees. The presence of the P5 protein enhanced binding in both strain types; however, they can still bind to T cells in its absence, likely due to the presence of other adhesins

on the bacterial surface. Activated human CD4<sup>+</sup> T cells express CEACAM1 (28),  $\beta$ 1 integrins (29), and Toll-like receptor (TLR) 2 and TLR4 (30). It has been demonstrated that the OMP-P2 and P6 interact with TLR2 (22,31,32), and the P5 protein interacts with CEACAM1 (33,34). Additionally, NTHi strain d1 expresses P5 protein bound strongly to Chinese hamster ovary (CHO)-CEACAM1 cells, whereas P5-deficient d3 strain did not (34). Moreover, *H. influenzae* expresses a range of adhesins that bind to host cells, such as *Haemophilus* surface fibrils that bind to vitronectin (35), and pili, which adhere to fibronectin and heparin-binding matrix proteins (36,37).

Immunity to microbial infection is organized by Th cells. Th1 cells are essential for immunity to intracellular pathogens via the production of IFN- $\gamma$ , which activates macrophages, and IL-2, which induces lymphocyte proliferation. On the contrary, Th2 cells produce IL-4, IL-5, IL-10, and IL-13, which support humoral immunity and play a crucial role in eliminating extracellular pathogens (38). Antimicrobial Th1 and Th2 responses are typically linked to resistance and susceptibility to infectious diseases, respectively. This was demonstrated in intracellular pathogens *Leishmania major* and *Mycobacterium leprae* (18,39). The interaction of *H. influenzae* with mucosal CD4<sup>+</sup> T cells is a significant factor in determining the outcome of *H. influenzae* infection. Herein, the results of this study have shown that certain live strains of NTHi and THi inhibited T cell proliferation and markedly reduced Th1 and Th2 cytokine production. This immunosuppressive effect may represent a mechanism by which the adaptive immune response is evaded.

Bacteria can manipulate the inhibitory signaling to avoid host defense. IgA proteases and phase variation of lipopolysaccharide enable NTHi to evade mucosal immune mechanisms and invade respiratory epithelial cells, allowing it to live intracellularly (3). On the contrary, *H. influenzae* can stimulate CD4<sup>+</sup> T cell immune responses (1). In response to the NTHi antigen, the activated Th (CD4<sup>+</sup>CD69<sup>+</sup>) cells produced Th1 cytokines (IFN- $\gamma$  and IL-2) in healthy controls (1). However, the bronchiectasis group had predominant Th2 cytokines such as IL-4 and IL-10 (1). In murine models, nasal immunization with NTHi antigen induced specific Th1 and Th2 responses (40). Furthermore, stimulation with P6 protein induced CD4<sup>+</sup> T cell proliferation in P6-immunized mice, and these cells upregulated mRNA for Th2 cytokines (41). The findings presented in this study may appear to be different from previous reports. Unlike prior studies that

used bacterial antigens (1,40,41). The bacterial strains used in this study are well-characterized, specific live strains, which may explain the difference.

The inhibition of T-cell proliferation can be explained by several mechanisms. *Haemophilus ducreyi*-reactive CD4<sup>+</sup> T cell proliferation was markedly increased by CD25<sup>+</sup>CD4<sup>+</sup> T cell depletion, underscoring the function of regulatory T (Treg) cells in regulating the immunological response to bacterial infection (42). Regulatory T cells can suppress the immune responses through cellular interactions and/or release of IL-10 and TGF- $\beta$  (43). It has been shown that IL-10 released by activated B lymphocytes in humans inhibited CD4<sup>+</sup>CD25<sup>+</sup> T-cell proliferation *in vitro* (44). Furthermore, Foxp3<sup>+</sup> CD25<sup>+</sup> Treg cells may produce suppressor cytokines, such as TGF- $\beta$  and IL-10, induce apoptosis or granzyme-mediated cytotoxicity, or compete with effector T cells for IL-2. After Treg activation, the cells may express galectin-1, which may arrest the cell cycle when interacting with receptors on effector T cells (45).

This study demonstrated the immunosuppressive properties of certain *H. influenzae* strains *in vitro*. However, it has some limitations that may affect its relevance to *in vivo* settings. One of the limitations is the lack of systemic immune components, such as circulating cytokines and complement proteins, which modulate immune responses *in vivo*. In addition, using isolated immune cell types rather than mixed populations found *in vivo* results in the absence of immune cell crosstalk and an incomplete immune response.

## Conclusion

The present study demonstrates that certain strains of *H. influenzae* inhibit the proliferation of primary human CD4<sup>+</sup> T cells and suppress the production of Th1 and Th2 cytokines. This immunosuppressive effect may contribute to the ability of *H. influenzae* to evade the adaptive immune response and establish respiratory colonization and persistence of the infection. The molecular mechanisms behind *H. influenzae*'s immunosuppressive effect on CD4<sup>+</sup> T cells require more research.



**Ethical Approval:** The study was approved by the Biomedical Research Ethics Committee of Umm Al-Qura University on December 25, 2024, with the decision number VDJB171224.

**Informed Consent:** N.A.

**Peer-review:** Externally peer-reviewed

**Author Contributions:** Concept – A.R.Y.; Design – A.R.Y.; Supervision – A.R.Y.; Data Collection and/or Processing – A.R.Y.; Analysis and/or Interpretation – A.R.Y.; Literature Review – A.R.Y.; Writer – A.R.Y.; Critical Reviews – A.R.Y.

**Conflict of Interest:** The author declares no conflict of interest.

**Financial Disclosure:** The author declared that this study has received no financial support.


**Acknowledgment:** I am grateful to Professor Mumtaz Virji for scientific support and to Dr. Andrew Herman for assistance with flow cytometry.

## References

- King PT, Hutchinson PE, Johnson PD, Holmes PW, Freezer NJ, Holdsworth SR. Adaptive immunity to nontypeable *Haemophilus influenzae*. Am J Respir Crit Care Med. 2003;167(4):587-92. [CrossRef]
- Turk DC. The pathogenicity of *Haemophilus influenzae*. J Med Microbiol. 1984;18(1):1-16. [CrossRef]
- Zhang J, Zhu Z, Zuo X, Pan H, Gu Y, Yuan Y, et al. The role of NTHi colonization and infection in the pathogenesis of neutrophilic asthma. Respir Res. 2020;21(1):170. [CrossRef]
- Broome CV. Epidemiology of *Haemophilus influenzae* type b infections in the United States. Pediatr Infect Dis J. 1987;6(8):779-82. [CrossRef]
- Murphy TF, Sethi S, Klingman KL, Brueggemann AB, Doern GV. Simultaneous respiratory tract colonization by multiple strains of nontypeable *Haemophilus influenzae* in chronic obstructive pulmonary disease: implications for antibiotic therapy. J Infect Dis. 1999;180(2):404-9. [CrossRef]
- Erwin AL, Smith AL. Nontypeable *Haemophilus influenzae*: understanding virulence and commensal behavior. Trends Microbiol. 2007;15(8):355-62. [CrossRef]
- Sethi S, Murphy TF. Infection in the pathogenesis and course of chronic obstructive pulmonary disease. N Engl J Med. 2008;359(22):2355-65. [CrossRef]
- Ganesan S, Comstock AT, Kinker B, Mancuso P, Beck JM, Sajjan US. Combined exposure to cigarette smoke and nontypeable *Haemophilus influenzae* drives development of a COPD phenotype in mice. Respir Res. 2014;15(1):11. [CrossRef]
- Weeks JR, Staples KJ, Spalluto CM, Watson A, Wilkinson TMA. The role of non-typeable *Haemophilus influenzae* biofilms in chronic obstructive pulmonary disease. Front Cell Infect Microbiol. 2021;11:720742. [CrossRef]
- Gilsdorf JR, McCrean KW, Marrs CF. Role of pili in *Haemophilus influenzae* adherence and colonization. Infect Immun. 1997;65(8):2997-3002. [CrossRef]
- Bakaletz LO, Barenkamp SJ. Localization of high-molecular-weight adhesion proteins of nontypeable *Haemophilus influenzae* by immunoelectron microscopy. Infect Immun. 1994;62(10):4460-8. [CrossRef]
- Barenkamp SJ, St Geme JW 3rd. Identification of a second family of high-molecular-weight adhesion proteins expressed by non-typable *Haemophilus influenzae*. Mol Microbiol. 1996;19(6):1215-23. [CrossRef]
- St Geme JW 3rd, de la Morena ML, Falkow S. A *Haemophilus influenzae* IgA protease-like protein promotes intimate interaction with human epithelial cells. Mol Microbiol. 1994;14(2):217-33. [CrossRef]
- Bookwalter JE, Jurcisek JA, Gray-Owen SD, Fernandez S, McGillivray G, Bakaletz LO. A carcinoembryonic antigen-related cell adhesion molecule 1 homologue plays a pivotal role in nontypeable *Haemophilus influenzae* colonization of the chinchilla nasopharynx via the outer membrane protein P5-homologous adhesin. Infect Immun. 2008;76(1):48-55. [CrossRef]
- Prasadara NV, Lysenko E, Wass CA, Kim KS, Weiser JN. Opacity-associated protein A contributes to the binding of *Haemophilus influenzae* to chag epithelial cells. Infect Immun. 1999;67(8):4153-60. [CrossRef]
- Sun L, Su Y, Jiao A, Wang X, Zhang B. T cells in health and disease. Signal Transduct Target Ther. 2023;8(1):235. [CrossRef]
- Ebert LM, Schaerli P, Moser B. Chemokine-mediated control of T cell traffic in lymphoid and peripheral tissues. Mol Immunol. 2005;42(7):799-809. [CrossRef]
- Abbas AK, Murphy KM, Sher A. Functional diversity of helper T lymphocytes. Nature. 1996;383(6603):787-93. [CrossRef]
- O'Garra A. Cytokines induce the development of functionally heterogeneous T helper cell subsets. Immunity. 1998;8(3):275-83. [CrossRef]
- Spellberg B, Edwards JE Jr. Type 1/Type 2 immunity in infectious diseases. Clin Infect Dis. 2001;32(1):76-102. [CrossRef]
- Moxon ER, Kroll JS. The role of bacterial polysaccharide capsules as virulence factors. Curr Top Microbiol Immunol. 1990;150:65-85. [CrossRef]
- Galdiero M, Galdiero M, Finamore E, Rossano F, Gambuzza M, Catania MR, et al. *Haemophilus influenzae* porin induces Toll-like receptor 2-mediated cytokine production in human monocytes and mouse macrophages. Infect Immun. 2004;72(2):1204-9. [CrossRef]

- 23 Abe Y, Murphy TF, Sethi S, Faden HS, Dmochowski J, Harabuchi Y, et al. Lymphocyte proliferative response to P6 of *Haemophilus influenzae* is associated with relative protection from exacerbations of chronic obstructive pulmonary disease. *Am J Respir Crit Care Med*. 2002;165(7):967-71. [\[CrossRef\]](#)
- 24 de Bree GJ, Daniels H, Schilfgaarde Mv, Jansen HM, Out TA, van Lier RA, et al. Characterization of CD4+ memory T cell responses directed against common respiratory pathogens in peripheral blood and lung. *J Infect Dis*. 2007;195(11):1718-25. [\[CrossRef\]](#)
- 25 Youssef AR, van der Flier M, Estevão S, Hartwig NG, van der Ley P, Virji M. Opa+ and Opa- isolates of *Neisseria meningitidis* and *Neisseria gonorrhoeae* induce sustained proliferative responses in human CD4+ T cells. *Infect Immun*. 2009;77(11):5170-80. [\[CrossRef\]](#)
- 26 Youssef AR, Elson CJ. Induction of IL-10 cytokine and the suppression of T cell proliferation by specific peptides from red cell band 3 and in vivo effects of these peptides on autoimmune hemolytic anemia in NZB mice. *Auto Immun Highlights*. 2017;8(1):7. [\[CrossRef\]](#)
- 27 Morgan E, Varro R, Sepulveda H, Ember JA, Apgar J, Wilson J, et al. Cytometric bead array: a multiplexed assay platform with applications in various areas of biology. *Clin Immunol*. 2004;110(3):252-66. [\[CrossRef\]](#)
- 28 Moller MJ, Kammerer R, Grunert F, von Kleist S. Biliary glycoprotein (BGP) expression on T cells and on a natural-killer-cell sub-population. *Int J Cancer*. 1996;65(6):740-5. [\[CrossRef\]](#)
- 29 Woods ML, Shimizu Y. Signaling networks regulating beta1 integrin-mediated adhesion of T lymphocytes to extracellular matrix. *J Leukoc Biol*. 2001;69(6):874-80.
- 30 Komai-Koma M, Jones L, Ogg GS, Xu D, Liew FY. TLR2 is expressed on activated T cells as a costimulatory receptor. *Proc Natl Acad Sci U S A*. 2004;101(9):3029-34. [\[CrossRef\]](#)
- 31 Chen R, Lim JH, Jono H, Gu XX, Kim YS, Basbaum CB, et al. Nontypeable *Haemophilus influenzae* lipoprotein P6 induces MUC5AC mucin transcription via TLR2-TAK1-dependent p38 MAPK-AP1 and IKKbeta-IkappaBalpha-NF-kappaB signaling pathways. *Biochem Biophys Res Commun*. 2004;324(3):1087-94. [\[CrossRef\]](#)
- 32 Berenson CS, Murphy TF, Wrona CT, Sethi S. Outer membrane protein P6 of nontypeable *Haemophilus influenzae* is a potent and selective inducer of human macrophage proinflammatory cytokines. *Infect Immun*. 2005;73(5):2728-35. [\[CrossRef\]](#)
- 33 Muenzner P, Rohde M, Kneitz S, Hauck CR. CEACAM engagement by human pathogens enhances cell adhesion and counteracts bacteria-induced detachment of epithelial cells. *J Cell Biol*. 2005;170(5):825-36. [\[CrossRef\]](#)
- 34 Hill DJ, Toleman MA, Evans DJ, Villullas S, Van Alphen L, Virji M. The variable P5 proteins of typeable and non-typeable *Haemophilus influenzae* target human CEACAM1. *Mol Microbiol*. 2001;39(4):850-62. [\[CrossRef\]](#)
- 35 Hallström T, Trajkovska E, Forsgren A, Riesbeck K. *Haemophilus influenzae* surface fibrils contribute to serum resistance by interacting with vitronectin. *J Immunol*. 2006;177(1):430-6. Erratum in: *J Immunol*. 2013;190(8):4431. [\[CrossRef\]](#)
- 36 Bresser P, Virkola R, Jonsson-Vihanne M, Jansen HM, Korhonen TK, van Alphen L. Interaction of clinical isolates of nonencapsulated *Haemophilus influenzae* with mammalian extracellular matrix proteins. *FEMS Immunol Med Microbiol*. 2000;28(2):129-32. [\[CrossRef\]](#)
- 37 Virkola R, Brummer M, Rauvala H, van Alphen L, Korhonen TK. Interaction of fimbriae of *Haemophilus influenzae* type B with heparin-binding extracellular matrix proteins. *Infect Immun*. 2000;68(10):5696-701. [\[CrossRef\]](#)
- 38 Mosmann TR, Coffman RL. TH1 and TH2 cells: different patterns of lymphokine secretion lead to different functional properties. *Annu Rev Immunol*. 1989;7:145-73. [\[CrossRef\]](#)
- 39 Reiner SL, Locksley RM. The regulation of immunity to leishmania major. *Annu Rev Immunol*. 1995;13:151-77. [\[CrossRef\]](#)
- 40 Kurono Y, Yamamoto M, Fujihashi K, Kodama S, Suzuki M, Mogi G, et al. Nasal immunization induces *Haemophilus influenzae*-specific Th1 and Th2 responses with mucosal IgA and systemic IgG antibodies for protective immunity. *J Infect Dis*. 1999;180(1):122-32. [\[CrossRef\]](#)
- 41 Kodama S, Suenaga S, Hirano T, Suzuki M, Mogi G. Induction of specific immunoglobulin A and Th2 immune responses to P6 outer membrane protein of nontypeable *Haemophilus influenzae* in middle ear mucosa by intranasal immunization. *Infect Immun*. 2000;68(4):2294-300. [\[CrossRef\]](#)
- 42 Li W, Tenner-Racz K, Racz P, Janowicz DM, Fortney KR, Katz BP, et al. Role played by CD4+FOXP3+ regulatory T Cells in suppression of host responses to *Haemophilus ducreyi* during experimental infection of human volunteers. *J Infect Dis*. 2010;201(12):1839-48. [\[CrossRef\]](#)
- 43 Roncarolo MG, Gregori S, Levings M. Type 1 T regulatory cells and their relationship with CD4+CD25+ T regulatory cells. *Novartis Found Symp*. 2003;252:115-27.
- 44 Bouaziz JD, Calbo S, Maho-Vaillant M, Saussine A, Bagot M, Bensussan A, et al. IL-10 produced by activated human B cells regulates CD4(+) T-cell activation *in vitro*. *Eur J Immunol*. 2010;40(10):2686-91. [\[CrossRef\]](#)
- 45 Shevach EM. Mechanisms of foxp3+ T regulatory cell-mediated suppression. *Immunity*. 2009;30(5):636-45. [\[CrossRef\]](#)

# Effects of HLA Typing Resolution on Hardy-Weinberg Equilibrium, Linkage Disequilibrium, and Hidden Heterozygosity

Emel Yantır<sup>1</sup> 

<sup>1</sup>Eskişehir Osmangazi University Faculty of Medicine, Department of Immunology, Eskişehir, Türkiye

## Abstract

**Objectives:** The resolution level of human leukocyte antigen (HLA) typing critically influences the interpretation of population genetic parameters. This study aimed to quantitatively evaluate the effects of 2-, 4-, and 8-digit typing resolutions on allelic diversity, Hardy-Weinberg equilibrium (HWE), linkage disequilibrium (LD), and asymmetric LD (ALD) in a Central Anatolian population.

**Materials and Methods:** High-resolution next-generation sequencing (NGS)-based HLA typing was performed for six loci (HLA-A, HLA-B, HLA-C, HLA-DRB1, HLA-DQB1, and HLA-DPB1) in 150 unrelated healthy donors. Population genetic analyses were conducted using PyPop v1.2.1 software, and the results were comparatively assessed across 2-, 4-, and 8-digit resolution levels.

**Results:** Higher typing resolution systematically increased allelic richness and revealed hidden heterozygosity. While several loci appeared to conform to HWE at lower resolutions, significant deviations emerged at higher resolutions. Linkage disequilibrium strength increased with resolution, and ALD analysis consistently demonstrated directional dominance between specific locus pairs, reflecting biological hierarchies within haplotypes. Low-resolution typing underestimated allelic diversity, obscured heterozygosity, masked evolutionary signals, and weakened LD, potentially leading to misinterpretations.

**Conclusion:** High-resolution HLA typing, particularly at the 8-digit level, is essential for the accurate interpretation of population genetic parameters, disease association studies, and donor-recipient matching in transplantation. Future studies should focus on developing cost-effective high-resolution typing methods to enhance global accessibility and improve data accuracy in global HLA research.

**Keywords:** HLA, population genetics, next-generation sequencing, typing resolution, Hardy-Weinberg equilibrium, linkage disequilibrium

## Correspondence

Emel Yantır

## E-mail

dremelyntr@gmail.com

## Received

September 19, 2025

## Accepted

October 20, 2025

## Published

December 4, 2025

## Suggested Citation

Yantır E. Effects of HLA typing resolution on Hardy-Weinberg equilibrium, linkage disequilibrium, and hidden heterozygosity. Turk J Immunol. 2025;13(3):177-86.

## DOI

10.36519/TJI.2025.864



This work is licensed under the Creative Commons Attribution-NonCommercial-Non-Derivatives 4.0 International License (CC BY-NC-ND 4.0).

## Introduction

The human leukocyte antigen (HLA) complex, encoded by the major histocompatibility complex (MHC), is characterized by its remarkable polymorphism and linkage disequilibrium (LD), which makes it crucial for both immunity and disease susceptibility (1). Balancing selection, which promotes a heterozygote advantage and enhances resistance to infection, is the main evolutionary force maintaining this diversity (2). This diversity poses a significant challenge in clinical settings, such as hematopoietic stem cell transplantation, whereas strong LD aids in forming ancestral haplotypes that are essential for tracking population migration and disease susceptibility (3).

Identifying HLA alleles depends on typing resolution, which ranges from 2-digit serological groups to 8-digit sequences that capture the most detailed level of allele diversity. Population genetics utilizes tools such as the Hardy-Weinberg equilibrium (HWE) and LD to analyze a population's genetic structure (1-3). However, the quantitative effect of the "resolution gap" on these parameters remains unclear. Low-resolution methods can group functionally distinct alleles, leading to a "dilution effect", which can obscure true genetic diversity and weaken statistical signals (4,5).

This study addressed a key methodological question: How does HLA typing resolution influence the estimation of population genetic parameters and the evolutionary inferences drawn from them? Specifically, our objectives were to:

1. Quantify changes in allelic diversity and heterozygosity at 2-, 4-, and 8-digit resolutions.
2. Assess the effect of resolution on the results of HWE and Ewens-Watterson (EW) neutrality tests; and
3. Evaluate how typing resolution alters the strength and directionality of LD and asymmetric LD (ALD).

By analyzing a single Central Anatolian population at three distinct resolution levels, we aimed to demonstrate that typing resolution is a fundamental determinant of how population genetic structure and evolutionary patterns are interpreted (3,6,7).

## Materials and Methods

The overall workflow of the study is summarized in Figure 1.

## Study Population and Methodological Considerations

This retrospective study included 150 unrelated healthy donors from the database of the Tissue Typing Laboratory, Eskişehir Osmangazi University, between January 2020 and July 2025. The study group consisted of 150 unrelated donors (52.7% female, 47.3% male) with

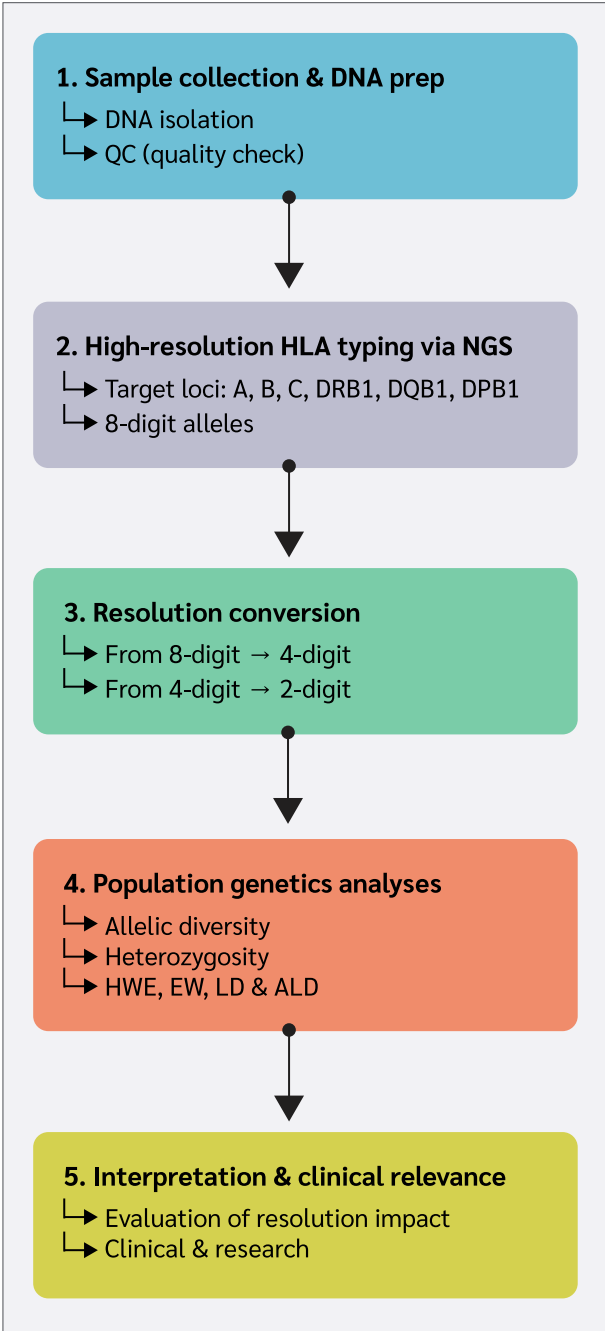


**Figure 1.** Overview of the study workflow. The diagram illustrates the sequential steps from sample collection to the final comparative interpretation of results across different HLA typing resolutions.

a mean age of  $38.6 \pm 19.4$  years. The cohort partially overlapped with the donor database used in our previous publication, while also incorporating newly recruited donors (8).

Most participants were of Central Anatolian origin, residing primarily in the city where the study was conducted or in neighboring provinces (8). As this was a retrospective study using a donor database, certain limitations were acknowledged. To minimize bias, individuals with known familial relationships were excluded based on a database cross-check and self-reporting by donors, ensuring that all participants were unrelated. No additional confounding factors were controlled for, as the primary objective was to compare the methodological resolutions within the same cohort rather than to conduct a case-control analysis.

The study was conducted in accordance with the principles of the Declaration of Helsinki, and the study protocol was approved by the Ethics Committee of Eskisehir Osmangazi University Faculty of Medicine (Approval No: 2025-06).

### Human Leukocyte Antigen Typing

Genomic DNA was isolated from peripheral blood collected into tubes with K3 EDTA using an automated system (EZ1 DNA Blood Kit 200  $\mu$ L; Qiagen, Hilden, Germany) according to the manufacturer's instructions. DNA concentrations were measured using the QIAxpert System (QIAGEN GmbH, Hilden, Germany), as described in our previous study (8,9). DNA samples purified to an A260/A280 ratio between 1.65 and 1.80 were used for subsequent next-generation sequencing (NGS) analysis.

High-resolution genotyping for HLA-A, HLA-B, HLA-C, HLA-DRB1, HLA-DQB1, and HLA-DPB1 loci was conducted using the MIA FORA NGS FLEX HLA Typing Kit (BioArray Solutions Ltd., New Jersey, USA), following the manufacturer's guidelines. Sequencing data were processed using the MIA FORA NGS FLEX HLA Genotyping Software (version 3.0), with reference to the IMGT/HLA database version 3.43.0 (10). For comparative analyses, 8-digit high-resolution data were converted to 2- and 4-digit resolutions by focusing on the initial two fields of the HLA allele identifiers.

### Population Genetics Analysis

Population genetics analyses for all three resolution levels were performed using Python for Population Genom-

ics (PyPop) v1.2.1 software (11). Alleles with frequencies below 1% were excluded from the HWE and LD analyses to minimize the potential for statistical artifacts arising from rare variants.

Compliance with HWE was evaluated using the Markov chain Monte Carlo (MCMC) exact test (12). Evidence of natural selection pressure was assessed via Slatkin's EW neutrality test (13). LD was measured using the normalized  $D'$  coefficient and  $W_n$  (a multiallelic extension of the  $r^2$  correlation measure) (14), and ALD analysis was performed based on the criteria defined by Thomson and Single (15). The statistical significance of LD measures was determined by a permutation test (1000 permutations) to account for multiple pairwise comparisons. For all analyses, statistical significance was set at  $p < 0.05$ .

## Results

### Impact of Resolution on Allelic Diversity and Genotype Counts

Analysis of six HLA loci demonstrated that as typing res-

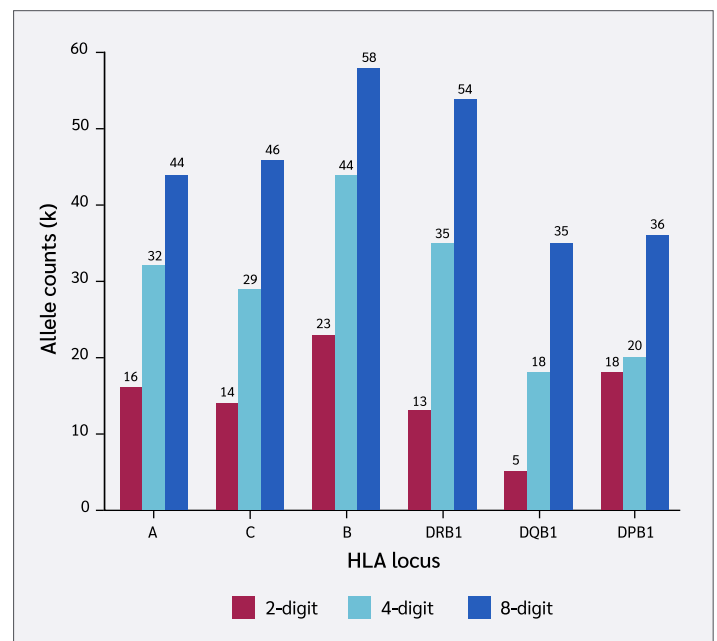


**Figure 2.** Allelic richness (k) by HLA locus across 2-, 4-, and 8-digit typing resolutions.

Bars show the number of unique alleles (k) observed at each HLA locus at 2-, 4-, and 8-digit resolution; exact counts are printed above bars. Data were derived by collapsing the same high-resolution NGS typings to lower resolutions. Allelic richness increases systematically with resolution, most notably at the B and DRB1.

**Table 1.** Observed and expected homozygote/heterozygote frequencies at different loci and resolution levels.

Locus	Resolution	Observed homozygotes (n)	Expected homozygotes (n)	Observed heterozygotes (n)	Expected heterozygotes (n)
HLA-A	2-digit	21	20.34	129	129.66
	4-digit	12	15.4	138	134.6
	8-digit	11	13.74	139	136.26
HLA-B	2-digit	22	11.6	128	138.4
	4-digit	14	7.06	136	142.94
	8-digit	11	6.57	139	145.2
HLA-C	2-digit	34	19.76	116	130.24
	4-digit	25	12.33	125	137.67
	8-digit	14	6.34	136	143.66
HLA-DRB1	2-digit	18	18.59	132	131.41
	4-digit	11	9.7	139	140.3
	8-digit	11	6.57	139	143.43
HLA-DQB1	2-digit	32	39.79	118	110.21
	4-digit	18	18.1	132	131.9
	8-digit	17	11.67	133	138.33
HLA-DPB1	2-digit	26	22.33	43	46.67
	4-digit	15	14.51	54	54.49
	8-digit	7	5.31	62	63.69

Due to typing limitations, the HWE analysis for the HLA-DPB1 locus was performed on a reduced sample size of N=69 individuals.

**Table 2.** Hardy-Weinberg equilibrium (HWE) exact test (Guo-Thompson MCMC) *p*-values.

Locus	2-digit ( <i>p</i> -value)	4-digit ( <i>p</i> -value)	8-digit ( <i>p</i> -value)
HLA-A	0.1463	0.4969	0.0216
HLA-C	0.0020	0.0024	0.0011
HLA-B	0.0002	0.0000	<0.0001
HLA-DRB1	0.2325	0.0458	0.0005
HLA-DQB1	0.7440	0.3513	0.0157
HLA-DPB1	0.0868	0.1290	<0.0001

**Table 3.** Summary of *p*-values for the Ewens-Watterson (EW) neutrality test and Hardy-Weinberg equilibrium (HWE) homozygosity test.

Locus	Resolution	EW test ( <i>p</i> -value)	HWE homozygosity test ( <i>p</i> -value)
HLA-C	2-digit	0.0168	0.0007
	4-digit	0.1662	0.0029
	8-digit	0.1662	<0.0001
HLA-B	2-digit	0.0096*	0.0040*
	4-digit	0.0456*	0.1842
	8-digit	0.0456*	0.1842
HLA-DRB1	2-digit	0.0063*	0.8993
	4-digit	0.1368	0.8993
	8-digit	0.1368	0.8993



**Table 4.** Linkage disequilibrium (LD) measures (D' and Wn) for major HLA locus pairs.

Locus pair	2-digit D'	4-digit D'	8-digit D'	2-digit Wn	4-digit Wn	8-digit Wn
HLA-A : HLA-C	0.46928	0.59824	0.75926	0.32873	0.48810	0.54729
HLA-A : HLA-B	0.55093	0.69351	0.73031	0.41791	0.55265	0.58476
HLA-C : HLA-B	0.85144	0.92100	0.93958	0.71223	0.75377	0.74748
HLA-B : HLA-DRB1	0.60246	0.77966	0.87513	0.46484	0.51672	0.56286
HLA-DRB1 : HLA-DQB1	0.94183	0.96729	0.95636	0.93373	0.84443	0.76977

Table 4 summarizes the strongest Linkage Disequilibrium (LD) findings; D' values for all 15 locus pairs are illustrated in Figure 3.

**Table 5.** Asymmetric linkage disequilibrium (ALD) values among selected HLA loci.

Locus pair	Resolution	LD (Wn)	ALD (L <sub>1</sub> → L <sub>2</sub> ) <sup>a</sup>	ALD (L <sub>1</sub> → L <sub>2</sub> ) <sup>b</sup>	p-value*
HLA-DRB1 : HLA-DQB1	2-digit	0.93373	0.60155	<b>0.94344</b>	<0.0001
	4-digit	0.84443	0.7411	<b>0.92872</b>	<0.0001
	8-digit	0.76977	0.6906	<b>0.87049</b>	<0.0001
HLA-C : HLA-B	2-digit	0.71223	<b>0.77876</b>	0.64005	<0.0001
	4-digit	0.75377	<b>0.81541</b>	0.66424	<0.0001
	8-digit	0.74748	<b>0.7978</b>	0.71408	<0.0001
HLA-B : HLA-DQB1	2-digit	0.50531	0.23721	<b>0.5383</b>	<0.0001
	4-digit	0.58367	0.39864	<b>0.62972</b>	<0.0001
	8-digit	0.5775	0.47329	<b>0.64707</b>	<0.0001
HLA-B : HLA-DRB1	2-digit	0.46484	0.36098	<b>0.51365</b>	<0.0001
	4-digit	0.51672	0.50716	<b>0.58582</b>	<0.0001
	8-digit	0.56286	0.55813	<b>0.60471</b>	<0.0001
HLA-A : HLA-B	2-digit	0.41791	<b>0.42723</b>	0.36501	<0.0001
	4-digit	0.55265	<b>0.53381</b>	0.44397	<0.0001
	8-digit	0.58476	<b>0.5973</b>	0.49967	<0.0001

<sup>a</sup>ALD (Locus 1 → Locus 2): Indicates the predictive power of the first locus (e.g., DRB1) in the first column of the table for the second locus (e.g., DQB1).

<sup>b</sup>ALD (Locus 2 → Locus 1): Indicates the predictive power of the second locus for the first.

\*Marked p-values were found to be statistically significant based on the results of 1000 permutation tests (p<0.05).

Values marked in **bold** indicate a stronger prediction direction for each locus pair.

olution improved, the number of distinct alleles (k) also increased (Figure 2). For instance, transitioning from a 2-digit to an 8-digit resolution increased allele richness from 16 to 44 for the HLA-A locus and from 23 to 58 for HLA-B.

Alongside the increase in allele numbers, there was a consistent decrease in the number of homozygous individuals across all loci with higher resolution, whereas the number

of heterozygous individuals increased (Table 1). For example, at the HLA-C locus, the number of observed homozygotes dropped from 34 at a 2-digit resolution to 14 at an 8-digit resolution. By contrast, the number of heterozygous individuals at this locus increased from 116 to 136.

### Hardy-Weinberg Equilibrium and Natural Selection Test Results

The population's adherence to the HWE was highly

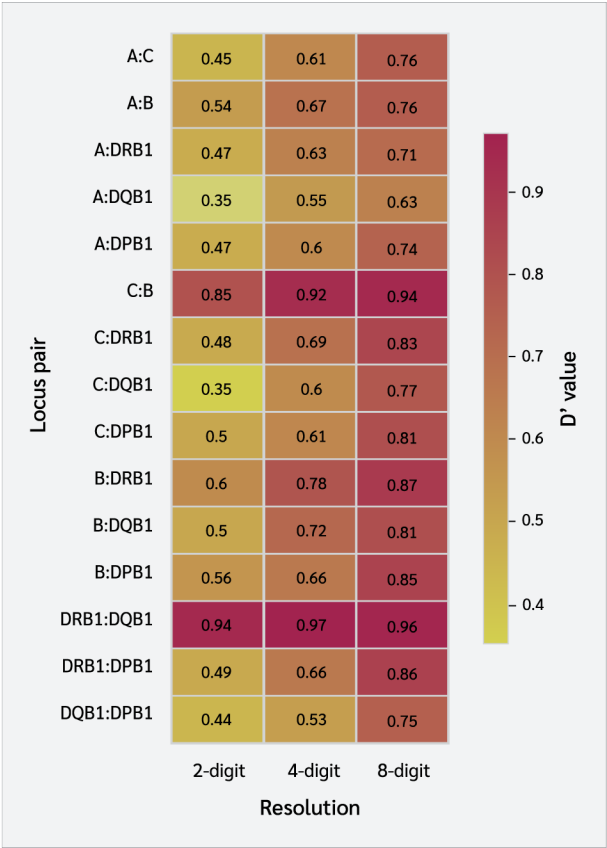


**Figure 3.** Linkage disequilibrium ( $D'$ ) values across HLA loci at different typing resolutions. Each cell represents the pairwise  $D'$  value between HLA loci, shown for 2-digit, 4-digit, and 8-digit resolution. The color scale indicates the strength of LD from low (yellow) to high (dark red), with exact values overlaid in each cell.

sensitive to typing resolution (Table 2). The HLA-C and HLA-B loci consistently and significantly deviated from HWE across all three resolution levels (all  $p < 0.01$ ). In contrast, the HLA-A, HLA-DQB1, and HLA-DPB1 loci conformed to HWE at lower resolutions but deviated significantly at the 8-digit level. The HLA-DRB1 locus deviated at both 4-digit ( $p = 0.0458$ ) and 8-digit ( $p = 0.0005$ ) resolutions.

The EW neutrality test revealed a different and more complex pattern (Table 3). The HLA-B locus showed significant deviation from neutrality at all resolutions. However, the HLA-C, HLA-DRB1, and HLA-DQB1 loci deviated significantly only at the 2-digit level, whereas the HLA-A and HLA-DPB1 loci did not deviate at any resolution.

**Linkage Disequilibrium (LD) and Asymmetric LD (ALD)**

The normalized  $D'$  coefficient was used to assess the LD

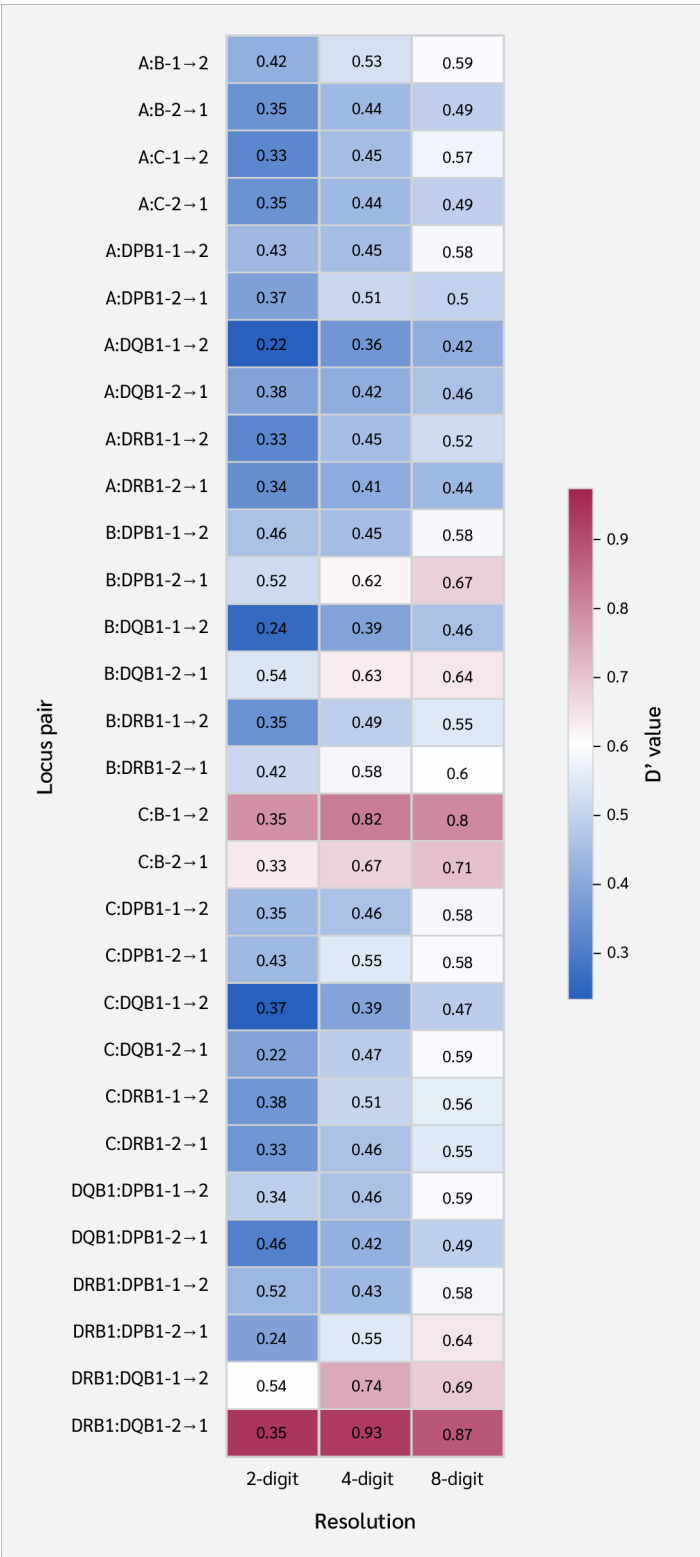


**Figure 4.** Asymmetric linkage disequilibrium (ALD) values between HLA loci at different typing resolutions. The heatmap shows directional ALD values for each HLA locus pair at 2-digit, 4-digit, and 8-digit resolution. Rows indicate the locus pair and the direction of the association (e.g., A:B-1 → 2 vs. A:B-2 → 1). The color scale represents the magnitude of ALD, ranging from low (blue) to high (red).

between pairs of loci. Generally, as typing resolution increased, there was a noticeable increase in the  $D'$  values (Table 4, Figure 3, Supplementary Table 1). For instance, the  $D'$  value for the HLA-A : HLA-C locus pair was 0.46928 at the 2-digit level and increased to 0.75926 at the 8-digit level. The strongest LD signals were detected at the 8-digit level between HLA-C : HLA-B ( $D'=0.93958$ ) and HLA-DRB1 : HLA-DQB1 ( $D'=0.95636$ ).

In the ALD analysis, a consistent and prevailing direction was observed between certain locus pairs, regardless of resolution levels (Table 5, Figure 4, Supplementary Table 2). Across all resolution levels analyzed, the predictive influence from HLA-C to HLA-B ( $C \rightarrow B$ ) and from HLA-DQB1 to HLA-DRB1 ( $DQB1 \rightarrow DRB1$ ) was more pronounced than that in the reverse direction.

## Discussion

The findings of this study demonstrated that increasing HLA typing resolution, from low to high, reshapes our understanding of the HLA genetic landscape. High-resolution typing uncovered previously "hidden" allelic diversity and heterozygosity, prompting a re-evaluation of HWE, natural selection, and LD. Our results highlighted how the "dilution effect" associated with low-resolution typing systematically diminishes or obscures evolutionary signals, resulting in a "blurred" view of the genetic landscape (16).

### "Dilution Effect": The Core Mechanism Obscuring the Genetic Landscape

The primary mechanism responsible for nearly all observed outcomes is the "dilution effect," which stems from the low resolution (8). Two-digit typing merges structurally and functionally distinct alleles (e.g., C\*07:01 and C\*07:02) into a single serological category (C\*07). This leads to an artificial decrease in the number of alleles, as demonstrated in our study: the number of alleles identified at the HLA-A locus increased from 16 at 2-digit to 32 at 4-digit and 44 at 8-digit resolution.

More critically, this merging leads to the artificial classification of individuals with different genotypes (e.g., C\*07:01/C\*07:02) as "homozygous" (C\*07/C\*07). This phenomenon, termed "hidden heterozygosity," directly accounts for the systematic reduction in the number of homozygotes observed in our study as resolution improved (11).

### Selection at the Haplotype Level: Synthesis of Complex Signals in HWE and EW Tests

Our analysis also demonstrated that deviations from the HWE are notably influenced by resolution and become particularly complex when considered in conjunction with selection tests. The HLA-C and HLA-B loci consistently deviated from HWE across all resolution levels (all  $p \leq 0.0024$ ), indicating the strong selection pressure. However, selection signals at these loci are not well understood. Hardy-Weinberg equilibrium analyses revealed that the number of homozygous individuals at these loci was significantly higher than expected. In contrast, the EW neutrality test indicated that the overall homozygosity ( $F$ ) at these loci was lower than expected under neutral evolution, suggesting a heterozygote advantage.

This apparent contradiction may result from selection acting on the entire haplotype rather than on the individual alleles. If a beneficial B-C haplotype becomes common in the population, certain genotypes may appear overrepresented in HWE analyses (17). This was more apparent when examining specific targets of selection at the genotypic level. The overall excess of homozygotes at the HLA-C locus was specifically driven by genotypes, such as C\*07+C\*07. The presence of many other rare haplotypes in the population maintained a low overall homozygosity ( $F$ ), creating a heterozygote advantage signal in the EW test (18). Thus, the differing outcomes of the two tests revealed two distinct aspects of the same evolutionary process: the rise of certain advantageous haplotype blocks and the maintenance of overall diversity (19).

### Linkage Disequilibrium and the True Power of Ancestral Haplotypes

Strong LD, the fundamental architecture of the HLA region, became increasingly evident with higher typing resolution in our study. This is a direct consequence of the elimination of the "dilution effect." High-resolution analysis directly reflected the true, non-random association between specific alleles and leads to a marked increase in LD measures such as  $D'$ . For example, the  $D'$  value for the HLA-A : HLA-C locus pair increased from 0.469 at the 2-digit level to 0.759 at the 8-digit level. This increase was particularly notable for some pairs; for instance, at 8-digit resolution, the  $D'$  value for the HLA-B : HLA-DRB1 pair was over 12% higher than that observed at 4-digit resolution.

These findings suggest that high-resolution typing does not create new links, but rather reveals the inherent strength of ancestral haplotype structures that have

been maintained by evolutionary forces. In particular, the HLA-C : HLA-B pair in Class I and the HLA-DRB1 : HLA-DQB1 pair in Class II were identified as nearly stable genetic blocks, exhibiting exceptionally high LD values. This suggests that previous evolutionary research using low-resolution datasets may have consistently underestimated the extent of MHC haplotype conservation.

Asymmetric LD analysis further clarified these relationships. Although ALD values varied depending on typing resolution, directional dominance (e.g., C→B and DQB1→DRB1) remained consistent regardless of resolution in certain locus pairs. This can be seen as a biological reflection of the functional or evolutionary hierarchy within haplotypes (20).

### Unveiling Hierarchical Structures in Haplotypes Through Asymmetric LD

Traditional LD metrics such as  $D'$  and  $r^2$  offer a single, symmetric value to describe the relationship between two loci. However, in systems with multiple alleles, such as HLA, where one locus has significantly more alleles than the other, this method does not provide a complete picture. To address this issue, ALD was developed by assessing the correlation between loci in both directions.

A key finding of our study was that the directional dominance identified by ALD (e.g., DQB1 → DRB1 and C → B) remained consistent across all resolution levels, even with a substantial increase in the number of alleles. This consistency strongly indicates that the observed patterns are not merely statistical anomalies but reflect genuine biological and evolutionary processes.

Our results demonstrated that the  $W(\text{DRB1}/\text{DQB1})$  value for the HLA-DRB1 : HLA-DQB1 pair was almost 1.00, indicating that knowing an allele at the HLA-DQB1 locus allows for the perfect prediction of the associated HLA-DRB1 allele. However, the predictive accuracy in the opposite direction,  $W(\text{DQB1}/\text{DRB1})$ , is not flawless. This asymmetry implies a functional or evolutionary hierarchy between these two loci. This situation might arise from selection pressures that aim to maintain the structural and functional integrity of the expressed DR-DQ heterodimer or from selection on one locus, causing a "genetic hitchhiking" effect on the other.

### The Broad Implications and Study Limitations

The results of this study have significant implications for

contemporary immunogenetic research. In the context of disease association studies, achieving high resolution is crucial for identifying the actual causal variant, as low-resolution findings can be deceptive (21). In the field of anthropological genetics, low resolution tends to systematically underestimate the strength of linkage disequilibrium, potentially leading to incorrect conclusions regarding population history. Regarding transplant compatibility, 8-digit resolution offers a vital evaluation of genomic compatibility throughout the entire linked MHC region, reducing the clinical risks associated with mismatches in minor histocompatibility antigens or immune-regulating genes, such as tumor necrosis factor (TNF) (22).

However, the broad adoption of high-resolution typing has encountered several obstacles. Increased expenses, the need for specialized equipment, and the demand for advanced bioinformatics expertise can pose significant challenges, especially in resource-constrained environments. Although this study established 8-digit typing as the scientific benchmark, future research should also aim to develop more affordable and accessible high-resolution methods to ensure that these advantages are globally applicable. Our findings, consistent with those of studies in other populations that reveal greater diversity with high-resolution, strongly support the investment in such technologies.

High-resolution HLA typing studies in African cohorts have demonstrated a marked increase in allelic richness and the unmasking of "hidden heterozygosity," closely paralleling our observations in the Central Anatolian population (16). In contrast, lower-resolution analyses in European datasets (7) have tended to underestimate haplotype conservation, whereas our results confirm that higher resolution sharpens LD signals and more accurately reflects ancestral haplotype structures.

Moreover, methodological advances in asymmetric LD analysis (6) provided a theoretical framework for our findings on stable directional dominance (e.g., C→B, DQB1→DRB1) across all resolution levels. Clinically, studies on transplantation immunogenetics (22) have shown that low-resolution matching increases the risk of graft-versus-host disease and rejection. Our demonstration that 8-digit typing represents the gold standard is, therefore, both clinically and evolutionarily relevant.

Of note, theoretical models of heterozygote advantage (19) suggested that MHC diversity itself may drive the

appearance of heterozygote advantage, offering a conceptual framework for the complex HWE and neutrality test outcomes that we observed. Taken together, these comparisons highlighted that our study not only provided a region-specific contribution but also reinforces broader international evidence that high-resolution typing is essential for accurate population genetic inference and clinical decision-making.

## Conclusion

This study quantitatively demonstrated that the resolution of HLA typing had a significant influence on the interpretation of population genetic parameters.

### Supplementary File

**Ethical Approval:** The study protocol was approved by the Non-Interventional Clinical Research Ethics Committee of Eskişehir Osmangazi University on April 29, 2025 with the decision number 2025-06.

**Informed Consent:** N.A.

**Peer-review:** Externally peer-reviewed

**Author Contributions:** Concept – E.Y.; Design – E.Y.; Supervision – E.Y.; Fundings – E.Y.; Materials – E.Y.; Data Collection and/or Pro-

Low-resolution data can lead to inaccurate conclusions by underestimating allelic diversity, concealing heterozygosity, hiding evolutionary signals, and weakening the LD power. Our principal findings revealed that as the resolution improved, allelic diversity became more apparent, HWE results underwent critical changes, LD signals became more pronounced, and biological hierarchies were validated. Collectively, these findings establish that high-resolution typing, particularly at the 8-digit level, is the gold standard for enhancing HLA population genetics, improving disease association analyses, and optimizing donor-recipient matching in transplantation. Future research should focus on cost-effective, high-resolution typing approaches to enhance the global accessibility and applicability of these insights.

cessing – E.Y.; Analysis and/or Interpretation – E.Y.; Literature Review – E.Y.; Writer – E.Y.; Critical Reviews – E.Y.

**Conflict of Interest:** The author declares no conflict of interest.

**Financial Disclosure:** The author declared that this study has received no financial support.

**Acknowledgment:** The author gratefully acknowledges the staff of the Tissue Typing Laboratory, Eskişehir Osmangazi University Faculty of Medicine, for their assistance in the data collection process.

## References

- Radwan J, Babik W, Kaufman J, Lenz TL, Winternitz J. Advances in the evolutionary understanding of MHC polymorphism. *Trends Genet.* 2020;36(4):298-311. [\[CrossRef\]](#)
- Parham P, Ohta T. Population biology of antigen presentation by MHC class I molecules. *Science.* 1996;272(5258):67-74. [\[CrossRef\]](#)
- Sakaue S, Gurajala S, Curtis M, Luo Y, Choi W, Ishigaki K, et al. Tutorial: a statistical genetics guide to identifying HLA alleles driving complex disease. *Nat Protoc.* 2023;18(9):2625-41. [\[CrossRef\]](#)
- Listgarten J, Brumme Z, Kadie C, Xiaojiang G, Walker B, Carrington M, et al. Statistical resolution of ambiguous HLA typing data. *PLoS Comput Biol.* 2008;4(2):e1000016. [\[CrossRef\]](#)
- Ewens WJ. The sampling theory of selectively neutral alleles. *Theor Popul Biol.* 1972;3(1):87-112. [\[CrossRef\]](#)
- Single RM, Strayer N, Thomson G, Paunic V, Albrecht M, Maier M. Asymmetric linkage disequilibrium: Tools for assessing multiallelic LD. *Hum Immunol.* 2016;77(3):288-94. [\[CrossRef\]](#)
- Evseeva I, Nicodemus KK, Bonilla C, Tonks S, Bodmer WF. Linkage disequilibrium and age of HLA region SNPs in relation to classic HLA gene alleles within Europe. *Eur J Hum Genet.* 2010;18(8):924-32. [\[CrossRef\]](#)
- Yantir E, Gündüz E, Çolak E. HLA alleles, genotype and haplotype analyzes from Central Anatolia Region of Turkey. *Balkan Med J.* 2023;40(5):358-66. [\[CrossRef\]](#)
- Sahin Tekin M, Yorulmaz G, Yantir E, Gunduz E, Colak E. A novel finding of an HLA allele's and a haplotype's relationship with SARS-CoV-2 vaccine-associated subacute thyroiditis. *Vaccines (Basel).* 2022;10(12):1986. [\[CrossRef\]](#)
- Robinson J, Barker DJ, Georgiou X, Cooper MA, Flicek P, Marsh SGE. IPD-IMGT/HLA database. *Nucleic Acids Res.* 2020;48(D1):D948-55. [\[CrossRef\]](#)
- Lancaster AK, Nelson MP, Single R, Solberg O, Tsai Y, Meyer D, et al. PyPop: Python for population genomics. Version 1.2.1. Zenodo; 2025. [\[CrossRef\]](#)
- Guo SW, Thompson EA. Performing the exact test of Hardy-Weinberg proportion for multiple alleles. *Biometrics.* 1992;48(2):361-72.
- Slatkin M. An exact test for neutrality based on the Ewens sampling distribution. *Genet Res.* 1994;64(1):71-4. [\[CrossRef\]](#)

- 14 Lewontin RC. The interaction of selection and linkage. I. General Considerations; Heterotic Models. *Genetics*. 1964;49(1):49-67. [\[CrossRef\]](#)
  - 15 Thomson G, Single RM. Conditional asymmetric linkage disequilibrium (ALD): extending the biallelic  $r^2$  measure. *Genetics*. 2014;198(1):321-31. [\[CrossRef\]](#)
  - 16 Banjoko AW, Ng'uni T, Naidoo N, Ramsuran V, Hyrien O, Ndhlovu ZM. High resolution class I HLA-A, -B, and -C diversity in Eastern and Southern African populations. *Sci Rep*. 2025;15(1):23667. [\[CrossRef\]](#)
  - 17 Meyer D, Thomson G. How selection shapes variation of the human major histocompatibility complex: a review. *Ann Hum Genet*. 2001;65(Pt 1):1-26. [\[CrossRef\]](#)
  - 18 Slatkin M. Joint estimation of selection intensity and mutation rate under balancing selection with applications to HLA. *Genetics*. 2022;221(2):iyac058. [\[CrossRef\]](#)
  - 19 Cherry JL. Heterozygote advantage cannot explain MHC diversity, but MHC diversity can explain heterozygote advantage. *bioRxiv* [Preprint]. May 31, 2025:2025.05.27.656382. [\[CrossRef\]](#)
  - 20 Pedersen MB, Asmussen SR, Sarfelt FM, Saksager AB, Sackett PW, Nielsen M, et al. Integration of HLA-DR linkage disequilibrium to MHC class II predictions. *bioRxiv* [Preprint]. May 24, 2023: 2023.05.24.542040. [\[CrossRef\]](#)
  - 21 Thorsby E. A short history of HLA. *Tissue Antigens*. 2009;74(2):101-16. [\[CrossRef\]](#)
  - 22 Petersdorf EW. The major histocompatibility complex: a model for understanding graft-versus-host disease. *Blood*. 2013;122(11):1863-72. [\[CrossRef\]](#)
-